Applications of four-wave mixing and cross phase modulation in highly nonlinear fibers

Seyedeh Bentolhoda Nazemosadat Arsanjani

2012

Seyedeh, B. N. A. (2012). Applications of four-wave mixing and cross phase modulation in highly nonlinear fibers. Doctoral thesis, Nanyang Technological University, Singapore.

https://hdl.handle.net/10356/48645

https://doi.org/10.32657/10356/48645

Applications of Four-Wave Mixing and Cross Phase Modulation in Highly Nonlinear Fibers

Seyedeh Bentolhoda Nazemosadat Arsanjani

School of Electrical & Electronic Engineering

A thesis submitted to the Nanyang Technological University

in partial fulfilment of the requirement for the degree of

Doctor of Philosophy

2012

Acknowledgements

"رب اشرح لی صدری و یسر لی امری واحلل عقده من لسانی یفقهوا قولی"

"Oh my Lord, grant me self-confidence, and ease my task for me, and remove the wrongs from my speech, so others understand my speech".

These are some verses of the Holy Quran which would come to my mind in the tough moments in these 4 years. There were times when the only thing which would make me go on was having faith in my God, Allah. I'm sure I haven't thanked Him for all that He has given me, but yet He has always took care of me, held my hands and shown me the right path. Thank you, Allah.

My deepest appreciation goes to my supervisor, Professor Perry P. Shum for his guidance, unceasing support and care throughout my PhD studies. Through the ups and downs of PhD he always encourages his students to go on and never lose hope, not just in words but also by using creative ways. He once sent me the music video of "When you believe" by Mariah Carey; I won't forget its effect on motivating me to carry on. I'm grateful to Dr Kenneth K. Y. Wong for his guidance and helpful suggestions. I would also like to express my gratitude to Prof. Lu Chao for his useful discussions and comments. Moreover, I would like to thank Nanyang Technological University for providing me with a postgraduate scholarship.

I also want to thank the students, researchers and staff of Network Technology Research Centre for their useful suggestions, help and friendship. In particular I would like to thank Dr Xiao Xiaosheng for his assistance and useful discussions. I'm also grateful to the graduate

students in Photonic Systems Research Laboratory in the University of Hong Kong for their helpful comments and friendship throughout my stay in Hong Kong, specially Mr. Yu Liang, Mr. Xu Xing and Ms Kim K. Y. Cheung for their patience in helping me in the lab.

The four years of my PhD life away from my family wouldn't have been possible without the lovely Iranian, Indian, Pakistani, Singaporean and Chinese friends I was surrounded with. Especial thanks goes to four of my dearest friends Farzaneh, Nazanin, Bahareh and Lobna for their warm friendship, love and support.

Last but not least I have to thank the dearest people I have in my life, my family. I might have been away from them during my PhD studies, but they were always the closest ones to me, in my heart. Talking to my mother, Parvaneh, cheered me up all the time by reminding me life isn't just studies and has many other aspects, the faith she had in me motivated me to go on. My father, Mohammad, has always given me hope, reminded me to believe in myself and made me calm by assuring me that his prayers are always with me. There are no words which can express how thankful I am to my caring parents who have offered me love and support throughout my life. If there is any honor in this degree it all goes to my parents. Thanks to my sister Zahra, and my brother Saeed, who are the ones who have always brought joy and happiness to my life.

Table of Contents

List of Figures

List of Tables

List of Acronyms

APSK	Amplitude and Phase Shift Keying
ASE	Amplified spontaneous emission
BER	Bit error rate
BPSK	Binary phase shift keying
CD	Chromatic dispersion
CSRZ	Carrier suppressed return-to-zero
CW	Continuous wave
DMUX	De-multiplexer
DPSK	Differential phase shift keying
DSF	Dispersion shifted fiber
DWDM	Dense wavelength division multiplexed
EDFA	Erbium-doped fiber amplifier
FOPA	Fiber optical parametric amplifier
FRA	Fiber Raman amplifier
FWM	Four-wave mixing
GVD	Group velocity dispersion
HNLF	Highly nonlinear fiber
MZDI	Mach-Zehnder delay interferometer
MZM	Mach-Zehnder modulator
NF	Noise figure
NLSE	Nonlinear Schrödinger Equation
NRZ	Non return-to-zero
O-E-O	Optical-electrical-optical
OOK	On-off keying
OSNR	Optical signal to noise ratio
OTDM	Optical time domain multiplexing

PALM	Parametric loop mirror
PMD	Polarization mode dispersion
PRBS	Pseudo random binary sequence
PSK	Phase shift keying
QN	Quantum noise
RZ	Return-to-zero
SBS	Stimulated Brillouin scattering
SMF	Single-mode fiber
SNR	Signal-to-noise ratio
SOA	Semiconductor optical amplifier
SOP	State of polarization
SPM	Self phase modulation
SRS	Stimulated Raman scattering
SSFM	Split-step Fourier method
TOD	Third order dispersion
WDM	Wavelength division multiplexing
XOR	Exclusive OR
XPM	Cross phase modulation
ZDW	Zero dispersion wavelength

Abstract

Wavelength Division Multiplexing (WDM) is one of the most common techniques used in fiber-optic communication systems in which multiple optical signals at various wavelengths are combined and transmitted through a single fiber. One of the key components in WDM systems are optical amplifiers. The most widely used amplifier is the Erbium-doped fiber amplifier (EDFA). However, its operating wavelength doesn't cover all the low loss wavelength range (1450-1650 nm) of optical fibers. Hence, to overcome the bandwidth limitation of EDFAs, alternative optical amplifiers have been investigated. One of the candidates is the fiber optical parametric amplifier (FOPA).

FOPAs operate based on a fiber nonlinearity known as four-wave mixing (FWM). FWM arises from the third order nonlinear susceptibility in a fiber and occurs when at least two waves with different frequencies co-propagate in the fiber. When a signal beam at angular frequency ω_s is launched into a fiber along with a strong optical pump beam at ω_p, the signal is amplified through a parametric process and another wave, called the idler, is generated at $2\omega_p - \omega_s$. For a modulated signal, the modulation format will be transferred to the idler; this feature enables the FOPA to be used for shifting the optical frequency of a signal in addition to amplifying it.

In order to use any optical amplifier in WDM systems, it should have a flat gain spectrum over its operating range, and FOPAs aren't an exception. A proposed method for achieving a FOPA with a flat gain spectrum is to set up the amplifier by cascading several fiber segments which have different parameters. A part of this research is allocated to optimizing the parameters of each of these fiber segments using a genetic algorithm such that the

resulting FOPA has a flat gain spectrum. It is shown that by optimizing the fourth order dispersion of each fiber section a broader flat gain spectrum can be achieved. Fluctuations of the zero dispersion wavelength (ZDW) have been considered for an amplifier which has optimum fourth order dispersion; the results show that as long as the average ZDW of each fiber segment is maintained close to the optimum value, ZDW fluctuations won't have a large effect on the flatness of the gain spectrum. The noise properties and the operation of a multi-section FOPA in the depleted pump regime have also been studied.

The four wave mixing behavior in a novel fiber loop mirror, composed of two dispersion shifted fibers along with a single mode fiber in between them, is theoretically investigated. Due to the phase shift which the SMF introduces this configuration provides higher conversion efficiency for signals in the vicinity of the pump, compared to previously reported fiber loop mirrors.

Furthermore, a new design for de-multiplexing and de-modulating a differential phase shift keying (DPSK) optical time-domain multiplexed signal is proposed and investigated. The scheme consists of a nonlinear medium and a dispersive fiber connected through a 3-dB coupler to form a fiber loop mirror.

Most optical signal processing operations are based on optical-electrical-optical (O/E/O) methods in which the operation bit rate is often limited by the electrical response time. In addition, utilizing ultrahigh speed photodiodes, data modulators and electronic devices are costly. Therefore, all-optical signal processing is highly desired.

In this research work applications of FWM and cross phase modulation (XPM) in all-optical signal processing are discussed. A multiple format conversion module based on FWM for converting non return-to-zero (NRZ)

or return-to-zero (RZ) on-off keying (OOK) modulation format to carrier-suppressed return-to-zero (CSRZ)-OOK and NRZ/RZ-DPSK signals to CSRZ-DPSK is presented.

Moreover, a scheme for performing all-optical logic exclusive-OR (XOR) between phase shift keying (PSK) data and OOK signals is described. This logic gate is based on XPM in a highly nonlinear fiber (HNLF).

All-optical generation of 4 levels and 8 levels RZ-amplitude and phase shift keying (APSK) modulation format based on FWM and XPM in a HNLF is presented.

Chapter 1

Introduction

1.1 Motivation

Optical fiber communication systems have attracted remarkable attention in the past two decades, as they are up to now the most promising technology in response to the exponentially growing demand for higher transmission capacity. This is due to the unique feature of optical fibers, which is their relatively low attenuation over a wide frequency range in the third telecommunication window around 1550 nm []. This telecommunication window offers a bandwidth of a few tens of THz. However, most of the installed fiber optic communication systems are only using a fraction of this huge available bandwidth.

To fully utilize the available bandwidth of optical fibers two methods can be considered. One approach is to transmit the signal at a higher bit rate by multiplexing signals in the time domain known as optical time division multiplexing (OTDM). Since the first 100 Gb/s OTDM transmission experiment over 36-km fiber link was reported in 1993 [2], OTDM technologies have made a lot of progress towards higher bit rates and longer transmission distances. For example, 160 Gb/s transmission over a record length of 4320 km [3] and 2.56 Tb/s transmission over 160 km have been reported [4]. An alternative technique is to multiplex several signals at different wavelengths and transmit them in a single fiber, which is called wavelength division multiplexing (WDM) [5]. In this technology by increasing the number of wavelengths, the transmission capacity will be

enhanced. A recent report, described the highest capacity of 101.7 Tb/s, where 370 WDM channels at 294 Gb/s were transmitted over 165 km of fiber [6].

WDM became possible only with the emergence of the Erbium-doped fiber amplifier (EDFA) [7], which provided amplification of multiple wavelengths simultaneously due to its relatively large bandwidth and low crosstalk. Erbium-doped fiber amplifier (EDFA) was invented in 1987 by a group of researchers in the University of Southampton [7]. The EDFA uses fiber doped with Erbium as a gain medium to amplify an optical signal. Amplification is a result of stimulated emission of photons from Erbium ions in the fiber. The dopant ions are pumped (usually at 980 nm or 1480 nm) to a higher energy state from where they can release their energy by stimulated emission of a photon which has the same wavelength as the input signal. This release of energy will bring the excited ions back to the lower energy level and meanwhile will amplify the input optical signal.

Although the combination of EDFA and WDM systems gives rise to higher bandwidths, but the EDFA amplification bandwidth is limited to the C-band (1530-1565 nm) [8]. Thus, the number of channels which can be combined using the WDM technique are limited by the EDFA bandwidth. Hence, to increase the transmission capacity of WDM systems it is important to have alternative amplifiers which can operate outside the EDFA bandwidth. The need of amplification outside the EDFA bandwidth has made researchers look for alternative amplifiers. Using the same EDFA technology, amplification has been demonstrated over both the L-band (1565-1610 nm) and S-band (1480-1510 nm) by using higher Erbium concentration [9] and doping Thulium in the fibers instead of Erbium [10], respectively.

Another possible solution is using optical amplifiers based on fiber nonlinearities. One such amplifier is the fiber Raman amplifier (FRA), which utilizes a nonlinear phenomenon in fibers known as the stimulated Raman

scattering (SRS) [11] for amplification [12]. Raman was the first to observe this scattering in 1928 [11]. In SRS the incident pump photon gives up its energy to create another photon with a lower energy at a lower frequency, while the remaining energy is absorbed by the medium in the form of molecular vibrations. When the pump and signal beams are injected into the fiber, energy is transferred from the pump to signal through SRS, which gives rise to Raman gain. The center wavelength of the gain bandwidth of these amplifiers depends on the pump wavelength, therefore with the proper selection of the pump wavelength FRAs can be used for amplifying signals at wavelengths outside the C-band. To obtain a wide gain bandwidth multiple pumps with different wavelengths and power levels can be used [13]. The Raman gain can be distributed in the transmission fiber which usually reduces the noise.

Another type of these amplifiers is the fiber optical parametric amplifier (FOPA) which is investigated in this research work. These amplifiers operate based on another fiber nonlinearity known as four wave mixing (FWM). FWM arises from the third order nonlinearity in a fiber and occurs when at least two waves with different frequencies co-propagate in the fiber. A refractive index modulation occurs at the difference frequency of the input waves, which creates an additional frequency component. Even though FWM was demonstrated experimentally for the first time by Stolen *et al.* in 1975 [14], but it was only until the last decade where FOPA gained a lot of attention. The first continuous wave (CW) FOPA was demonstrated in Photonics and Networking Research Laboratory (PNRL) in 1996 [15] where a signal gain of 5 dB and idler conversion efficiency of 4 dB was measured.

A continuous wave pumped FOPA with 70 dB gain [16], a pulsed FOPA over a record 400 nm bandwidth [17] and highly efficient parametric amplification and wavelength conversion in a one pump amplifier with near-complete pump depletion [18] are some of the recent results achieved in this

field. A CW bandwidth of 100 nm was also demonstrated using a single pump FOPA with a 4 W pump [19]. Distributed parametric amplification has been achieved in a 75 km long fiber [20]. Using double side band modulation, a phase sensitive parametric amplifier has been experimentally shown where data at 2.5 Gb/s was transmitted over a 60 km long fiber [21].

Unlike EDFAs, FOPAs can operate at any arbitrary wavelength. Similar to FRAs, the gain shape of FOPAs can also be controlled. In the meantime, the FOPA gain is approximately twice as high as that of the FRA, for the same fiber parameters [22]. This is due to the properties of silica and may be related to the higher value of the nonlinear refractive index compared to the peak Raman gain coefficient. This higher gain makes the FOPA more suitable for lumped amplification and all-optical signal processing applications. An important difference between these two amplifiers is the generation of an idler in the parametric process, which can be used for wavelength conversion [23].

FOPAs have a noise figure less than 3 dB quantum limit which can be even reduced to 0 dB when it is operated in a phase sensitive mode[24] [25]. The gain in Raman amplifier is bi-directional, therefore the beams can either co- or counter-propagate inside the fiber. However, FOPAs are uni-directional amplifiers which makes them less sensitive to saturation effects arising from the generated internal amplified spontaneous emission (ASE) [19].

Raman amplification has an inherent polarization dependence of gain which can be reduced by depolarization of the pump light [26, 27]. A depolarized pump can be achieved by orthogonal polarization multiplexing or by using various types of depolarizers. Parametric amplification is also a polarization-sensitive process which may cause problems for implementation in optical communication systems. This issue can be solved by using dual-pump waves with orthogonal polarization [28]. Polarization-independent operation can also be achieved in a single pump OPA by using a polarization

beam splitter in a Sagnac loop configuration [29]. A brief comparison between EDFA, FRA and FOPA can be seen in table 1.1 [30].

Table 1.1 Comparison between EDFA, FRA and FOPA

	EDFA	FRA	FOPA
Highest gain	54 dB [31]	45 dB [32]	70 dB [16]
Highest Bandwidth	40 nm	135 nm [33]	400 nm [17]
Center wavelength	Fixed	λ_{pump} dependent	λ_{pump} dependent
Noise figure	4 dB	4 dB	3.7 dB with 17 dB gain [34]
Average Pump power	10-100mW	≈1W	≈1W
Cross talk	No	No	Yes
Response time	milli-seconds	femto-seconds	femto-seconds
Polarization dependence	Small	Moderate	Large
Wavelength Conversion	No	No	Yes

An important concern in using FOPAs for amplification of WDM communication signals is that the nonlinearity of the amplifying medium may lead to detrimental inter-channel crosstalk [35], which arises from spurious FWM and cross-gain modulation (XGM) due to pump depletion [36]. This crosstalk can be reduced by using highly uniform fibers [37, 38], orthogonal signal polarizations [39] and short fibers [40]. Substantial crosstalk suppression has been achieved by using return-to-zero differential phase-shift

keying (RZ-DPSK) modulation format [41]. The pattern-independent amplitude and sub-unity duty cycle of RZ-DPSK modulated signals is effective in reducing XGM and FWM effects.

In a recently reported experiment where the signal-signal FWM crosstalk was reduced by using a short nonlinear fiber and a high-power pump, optical parametric amplification of 26×43.7 Gb/s RZ-DPSK DWDM channels with less than 1 dB penalty was demonstrated [42]. This work shows the ability of current FOPAs in handling amplification of WDM signals up to 1 Tb/s, and indicates that with further improvements FOPA could be a suitable candidate for wideband amplification in future optical communication networks.

Besides operating as amplifiers, FOPAs have characteristics which make them have the potential to be used for a variety of applications [22]. In addition to being an amplifier, due to the generation of a new wave, FOPA can simultaneously be used as a wavelength converter [43, 44] which is required for wavelength routing in optical networks. The intrinsic spectrum inversion of idlers in FOPAs can be used for dispersion compensation in long-haul transmission systems. Pulse generation [45], optical time division de-multiplexing [46, 47] and all-optical sampling [48] are other applications of FOPAs. These various features and applications of FOPAs are enough to motivate one to do research in this field.

Due to the requirement of higher network capacity, the data bit rate and channel number of WDM systems have been rapidly increasing. Consequently, the speed of signal processing in optical networks has been rising as well. Manipulating and analyzing high-speed optical signals with the present electronic devices is a major issue, since the electronic response time limits the operation bit rate. Carrying out the processing in electrical domain will also give rise to cumbersome optical-electrical-optical (O/E/O) conversions. Thus to prevent these issues, all-optical signal processing devices

are essential for providing ultrafast data processing and switching which will be crucial in network nodes of future ultrahigh speed optical communication systems.

A variety of all-optical signal processing devices such as switches [49-51], wavelength converters [52-54], de-multiplexers [46, 55], logic gates [56, 57], data format converters [58, 59] and regenerators [60, 61] have been investigated. Due to the fast response (femto-second time scale) of nonlinear effects in optical fibers, in this research work, some all-optical signal processing techniques based on two major nonlinear effects (cross phase modulation (XPM) and FWM) have been investigated.

1.2 Objectives

Most of this research work is focused on the fiber optical parametric amplifier, which is the main application of FWM. An objective of this work is to investigate the properties of FOPA used as an amplifier and also as a wavelength converter. Besides FWM, another nonlinear phenomenon which is considered in this research work is XPM. Finding new approaches for all-optical signal processing using these two nonlinear effects is another aim of this research.

1.3 Contribution

For any amplifier it is desired to have a flat gain spectrum in order to be used in WDM systems, and FOPAs aren't an exception. Therefore a part of this research is allocated to this issue by optimizing the parameters of a single pump FOPA to obtain a flat gain spectrum. The optimization is done using a genetic algorithm for a FOPA composed of several cascaded fiber segments. It

is shown that by optimizing the fourth order dispersion of each fiber segment a broad gain spectrum with low ripple will be achieved. Fluctuations of the zero dispersion wavelength (ZDW) have been considered for an amplifier which has optimum fourth order dispersion; the results show that as long as the average ZDW of each fiber segment is maintained close to the optimum value, ZDW fluctuations won't have a large effect on the flatness of the gain spectrum. The noise properties and the operation of a multi-section FOPA in the depleted pump regime have also been studied.

The FWM behavior in a novel loop mirror configuration, composed of two dispersion shifted fibers along with a single mode fiber in between them is studied. This loop, which can be used for separating the generated idler from the input pump and signal without using a filter, provides higher conversion efficiency compared to previously reported fiber loop mirrors.

Some applications of FWM and XPM in signal processing are discussed. A novel method for de-multiplexing return-to-zero differential phase shift keying (RZ-DPSK) optical time domain multiplexed (OTDM) signals and demodulating the de-multiplexed channel at the same time, is investigated.

It is shown that FWM can be used for modulation format conversion between return-to-zero (RZ) and non return-to-zero (NRZ) on-off keying (OOK) modulation formats to carrier suppressed return-to-zero on-off keying (CSRZ-OOK) format and also for NRZ/RZ-DPSK format to CSRZ-DPSK.

Moreover, a scheme for performing logic exclusive-OR (XOR) between an amplitude modulated signal and a phase modulated one is described. This logic gate is based on XPM in a highly nonlinear fiber (HNLF).

In the end, all-optical generation of return-to-zero 4 levels and 8 levels amplitude and phase shift keying (RZ-8-APSK) modulation format based on FWM and XPM in a highly nonlinear fiber is presented.

1.4 Overview

In Chapter 2, the theory of pulse propagation in nonlinear dispersive media in the slowly varying envelope approximation is explained and the nonlinear Schrödinger equation (NLSE) which describes the propagation of optical pulses in single mode fibers is derived. Then, a numerical approach for solving this equation known as the split-step Fourier method (SSFM) is discussed.

A brief description of chromatic dispersion and fiber loss in fibers are provided. In the end, an introduction to various nonlinear effects in fibers including self phase modulation, cross phase modulation, four wave mixing, stimulated Brillouin scattering and Stimulated Raman scattering, is given.

In Chapter 3, first basic concepts of optical amplifiers are mentioned. Then the principles and characteristics of fiber optical parametric amplification are introduced.

Chapter 4 discusses the optimization procedure of a single pump FOPA using a genetic algorithm. After optimizing the fiber parameters for achieving a FOPA with a flat gain spectrum, the effect of optimizing the fourth order dispersion of the fiber on the gain flatness is studied. The effects of zero dispersion wavelength fluctuations on the gain spectrum, noise properties of the amplifier and its operation in the pump depletion regime are investigated as well.

Chapter 5 explores the FWM conversion efficiency inside a loop mirror. It also contains a novel method for de-multiplexing and demodulating a RZ-DPSK OTDM signal using a fiber loop mirror.

Some applications of FWM and XPM in all-optical signal processing are mentioned in Chapter 6; a modulation format converter, a logic exclusive-OR gate and all-optical generation of RZ-8-APSK modulated signals are discussed.

In the end, Chapter 7 summarizes the results of this work.

Chapter 2

Signal Propagation in Optical Fibers

As an optical wave propagates through a fiber it experiences different effects, due to linear and nonlinear phenomena within the fiber. Optical loss and chromatic dispersion are linear degrading effects, while self-phase modulation (SPM), cross-phase modulation (XPM), four-wave mixing (FWM), stimulated Raman scattering (SRS) and stimulated Brillouin scattering (SBS) are nonlinear effects in fibers. Before getting into a detailed explanation of each of these effects, the nonlinear Schrödinger equation (NLSE) which is used to describe the signal propagation in optical fibers is presented. Details of the split-step Fourier method (SSFM), which is a numerical method for solving the NLSE, are also provided in this chapter.

2.1 Nonlinear Schrödinger Equation

Applying an intense electromagnetic field to any dielectric medium such as optical fiber will result in a nonlinear response. As light propagates through a medium, the bound electrons will start to oscillate under the influence of the applied field. The oscillating dipoles add up to a polarization **P**, which is normally used for describing the material response. When the light intensity is small, the bound electrons can follow the applied electric field **E**, resulting in a linear relationship between **P** and **E**. Meanwhile, large light intensities will cause non-harmonic motion of bound electrons which means the induced polarization becomes a nonlinear function of the applied electric field. The starting point for deriving a basic equation which

governs the propagation of optical waves in nonlinear dispersive fibers is the set of Maxwell's equations, given by

$$\nabla \times \mathbf{E} = -\frac{\partial \mathbf{B}}{\partial t} \tag{2.1.1}$$

$$\nabla \times \mathbf{H} = \mathbf{J} + \frac{\partial \mathbf{D}}{\partial t} \tag{2.1.2}$$

$$\nabla . \mathbf{D} = \rho \tag{2.1.3}$$

$$\nabla . \mathbf{B} = 0 \tag{2.1.4}$$

where **E** and **H** are electric and magnetic field vectors, and **D** and **B** are the electric and magnetic flux densities, respectively. **J** is the current density vector and ρ is the charge density. In mediums such as optical fibers there won't be any free charges so $\mathbf{J} = 0$ and $\rho = 0$. The electric and magnetic flux densities which arise in response to the **E** and **H** fields propagating inside the waveguide can be found by:

$$\mathbf{D} = \varepsilon_0 \mathbf{E} + \mathbf{P} \tag{2.1.5}$$

$$\mathbf{B} = \mu_0 \mathbf{H} + \mathbf{M} \tag{2.1.6}$$

where **P** and **M** are the induced electric and magnetic polarizations, respectively. ε_0 is the vacuum permittivity while μ_0 is the vacuum permeability. Since fibers are nonmagnetic mediums $\mathbf{M} = 0$. The equation which describes the propagation of light in optical fibers can be found by taking the curl of Eq. (2.1.1) and using Eqs. (2.1.2), (2.1.5) and (2.1.6) to obtain:

$$\nabla \times \nabla \times \mathbf{E} = -\frac{1}{c^2}\frac{\partial^2 \mathbf{E}}{\partial t^2} - \mu_0 \frac{\partial^2 \mathbf{P}}{\partial t^2} \tag{2.1.7}$$

where c is the speed of light in vacuum and $\varepsilon_0 \mu_0 = 1/c^2$. The left hand side of this equation can be simplified to

$$\nabla \times \nabla \times \mathbf{E} = \nabla (\nabla . \mathbf{E}) - \nabla^2 \mathbf{E} = -\nabla^2 \mathbf{E} \tag{2.1.8}$$

where the relation $\nabla.\mathbf{D} = \varepsilon\nabla.\mathbf{E} = 0$ is considered. The relation between the induced polarization vector and the electric field is

$$\mathbf{P} = \varepsilon_0(\chi^{(1)}.\mathbf{E} + \chi^{(2)}:\mathbf{EE} + \chi^{(3)}\vdots\mathbf{EEE} + \cdots) \tag{2.1.9}$$

where $\chi^{(i)}$ (i=1,2..) is the *i*th order susceptibility. The first order susceptibility $\chi^{(1)}$ stands for the linear response and is related to the linear refractive index by $n_0^2 = 1 + \chi^{(1)}$, while the higher order ones ($i \geq 2$) represent the nonlinear response. The second order susceptibility is zero in media which have inversion symmetry at molecular level. Since fibers are made of silica glass (SiO_2), which has symmetric molecules, $\chi^{(2)}$ is negligible in fibers. Hence, the dominant nonlinear effects in silica fibers stem from the third order susceptibility which is responsible for a phenomenon known as the Kerr effect. This effect is due to the intensity dependence of the refractive index in a fiber. Only high intensity light waves propagating through the nonlinear fiber will give rise to nonlinear effects. This is because $\chi^{(3)}$ is very small and based on Eq. (2.1.9), in order to have a large nonlinear polarization, **EEE** should be large. The presence of a strong light wave with effective optical field intensity I in a medium with a third order susceptibility modifies its refractive index according to:

$$\tilde{n}(\omega, I) = n_0(\omega) + n_2 I \tag{2.1.10}$$

where $n_0(\omega)$ is the fiber refractive index in a weak field and n_2 is the fiber nonlinear refractive index.

If only the third order nonlinear effects governed by $\chi^{(3)}$ are considered, the induced polarization can be written as

$$\mathbf{P}(\mathbf{r},t) = \mathbf{P}_L(\mathbf{r},t) + \mathbf{P}_{NL}(\mathbf{r},t) \tag{2.1.11}$$

where the linear part $\mathbf{P}_L$ and nonlinear part $\mathbf{P}_{NL}$ are related to the electrical field by

$$\mathbf{P}_L(\mathbf{r},t) = \varepsilon_0 \int_{-\infty}^{\infty} \chi^{(1)}(t-t').\mathbf{E}(\mathbf{r},t')\,dt' \tag{2.1.12}$$

$$\mathbf{P}_{NL}(\mathbf{r},t) = \varepsilon_0 \iiint_{-\infty}^{\infty} \chi^{(3)}(t-t_1, t-t_2, t-t_3) \vdots \mathbf{E}(\mathbf{r},t_1)\mathbf{E}(\mathbf{r},t_2)\mathbf{E}(\mathbf{r},t_3)\,dt_1 dt_2 dt_3 \tag{2.1.13}$$

By using Eqs. (2.1.8) and (2.1.11), Eq. (2.1.7) can be written in the form

$$\nabla^2\mathbf{E} - \frac{1}{c^2}\frac{\partial^2\mathbf{E}}{\partial t^2} = \mu_0 \frac{\partial^2\mathbf{P}_L}{\partial t^2} + \mu_0 \frac{\partial^2\mathbf{P}_{NL}}{\partial t^2} \tag{2.1.14}$$

To be able to solve the above equation, one should simplify it by making some assumptions. As a first step, $\mathbf{P}_{NL}$ is considered as a small perturbation to $\mathbf{P}_L$, which is valid as the refractive index changes are typically in the order of 10^{-6}. Second, it is assumed that the polarization state of the optical field will remain unchanged during propagation so that a scalar approach is valid. It is also assumed that the optical field is quasi-monochromatic, which means that the center frequency of the pulse ω_0 is much greater than its spectral width $\Delta\omega$. Given that $\omega_0 \sim 10^{15}\ s^{-1}$, this assumption is valid for pulses as short as 0.1 ps. The electric field can be written in the form

$$\mathbf{E}(\mathbf{r},t) = \frac{1}{2}\hat{x}[E(\mathbf{r},t)\exp(-i\omega_0 t) + c.c.] \tag{2.1.15}$$

where $\hat{x}$ is the polarization unit vector, $\mathbf{E}(\mathbf{r},t)$ is a slowly varying function of time and c.c. stands for complex conjugate. Similarly, the induced polarization components can also be expressed as

$$\mathbf{P}_{\mathrm{L}}(\mathbf{r},t) = \frac{1}{2}\hat{x}[\mathrm{P}_{\mathrm{L}}(\mathbf{r},t)\exp(-i\omega_0 t) + c.c.] \tag{2.1.16}$$

$$\mathbf{P}_{\mathrm{NL}}(\mathbf{r},t) = \frac{1}{2}\hat{x}[\mathrm{P}_{\mathrm{NL}}(\mathbf{r},t)\exp(-i\omega_0 t) + c.c.] \tag{2.1.17}$$

Typical nonlinear response time is much shorter than any practical optical pulse width, hence it is assumed to be instantaneous. The instantaneous response leads to considerable simplifications since the time dependence of $\chi^{(3)}$ in Eq. (2.1.13) is

$$\chi^{(3)}(t-t_1, t-t_2, t-t_3) = \chi^{(3)}\delta(t-t_1)\delta(t-t_2)\delta(t-t_3) \tag{2.1.18}$$

Hence Eq. (2.1.13) reduces to

$$\mathbf{P}_{\mathrm{NL}}(\mathbf{r},t) = \varepsilon_0\chi^{(3)} \vdots \mathbf{E}(\mathbf{r},t)\mathbf{E}(\mathbf{r},t)\mathbf{E}(\mathbf{r},t) \tag{2.1.19}$$

When Eq. (2.1.15) is substituted in Eq. (2.1.19), the nonlinear induced polarization will have a term oscillating at the third harmonic frequency $3\omega_0$, which is negligible in optical fibers. Thus P_{NL} can be written as

$$\begin{aligned}\mathbf{P}_{\mathrm{NL}}(\mathbf{r},t) &= \frac{1}{8}\varepsilon_0\chi^{(3)}[\mathrm{E}(\mathbf{r},t)\mathrm{e}^{-i\omega_0 t} + \mathrm{E}^*(\mathbf{r},t)\mathrm{e}^{i\omega_0 t}]^3 \\ &= \frac{1}{8}\varepsilon_0\chi^{(3)}[\left(\mathrm{E}^3(\mathbf{r},t)\mathrm{e}^{-i3\omega_0 t} + c.c.\right) \\ &\quad + 3|\mathrm{E}(\mathbf{r},t)|^2(\mathrm{E}(\mathbf{r},t)\mathrm{e}^{-i\omega_0 t} + \mathrm{c.c.})] \approx \varepsilon_0\varepsilon_{\mathrm{NL}}\mathrm{E}(\mathbf{r},t)\end{aligned} \tag{2.1.20}$$

where $\varepsilon_{\mathrm{NL}}$ is the nonlinear contribution to the dielectric constant defined as

$$\varepsilon_{\mathrm{NL}} = \frac{3}{4}\chi^{(3)}|\mathrm{E}(\mathbf{r},t)|^2 \tag{2.1.21}$$

Since $\varepsilon_{\mathrm{NL}}$ has a perturbative nature (similar to P_{NL}), it is assumed to be constant during the derivation of the propagation equation. For obtaining the wave equation for $\mathrm{E}(\mathbf{r},t)$ it is easier to work in the Fourier domain. Equation (2.1.14) can be written in the Fourier domain as follows

$$\nabla^2\widetilde{\mathrm{E}}(\mathbf{r},\omega) + \varepsilon(\omega)k_0^2\widetilde{\mathrm{E}}(\mathbf{r},\omega) = 0 \tag{2.1.22}$$

where $k_0 = \omega/\mathrm{c}$ and $\varepsilon(\omega) = 1 + \chi^{(1)} + \varepsilon_{\mathrm{NL}}$. The solution of this wave equation is assumed to be

$$\widetilde{\mathrm{E}}(\mathbf{r},\omega-\omega_0) = F(x,y)\tilde{A}(\mathrm{z},\omega-\omega_0)\exp(i\beta_0 z) \tag{2.1.23}$$

where $\tilde{A}(\mathrm{z},\omega-\omega_0)$ is a slowly varying function of z, $F(x,y)$ is the field distribution in the (x,y) plane and corresponds to the mode structure and β_0 is the wave number. Equations (2.1.22) and (2.1.23) lead to

$$\frac{\partial^2 F}{\partial x^2} + \frac{\partial^2 F}{\partial y^2} + [\varepsilon(\omega)k_0^2 - \tilde{\beta}^2]F = 0 \tag{2.1.24}$$

$$2i\beta_0\frac{\partial\tilde{A}}{\partial z} + [\tilde{\beta}^2 - \beta_0^2]\tilde{A} = 0 \tag{2.1.25}$$

Since $\tilde{A}(\mathrm{z},\omega-\omega_0)$ is a slowly varying function of z, $\partial^2\tilde{A}/\partial z^2$ is neglected in Eq. (2.1.25). The dielectric constant can be approximated by

$$\varepsilon(\omega) = (n_0 + \Delta n)^2 \approx n_0^2 + 2n\Delta n \tag{2.1.26}$$

$$\Delta n = n_2|E|^2 + i\frac{\alpha}{2k_0} \tag{2.1.27}$$

where n_0 is the fiber refractive index, Δn is a small perturbation, n_2 is the fiber nonlinear refractive index and α is the fiber loss. First-order perturbation theory can be used to solve Eq. (2.1.24). ε(ω) is first replaced by n_0^2 to obtain the modal distribution $F(x,y)$ and the corresponding wave number β(ω) and then the effect of Δn is included. While in the first-order perturbation theory Δn doesn't affect $F(x,y)$, the eigenvalue $\tilde{\beta}$ becomes

$$\tilde{\beta}(\omega) = \beta(\omega) + \Delta\beta \tag{2.1.28}$$

where $\Delta\beta$ includes the effect of fiber loss and nonlinearity and can be found by

$$\Delta\beta = \frac{k_0 \iint_{-\infty}^{\infty} \Delta n|F(x,y)|^2 dxdy}{\iint_{-\infty}^{\infty} |F(x,y)|^2 dxdy} \tag{2.1.29}$$

By substituting Eq. (2.1.29) in Eq. (2.1.25) and using the approximation $\tilde{\beta}^2 - \beta_0^2 \sim 2\beta_0(\tilde{\beta} - \beta_0)$, we have

$$\frac{\partial \tilde{A}}{\partial z} = i(\beta(\omega) + \Delta\beta - \beta_0)\tilde{A} \tag{2.1.30}$$

where it is useful to use the Taylor expansion of $\beta(\omega)$ about the center frequency ω_0

$$\beta(\omega) = \beta_0 + \beta_1(\omega - \omega_0) + \frac{1}{2}\beta_2(\omega - \omega_0)^2 + \frac{1}{6}\beta_3(\omega - \omega_0)^3 + \cdots \tag{2.1.31}$$

The propagation equation for $A(z,t)$ is found by taking the inverse Fourier transform of Eq. (2.1.30) and going back to the time domain. For the inverse Fourier transform operation $\omega - \omega_0$ is replaced by $i\frac{\partial}{\partial t}$. Thus, the

resulting equation for $A(z,t)$ when Eq. (2.1.31) is also taken into account becomes

$$\frac{\partial A}{\partial z} = -\beta_1 \frac{\partial A}{\partial t} - i\frac{1}{2}\beta_2 \frac{\partial^2 A}{\partial t^2} + i\Delta\beta A \tag{2.1.32}$$

By evaluating $\Delta\beta$ using Eqs. (2.1.27) and (2.1.29) and substituting it in the above equation, we have

$$\frac{\partial A}{\partial z} + \beta_1 \frac{\partial A}{\partial t} + i\frac{1}{2}\beta_2 \frac{\partial^2 A}{\partial t^2} + \frac{\alpha}{2}A = i\gamma|A|^2 A \tag{2.1.33}$$

where γ is the nonlinear coefficient of the fiber which is related to its nonlinear refractive index through

$$\gamma = \frac{2\pi n_2}{\lambda A_{eff}} \tag{2.1.34}$$

A_{eff} is the effective core area of the fiber, defined as

$$A_{eff} = \frac{\left(\iint_{-\infty}^{\infty} |F(x,y)|^2 dxdy\right)^2}{\iint_{-\infty}^{\infty} |F(x,y)|^4 dxdy} \tag{2.1.35}$$

The effective core area depends on fiber parameters such as the core radius and the core-cladding index difference. It can vary from $20\,\mu m^2$ for some dispersion compensating fibers to values more than $100\,\mu m^2$ for large-effective area fibers (LEAF). An appropriate amount for n_2 is $2.6 \times 10^{-20}\,\frac{m^2}{W}$.

It should be noted that in obtaining Eq. (2.1.33) the pulse amplitude unit is assumed normalized so that $|A|^2$ is the optical power. As seen in this equation, dispersion and nonlinearity act simultaneously on an optical pulse while it propagates along the fiber length. The effects of chromatic dispersion are included through β_1 and β_2, fiber nonlinearity through γ and fiber losses through α. By using the transformation $(z,t) \rightarrow (z, T = t - \frac{z}{v_g} \equiv t - \beta_1 z)$ the propagation equation can be re-written in terms of a reference frame moving with the pulse at the group velocity v_g, in the form

$$\frac{\partial A}{\partial z}+\frac{i\beta_2}{2}\frac{\partial^2 A}{\partial T^2}+\frac{\alpha}{2}A=i\gamma|A|^2A \tag{2.1.36}$$

Equation (2.1.36) is referred to as the nonlinear Schrödinger equation (NLSE). Since the NLSE is a nonlinear partial equation, it doesn't generally have analytic solutions. Thus, a numerical approach is often required for studying nonlinear effects in optical fibers. The most common scheme which has been used for solving the pulse propagation equation in nonlinear dispersive media has been the split-step Fourier method (SSFM) [62, 63]. In SSFM the fiber span is divided to many short sections, where the dispersion and nonlinearity are treated separately in each section. In the next section, more details on SSFM is provided.

2.2 Split-Step Fourier Method

The split-step Fourier method (SSFM) is a pseudo-spectral numerical method which is generally used for solving the nonlinear Schrödinger equation. In this method the solution is computed in small steps, were the linear and nonlinear steps are treated separately. The linear step is computed in the frequency domain while the nonlinear one is calculated in the time domain. A brief description of this method is presented in this section.

To understand the SSFM, it is useful to write the NLSE in the following form:

$$\frac{\partial A}{\partial z}=(\widehat{D}+\widehat{N})A \tag{2.2.1}$$

where

$$\widehat{D}=-\frac{i\beta_2}{2}\frac{\partial^2}{\partial T^2}-\frac{\alpha}{2} \tag{2.2.2}$$

$$\widehat{N} = i\gamma|A|^2 \tag{2.2.3}$$

$\widehat{D}$ is a differential operator which describes dispersion and absorption in a linear medium, while $\widehat{N}$ is a nonlinear operator which introduces fiber nonlinearity effects on the propagating pulse. Although dispersion and nonlinearity act together along the fiber length but in order to obtain an approximate solution to NLSE in SSFM it is assumed that dispersive and nonlinear effects act separately on the propagation of the optical field over a small distance h . Thus, propagation over one segment of length h from z to $z + h$ is carried out in two steps, where in the first step nonlinearity acts alone and $\widehat{D}$ is considered zero, while in the second step $\widehat{N} = 0$ and dispersion acts alone. The solution is

$$A(z + h, T) \approx \exp\left(h\widehat{D}\right) \exp\left(h\widehat{N}\right) A(z, T) \tag{2.2.4}$$

The execution of the linear dispersion operator $\exp\left(h\widehat{D}\right)$ can be carried out in the frequency domain, thus

$$\exp\left(h\widehat{D}\right) A(z, T) = F^{-1}\{\exp\left(h\widehat{D}(i\omega)\right) F[\, A(z, T)]\} \tag{2.2.5}$$

where $\widehat{D}(i\omega) = \frac{i\beta_2}{2}\omega^2 - \frac{\alpha}{2}$ is the dispersion operator in the Fourier domain and F and F^{-1} denote the Fourier and inverse Fourier transformations, respectively.

The exact solution of Eq. (2.2.1) is given by

$$A(z + h, T) = \exp[\, h(\widehat{D} + \widehat{N})]A(z, T) \tag{2.2.6}$$

The accuracy of the SSFM can be found by using the Baker-Hausdorff formula:

$$\exp\left(h\widehat{D}\right) \exp\left(h\widehat{N}\right)$$

$$= \exp\left(h\widehat{D} + h\widehat{N} + \frac{h^2}{2}\left[\widehat{D}, \widehat{N}\right] + \frac{h^3}{12}\left[\widehat{D} - \widehat{N}, \left[\widehat{D}, \widehat{N}\right]\right] + \cdots\right) \tag{2.2.7}$$

where $[\widehat{D},\widehat{N}] = \widehat{D}\widehat{N} - \widehat{N}\widehat{D}$. By comparing Eqs. (2.2.4) and (2.2.6) and considering Eq. (2.2.7) it is found that the dominant error term is $^1/_2\, h^2[\widehat{D},\widehat{N}]$. Hence, the SSFM is accurate to second order of step size h.

To increase the accuracy of this method, symmetrized SSFM can be used, which is given by

$$A(z+h,T) \approx \exp(\frac{h}{2}\widehat{D})\exp(h\widehat{N})\exp(\frac{h}{2}\widehat{D})\,A(z,T) \tag{2.2.8}$$

The accuracy of this method using the Baker-Hausdorff formula is

$$\begin{aligned}
&\exp\left(\frac{h}{2}\widehat{D}\right)\exp(h\widehat{N})\exp\left(\frac{h}{2}\widehat{D}\right)\\
&= \{\exp\left(\frac{h}{2}\widehat{D} + h\widehat{N} + \frac{h^2}{4}[\widehat{D},\widehat{N}] + \frac{h^3}{48}\left[\widehat{D},[\widehat{D},\widehat{N}]\right] - \frac{h^3}{24}\left[\widehat{N},[\widehat{D},\widehat{N}]\right]\right)\}\exp\left(\frac{h}{2}\widehat{D}\right)\\
&= \exp\left(\frac{h}{2}\widehat{D} + h\widehat{N} + \frac{h^2}{4}[\widehat{D},\widehat{N}] + \frac{h^3}{48}\left[\widehat{D},[\widehat{D},\widehat{N}]\right] - \frac{h^3}{24}\left[\widehat{N},[\widehat{D},\widehat{N}]\right] + \frac{h}{2}\widehat{D} + \frac{1}{2}[\frac{h}{2}\widehat{D}\right.\\
&\qquad \left. + h\widehat{N} + \frac{h^2}{4}[\widehat{D},\widehat{N}] + \frac{h^3}{48}\left[\widehat{D},[\widehat{D},\widehat{N}]\right] - \frac{h^3}{24}\left[\widehat{N},[\widehat{D},\widehat{N}]\right], \frac{h}{2}\widehat{D}]\right)\\
&= \exp\left(\frac{h}{2}\widehat{D} + h\widehat{N} + \frac{h^2}{4}[\widehat{D},\widehat{N}] + \frac{h^3}{48}\left[\widehat{D},[\widehat{D},\widehat{N}]\right] - \frac{h^3}{24}\left[\widehat{N},[\widehat{D},\widehat{N}]\right] + \frac{h}{2}\widehat{D}\right.\\
&\qquad \left. + \frac{1}{2}(\frac{h^2}{4}[\widehat{D},\widehat{D}] + \frac{h^2}{2}[\widehat{N},\widehat{D}] + \frac{h^3}{8}[[\widehat{D},\widehat{N}],\widehat{D}])\right)\\
&= \exp\left(\frac{h}{2}\widehat{D} + h\widehat{N} + \frac{h^2}{4}[\widehat{D},\widehat{N}] + \frac{h^3}{48}\left[\widehat{D},[\widehat{D},\widehat{N}]\right] - \frac{h^3}{24}\left[\widehat{N},[\widehat{D},\widehat{N}]\right] + \frac{h}{2}\widehat{D} + \frac{h^2}{4}[\widehat{N},\widehat{D}]\right.\\
&\qquad \left. + \frac{h^3}{16}[[\widehat{D},\widehat{N}],\widehat{D}]\right)\\
&= \exp\left(h\widehat{D} + h\widehat{N} + \frac{h^3}{48}\left[\widehat{D},[\widehat{D},\widehat{N}]\right] - \frac{h^3}{24}\left[\widehat{N},[\widehat{D},\widehat{N}]\right] + \frac{h^3}{16}[[\widehat{D},\widehat{N}],\widehat{D}]\right)
\end{aligned} \tag{2.2.9}$$

It should be noted that in Eq. (2.2.9), only up to the third order terms have been written and $[\widehat{D},\widehat{D}] = 0$ has been used. Thus, as seen in this equation the leading error term in the symmetrized method results from the third order of

h, which makes it more accurate than the previous method. Thus, this method is used throughout this thesis.

In this method the optical field is first propagated for a distance of $h/2$ using Eq. (2.2.5) where only dispersion is considered. At $z + h/2$, a nonlinear term is multiplied in the optical field, which accounts for the nonlinearity effect over the fiber section with length h. In the remaining $h/2$ propagation distance, the optical field is again propagated with the assumption that only dispersion is present in the fiber.

For higher accuracy in the dispersion operator, a more precise description of the propagation constant $\beta(\omega)$ is required for pulses close to the zero dispersion wavelength and also ultra-short pulses. By considering the Taylor expansion of the propagation constant, the dispersion operator is

$$\widehat{D} = \sum_{k=2}^{n} -i^{k-1} \frac{\beta_k}{k!} \frac{\partial^k}{\partial T^k} \tag{2.2.10}$$

where

$$\beta_k = \left(\frac{d^k \beta}{d\omega^k}\right)_{\omega=\omega_0} \qquad (k = 2,3, \dots) \tag{2.2.11}$$

2.3 Linear Effects in Fibers

2.3.1 Optical Loss

When an optical signal propagates inside a fiber, its power is attenuated due to material absorption and Rayleigh scattering. Even small amounts of impurities in silica glass can lead to significant absorption. Since the most important impurity which causes fiber loss is the OH ion, during the fiber fabrication process special precautions are taken to make sure the OH ion level is less than one part in one hundred million.

Rayleigh scattering arises from density fluctuations frozen into the fused silica during manufacture, which causes the scattering of light in all directions. This loss which is intrinsic to the fiber is dominant at short wavelengths.

The power loss during transmission of optical signals inside the fiber can be measured by

$$P_T = P_0 \exp(-\alpha L) \tag{2.3.1}$$

where P_0 is the signal power launched into a fiber of length L, P_T is the transmitted power and α is the attenuation constant. Usually fiber loss is expressed in units of dB/km using the relation

$$\alpha_{dB} = \frac{-10}{L} \log\left(\frac{P_T}{P_0}\right) = 4.343\alpha \tag{2.3.2}$$

The loss of most communication fibers near 1550 nm wavelength is around 0.2 dB/km.

2.3.2 Chromatic Dispersion

The refractive index $n(\omega)$ of a fiber depends on the optical frequency of the light wave passing through it. A signal wave with angular frequency ω which propagates as a single frequency component along the fiber will reach the output after a time $T = L/v_g$, where L is the fiber length and v_g is the group velocity of light given by

$$v_g = \frac{d\omega}{d\beta} \tag{2.3.3}$$

$\beta(\omega)$ is the propagation constant and is given by $\beta = n(\omega)\,{}^{\omega}/_{c}$, where c is the speed of light in vacuum. A pulse with a spectral width $\Delta\omega$ will be broadened due to the frequency dependence of its group velocity which is known as

group velocity dispersion (GVD). The different spectral components associated with the pulse will propagate at different speeds inside the fiber and therefore won't arrive at the fiber output simultaneously. Fiber dispersion effects can be explained by the Taylor expansion of the propagation constant about the center frequency ω_0 of the pulse spectrum

$$\beta(\omega) = \sum_{j=0}^{\infty} \frac{\beta_j}{j!}(\omega - \omega_0)^j$$

$$= \beta_0 + \beta_1(\omega - \omega_0) + \frac{1}{2}\beta_2(\omega - \omega_0)^2 + \frac{1}{6}\beta_3(\omega - \omega_0)^3 + \cdots \quad (2.3.4)$$

where

$$\beta_m = \left(\frac{d^m \beta}{d\omega^m}\right)_{\omega=\omega_0} \qquad (m = 0,1,2, \dots) \quad (2.3.5)$$

β_1 is the reciprocal of group velocity and the amount of pulse broadening is determined by the GVD parameter β_2. The relation between the dispersion parameter D and β_2 can be found by

$$D = -\frac{2\pi c}{\lambda^2}\beta_2 \quad (2.3.6)$$

β_2 is positive in the normal dispersion regime, vanishes around a wavelength referred to as zero dispersion wavelength (ZDW) and becomes negative in the anomalous dispersion region. In the normal dispersion regime, since the lower frequency components are closer to the ZDW, they travel faster than the higher frequency components, while the reverse occurs for waves travelling in the anomalous dispersion regime.

The coefficient β_3, known as the third order dispersion (TOD) parameter, becomes more effective when β_2 approaches zero. Higher-order dispersive effects should be considered for ultra-short optical pulses, and also for input wavelengths which are in the vicinity of ZDW within a few nanometers.

2.4 Nonlinear Effects in Fibers

The Kerr effect in an optical fiber is responsible for nonlinear effects known as self phase modulation (SPM), cross phase modulation (XPM) and four wave mixing (FWM), which are governed by the nonlinear coefficient γ of the fiber. Since most optical fibers which are used for communication have a small nonlinear coefficient ($\sim 1\ W^{-1}km^{-1}$), they can't be used for nonlinear applications. To overcome this issue, several kinds of fibers referred to as highly nonlinear fibers (HNLFs), have been developed.

Based on Eq. (2.2.3), the value of γ can be increased by increasing the nonlinear refractive index n_2 or decreasing the effective mode area A_{eff}. By reducing the core size and increasing its Germania content, higher nonlinear coefficient can be achieved [64, 65]. However, the loss of such a fiber will be increased due to the scattering caused by the doping molecules.

The nonlinear phenomena due to the Kerr effect are elastic, meaning that no energy is exchanged between the electromagnetic field and the nonlinear medium. On the other hand, some nonlinear effects such as stimulated Brillouin scattering (SBS) and stimulated Raman scattering (SRS) are caused by stimulated inelastic scattering in which part of the optical field's energy is transferred to the dielectric medium. These two phenomena are associated with the vibrational excitation modes of silica. Acoustic phonons are involved in stimulated Brillouin scattering while the participants of stimulated Raman scattering are optical phonons.

2.4.1 Self Phase Modulation

Self phase modulation (SPM) is a manifestation of the intensity dependence of the refractive index in optical fibers. An optical field propagating in an optical fiber will go through a self-induced nonlinear phase shift known as self phase modulation. To obtain the magnitude of the phase shift, one should consider that the phase of a signal with intensity $I(t)$, propagating through a fiber varies with the distance according to

$$\phi = \frac{2\pi}{\lambda}\tilde{n}z = \frac{2\pi}{\lambda}(n_0 + n_2 I(t))z \tag{2.4.1}$$

where λ is the wavelength of the optical wave and z is the propagation distance. The first term in Eq. (2.4.1) represents the linear phase shift due to signal propagation; the second term is the nonlinear phase shift which is due to SPM. Hence, when an optical pulse is transmitted through a fiber, it will experience a time-dependant phase shift ($\Delta\phi_{SPM}(t) = \frac{2\pi}{\lambda}n_2 I(t)z$) as a result of its time-dependant intensity.

A temporally varying phase means that the instantaneous optical frequency differs across the pulse from its central value ω_0. As shown in Fig. 2.1, in the leading edge of the pulse the instantaneous frequency is downshifted from the central frequency ω_0 (red shift), whereas in the trailing edge the instantaneous frequency is upshifted (blue shift) which leads to spectral broadening of the pulse. Thus, the time dependence of $\Delta\phi_{SPM}$ is responsible for SPM-induced spectral broadening.

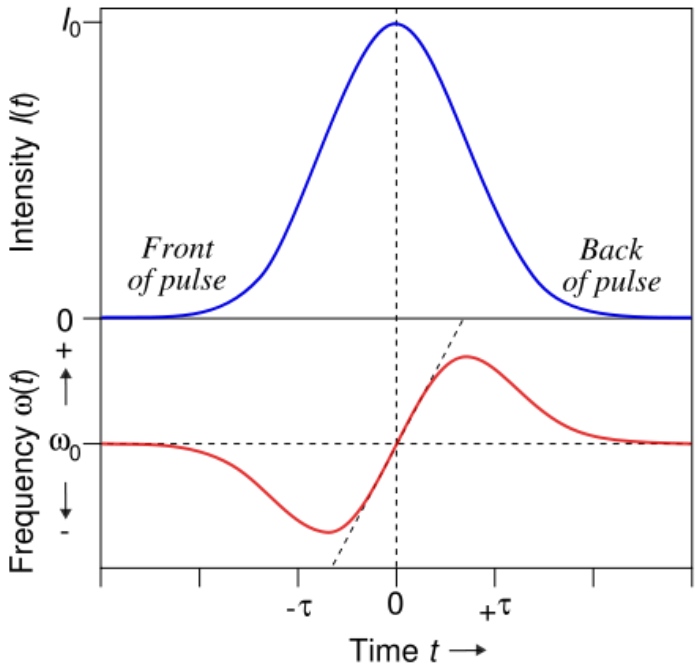

Fig. 2.1 The frequency shift (bottom curve) of a pulse (top curve) propagating through a nonlinear medium due to self-phase modulation. The front of the pulse is shifted to lower frequencies, the back to higher frequencies. In the centre of the pulse the frequency shift is approximately linear [66].

2.4.2 Cross Phase Modulation

When at least two optical fields with different frequencies propagate inside a fiber concurrently, they will not only experience an SPM induced phase shift but will also induce a phase shift on each other. This effect is known as cross phase modulation (XPM). The reason behind XPM is that each optical wave will change the fiber refractive index due to the Kerr nonlinearity and consequently will affect the other waves in the form of a nonlinear phase shift. Thus the effective refractive index seen by each optical wave not only depends on its own intensity but also on the intensity of other co-propagating beams. The XPM phase shift induced on an optical signal with the center wavelength λ_i by other co-propagating fields is

$$\Delta\phi_{\mathrm{XPM}} = \frac{2\pi}{\lambda_i} n_2 \left[2 \sum_{i \neq j} I_j(t)\right] z \tag{2.4.2}$$

where $I_j(t)$ is the intensity of the co-propagating signals. XPM phase shift takes place only when two pulses overlap in the time domain. The factor of 2 on the right hand side of Eq. (2.4.2) shows that for the same amount of power, XPM is twice as effective as SPM.

2.4.3 Four-Wave Mixing

Four-wave mixing also arises from the third order nonlinearity in a fiber and occurs when two intense pump waves with different frequencies (ω_1, ω_2) propagate together in the fiber. These waves force the bound electrons to oscillate almost instantly at any frequency resulting from the mixing of these waves. Although the electrons are confined to their original atom due to the potential provided by silica molecules, they respond to the intense applied electromagnetic field by emitting waves at two new frequencies (ω_3, ω_4) in addition to their original frequencies [67].

In quantum mechanical terms, FWM occurs when two photons at ω_1 and ω_2 are annihilated and two photons at ω_3 and ω_4 are simultaneously created, such that the net energy and momentum are conserved. The photon energy and momentum are $h\omega$ and $h\beta$, respectively, where β is the propagation constant. Therefore the conservation relations for a FWM process are:

$$\omega_1 + \omega_2 = \omega_3 + \omega_4 \tag{2.4.3}$$

$$\Delta\beta = \beta(\omega_3) + \beta(\omega_4) - \beta(\omega_1) - \beta(\omega_2) = 0 \tag{2.4.4}$$

Since $\beta(\omega_j)$ governs the phase shift experienced by the *j*th wave, Eq. (2.4.4) is referred to as the phase-matching condition.

If only the pump beams are launched into the fiber, the two other waves will grow from noise at frequencies which satisfy the phase-matching condition. However, a seeded FWM process will have a higher efficiency. Therefore if a weak signal at ω_3 is launched into the fiber along with the pump beams, the new created photons at the signal frequency will amplify the signal wave while a new wave known as the *idler wave* will be generated at ω_4 simultaneously. The gain causing this amplification is referred to as parametric gain. FWM will still occur even if only one pump beam is incident on the fiber instead of the general case of two independent pump beams. In this case which is referred to as degenerate FWM, the two pump photons will have the same frequency ($\omega_1 = \omega_2$).

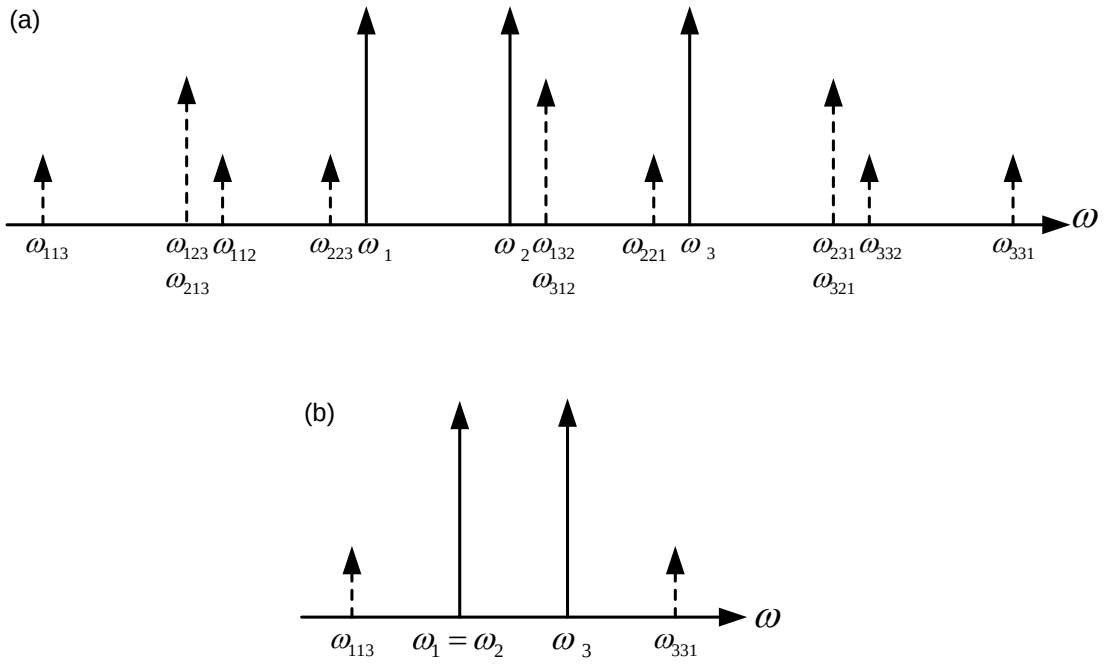

Fig. 2.2 FWM components at frequencies $\boldsymbol{\omega_{ijk} = \omega_i + \omega_j - \omega_k}$. FWM terms are generated in (a) non-degenerate case with three input fields at $\boldsymbol{\omega_1, \omega_2}$ and $\boldsymbol{\omega_3}$ and (b) degenerate case with two input signals.

Without loss of generality we will consider the degenerate case with the interaction of three co-polarized waves. The angular frequencies and the slowly varying electric field amplitudes of the pump, signal and idler are ω_p ω_s, ω_i and $A_p(z), A_s(z)$ and $A_i(z)$, respectively. By assuming continuous-wave operation, the following coupled equations describe the complex field amplitude changes along the fiber length [63, 68]:

$$\frac{dA_p}{dz} = i\gamma[\left(|A_p|^2 + 2(|A_s|^2 + |A_i|^2)\right)A_p + 2A_sA_iA_p^* \exp(\mathrm{i}\Delta\beta z)] \quad (2.4.5)$$

$$\frac{dA_s}{dz} = i\gamma[\left(|A_s|^2 + 2\left(|A_i|^2 + |A_p|^2\right)\right)A_s + A_i^*{A_p}^2 \exp(-\mathrm{i}\Delta\beta z)] \quad (2.4.6)$$

$$\frac{dA_i}{dz} = i\gamma[\left(|A_i|^2 + 2\left(|A_s|^2 + |A_p|^2\right)\right)A_i + A_s^*{A_p}^2 \exp(-\mathrm{i}\Delta\beta z)] \quad (2.4.7)$$

The first three terms on the right hand side of Eqs. (2.4.5)-(2.4.7) are the nonlinear phase shifts due to SPM and XPM. The last term describes the FWM energy transfer between the interacting waves. If the loss is considered, $-{\alpha}/{2}\,A_j$, $(j = p, s, i)$ should be added to the right hand side of these equations, where α is the attenuation constant.

When the power of the signal is much smaller than the pump and when the fiber attenuation can be neglected, closed form analytical solutions can be derived for the coupled equations, which will be explained in the next chapter. However, when the power of the signal is high relative to the pump power level, the coupled equations should be solved numerically using for instance the Runge-Kutta method.

The above equations describe the interaction of three continuous wave beams. However, if the participating waves are optical pulses, A_j should not only be a function of z but also should be considered a slowly varying

function of time as well. In this case, based on Eq. (2.1.33) and the coupled equations (2.4.5)-(2.4.7), the following equations are obtained [69]

$$\frac{\partial A_p}{\partial z}+\beta_{1p}\frac{\partial A_p}{\partial t}+i\frac{1}{2}\beta_{2p}\frac{\partial^2 A_p}{\partial t^2}+\frac{\alpha_p}{2}A_p = i\gamma[\left(\left|A_p\right|^2+2(|A_s|^2+|A_i|^2)\right)A_p+2A_sA_iA_p^*\exp(\mathrm{i}\Delta\beta z)] \tag{2.4.8}$$

$$\frac{\partial A_s}{\partial z}+\beta_{1s}\frac{\partial A_s}{\partial t}+i\frac{1}{2}\beta_{2s}\frac{\partial^2 A_s}{\partial t^2}+\frac{\alpha_s}{2}A_s = i\gamma[\left(|A_s|^2+2\left(|A_i|^2+\left|A_p\right|^2\right)\right)A_s+A_i^*{A_p}^2\exp(-\mathrm{i}\Delta\beta z)] \tag{2.4.9}$$

$$\frac{\partial A_i}{\partial z}+\beta_{1i}\frac{\partial A_i}{\partial t}+i\frac{1}{2}\beta_{2i}\frac{\partial^2 A_i}{\partial t^2}+\frac{\alpha_i}{2}A_i = i\gamma[\left(|A_i|^2+2\left(|A_s|^2+\left|A_p\right|^2\right)\right)A_i+A_s^*{A_p}^2\exp(-\mathrm{i}\Delta\beta z)] \tag{2.4.10}$$

where $\beta_{mx,}(x=p,s,i)$ is the mth order dispersion parameter at the pump, signal and idler wavelength, respectively. By transforming to a frame of reference that is moving with the group velocity of the pump pulse $T=t-z/v_{gp}$, the above set of equations can be written in the form

$$\frac{\partial A_p}{\partial z}+i\frac{1}{2}\beta_{2p}\frac{\partial^2 A_p}{\partial T^2}+\frac{\alpha_p}{2}A_p = i\gamma[\left(\left|A_p\right|^2+2(|A_s|^2+|A_i|^2)\right)A_p+2A_sA_iA_p^*\exp(\mathrm{i}\Delta\beta z)] \tag{2.4.11}$$

$$\frac{\partial A_s}{\partial z}+(\frac{1}{v_{gs}}-\frac{1}{v_{gp}})\frac{\partial A_s}{\partial T}+i\frac{1}{2}\beta_{2s}\frac{\partial^2 A_s}{\partial T^2}+\frac{\alpha_s}{2}A_s = i\gamma[\left(|A_s|^2+2\left(|A_i|^2+\left|A_p\right|^2\right)\right)A_s+A_i^*{A_p}^2\exp(-\mathrm{i}\Delta\beta z)] \tag{2.4.12}$$

$$\frac{\partial A_i}{\partial z}+(\frac{1}{v_{gi}}-\frac{1}{v_{gp}})\frac{\partial A_i}{\partial T}+i\frac{1}{2}\beta_{2i}\frac{\partial^2 A_i}{\partial T^2}+\frac{\alpha_i}{2}A_i = i\gamma[\left(|A_i|^2+2\left(|A_s|^2+\left|A_p\right|^2\right)\right)A_i+A_s^*{A_p}^2\exp(-\mathrm{i}\Delta\beta z)] \tag{2.4.13}$$

Under general conditions a numerical approach is required for solving the resulting coupled NLS equations, which describe FWM of pico-second pulses.

2.4.4 Stimulated Brillouin Scattering

Due to the electrostriction process, when an intense light wave is launched into a fiber its oscillating electric field will generate an acoustic wave at another frequency [70]. This acoustic wave will propagate in the same direction as the light wave and scatter it through stimulated Brillouin scattering (SBS) to a frequency down-shifted counter-propagating lightwave. The amount of this counter-propagating lightwave depends on the SBS threshold. Once the input power is beyond the SBS threshold, the backward-propagating stokes wave will carry most of the input power. The SBS threshold can be estimated as [63, 71]

$$P_{th} \approx \frac{21kA_{eff}}{g_0 L_{eff}} \left(\frac{\Delta\nu_B + \Delta\upsilon_P}{\Delta\nu_B}\right) \tag{2.4.14}$$

where L_{eff} is the effective interaction length, k is the polarization factor, g_0 is the peak Brillouin gain coefficient and $\Delta\nu_B$ and $\Delta\upsilon_P$ are the Brillouin gain linewidth and the pump spectral width, respectively.

Since the maximum transmitted optical power in fibers will be limited by SBS, there are several methods for increasing the SBS threshold and thus reducing or suppressing SBS. The frequency components falling outside the SBS gain bandwidth $\Delta\nu_B$ won't generate SBS gain; therefore the most common technique for increasing SBS threshold is to increase the bandwidth of the optical carrier through phase or frequency modulation [15, 72].

2.4.5 Stimulated Raman Scattering

In any molecular medium, due to spontaneous Raman scattering the incident pump photon gives up a small fraction of its energy to create another

photon with a lower energy at a lower frequency known as the Stokes wave. Meanwhile, the medium absorbs the remaining energy in the form of molecular vibrations [73]. This effect which was first found by Raman in 1928 is known as the Raman effect [74]. In 1962, it was revealed that for intense pump fields, Stimulated Raman scattering (SRS) occurs and the Stokes wave grows rapidly inside the medium since most of the incident pump energy is transferred to it [75].

2.5 Summary

In the beginning of this chapter, the theory of pulse propagation in nonlinear dispersive media in the slowly varying envelope approximation is considered in order to derive the nonlinear Schrödinger equation (NLSE). Then, the split-step Fourier method (SSFM) which is a numerical method used for solving the NLSE is explained.

A description of chromatic dispersion, due to its importance in the study of nonlinear effects in fibers, along with fiber loss is given. In the end, a brief introduction to various nonlinear effects arising from the Kerr effect and stimulated inelastic scattering is provided. The Kerr effect results from the dependence of the refractive index on the optical intensity, which brings on SPM, XPM and FWM. The stimulated inelastic scattering arises from the interaction of the optical field with acoustic phonons in the fiber (SBS) or with optical phonons (SRS).

Chapter 3

Fiber Optical Parametric Amplifiers

3.1 Basic Concepts of Optical Amplifiers

Optical amplifiers, which are the key enabling technology for WDM systems, can amplify multiple wavelengths in the optical domain without requiring conversion to the electrical domain. Ever since EDFAs were successfully implemented as optical amplifiers, a lot of research has been done not only on the EDFA itself, but also on other types of optical amplifiers which use different material and working mechanisms. Some of the characteristics of optical amplifiers which we will be dealing with later on in this research work include:

- **Gain**: The ratio of output signal power to input signal power which is usually expressed in decibels (dB).

$$G(dB) = 10\log(\frac{P_{s,out}}{P_{s,in}}) \tag{3.1.1}$$

- **Bandwidth:** The wavelength range in which the gain drops 3 dB from its maximum.
- **Center wavelength:** The wavelength which is the center of the gain bandwidth.
- **Noise figure:** The amplifier noise figure (NF) shows how much the signal-to-noise ratio (SNR) is degraded after passing through the amplifier. In other words it describes the extra noise added by the amplifier and is defined as the ratio of the input SNR to the output one.

$$NF(dB) = 10\log(\frac{SNR_{in}}{SNR_{out}}) \quad (3.1.2)$$

- **Polarization dependence:** Ideally the signal gain should not depend on its state of polarization (SOP); however in practice this is not the case for some amplifiers.

3.2 Fiber Optical Parametric Amplifiers

Parametric amplification occurs when FWM takes effect between a strong optical pump beam at ω_p and a weak signal beam at ω_s propagating in a highly nonlinear fiber (HNLF). When the two beams are co-propagating in the fiber their frequencies are beating with each other due to Kerr effect. As a result the refractive index of the fiber is modulated with the frequency $\omega_p - \omega_s$. The modulated refractive index acts as a phase modulator for the pump beam and creates sidebands at $\omega_p - (\omega_p - \omega_s) = \omega_s$ and $\omega_p + (\omega_p - \omega_s) = \omega_i$. Therefore the signal is amplified due to parametric gain, while a new wave, generally called idler, is generated simultaneously.

FOPAs have important characteristics which make them have the potential to be used for a variety of applications [76]. These properties are listed below:

- **Large gain and bandwidth**

  By using one or two pumps, FOPAs can provide relatively larger gain and bandwidth compared to EDFA and FRAs. Simultaneous amplification of seven channels was realized in an experiment in 2003 using a single pump FOPA [36]. In another experiment a dual pump FOPA with 38-dB gain with 1.5-dB ripple over a bandwidth of more than 47 nm was achieved [77].

- **Arbitrary center wavelength**

The center wavelength, λ_c, of the gain region in FOPAs can be any arbitrary wavelength. However it should be noted that the zero dispersion wavelength (ZDW) of the fiber should be close to λ_c. This property exists in FRAs as well but not in EDFAs.

- **Wavelength conversion**

Besides amplifying the input signal, a new wavelength component is generated by the FOPA. This feature can be used for creating new wavelengths for wavelength routing in optical networks. The signal to idler conversion efficiency can be as high as the signal gain, therefore leading to large conversion efficiencies which can't be obtained with other wavelength conversion techniques. Dual pump FOPAs can produce multiple idlers at the same time. This feature was used in an experiment to convert the signal to three different bands simultaneously [78]. By using dual pump FOPAs with orthogonally polarized pumps, polarization-insensitive wavelength conversion can be achieved [79].

- **Spectral inversion**

In FOPAs the idler spectrum is symmetric to the signal spectrum with respect to the central frequency. This feature can be used for dispersion compensation in communication systems [80].

- **Phase conjugation**

The idler's phase is opposite to that of the original signal. Some nonlinear effects such as cross phase modulation which affect the phase of the waves can be counteracted using this idler property.

- **High speed optical signal processing**

The ultrafast nature of the nonlinear response of FOPAs is useful for many applications. Generally high speed modulation of the pump will result in modulation of the signal and idler which can be used for applications such as pulse generation [45] ,regeneration of signal pulses and all-optical sampling [48]. optical time division de-multiplexing [46, 47] is another application of FOPAs.

- **Low noise figure**

FOPAs can theoretically have a noise figure of 0 dB while operating in phase sensitive mode [24]. A noise figure of 4.2 dB with maximum gain of 27.2 dB [81]and 3.7 dB with 17 dB gain [34] has been measured for FOPAs.

- **Unidirectional gain**

Unlike EDFA and FRA, in a FOPA only the signal waves which co-propagate with the pump get amplified. Therefore, it doesn't provide gain for the reflections from the end of the amplifier.

- **Distributed amplification**

Similar to Raman amplification, parametric amplification can be implemented along the transmission fibers as well as between them.

3.2.1 Parametric Amplification

The configuration of a single-pump optical parametric amplifier is shown in Fig. 3.1. The signal at ω_s ,which is to be amplified, is coupled into a highly nonlinear fiber along with a strong optical pump wave at ω_p. In practice, in order to suppress the effects of SBS, the pump is first broadened by phase modulation [82]. By adjusting the pump and signal wavelengths

near the zero-dispersion wavelength, FWM takes place and the weak signal is amplified through parametric amplification, while the idler wave is generated at $\omega_i = 2\omega_p - \omega_s$. An optical band-pass filter at the end of the HNLF is required to separate the amplified signal from the residual pump power and the generated idler.

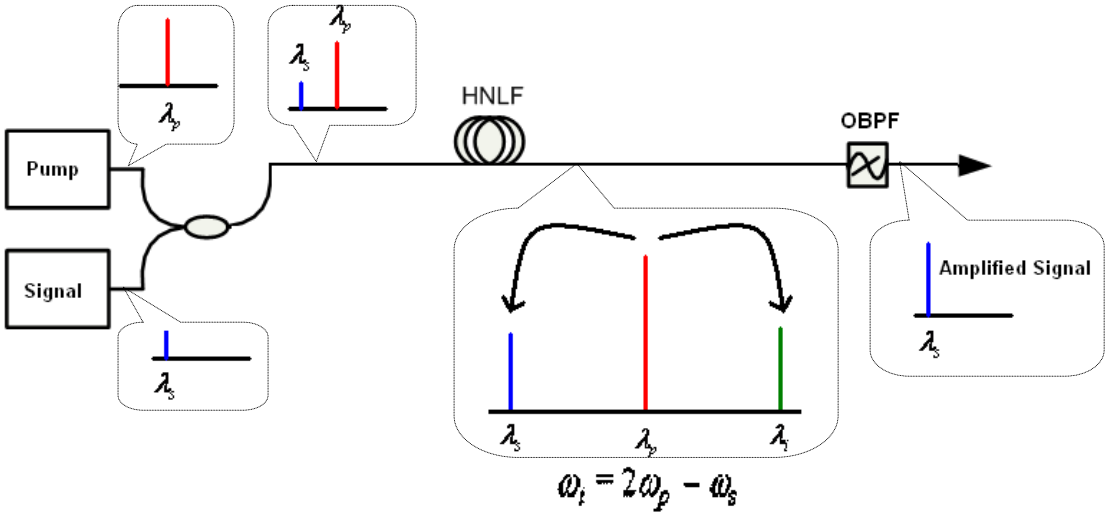

Fig. 3.1 Single pump FOPA configuration**.** OBPF: Optical band-pass filter.

3.2.2 Parametric Gain

Equations (2.4.5)-(2.4.7) describe the basics of FOPAs with the assumption of quasi-CW conditions. To find an analytical solution for them we assume the pump is much more intense than the signal and idler; which means the pump isn't depleted. In this case the solution of (2.4.5) is found by [63]

$$A_p(z) = \sqrt{P_p}\exp(i\gamma P_p z) \tag{3.2.1}$$

where $P_p = |A_p(0)|^2$ is the pump power. By substituting (3.2.1) in (2.4.6) and (2.4.7), we have

$$\frac{dA_s}{dz} = i\gamma(2P_p A_s + A_i^* A_p^2 \exp(-i\Delta\beta z)) \tag{3.2.2}$$

$$\frac{dA_i^*}{dz} = -i\gamma(2P_p A_i^* + A_s {A_p^*}^2 \exp(i\Delta\beta z)) \tag{3.2.3}$$

B_j is introduced as

$$B_j = A_j \exp\left(-2i\gamma P_p z\right), \text{ for } j = s, i \tag{3.2.4}$$

Using B_j , Eqs. (3.2.2) and (3.2.3) can be rewritten in the following form

$$\frac{dB_s}{dz} = i\gamma P_p B_i^* \exp(-i2kz) \tag{3.2.5}$$

$$\frac{dB_i^*}{dz} = -i\gamma P_p B_s \exp(i2kz) \tag{3.2.6}$$

where k is the total phase mismatch, containing the linear propagation constant mismatch and the nonlinear phase shift

$$\boldsymbol{k = \frac{\Delta\beta}{2} + \gamma P_p} \tag{3.2.7}$$

The linear propagation constant mismatch is given by

$$\Delta\beta = \beta(\omega_s) + \beta(\omega_i) - 2\beta\left(\omega_p\right) \tag{3.2.8}$$

By expanding $\beta(\omega_s)$ around ω_p we have

$$\beta(\omega_s) = \beta\left(\omega_p\right) + \beta_1(\omega_p)(\omega_s - \omega_p) + \frac{1}{2}\beta_2(\omega_p)\left(\omega_s - \omega_p\right)^2 + \frac{1}{6}\beta_3(\omega_p)\left(\omega_s - \omega_p\right)^3 + \cdots \tag{3.2.9}$$

Similarly we can expand $\beta(\omega_i)$ around ω_p and use $\Omega = \omega_p - \omega_s = -(\omega_p - \omega_i)$ which is the frequency detuning between the signal (idler) and pump, to obtain [83]

$$\Delta\beta = 2\sum_{m=1}^{\infty}\frac{\beta_{2m}(\omega_p)}{(2m)!}(\omega_s-\omega_p)^{2m} \tag{3.2.10}$$

where $\beta_{2m}(\omega_p)$ denotes the $(2m)$th derivative of β at ω_p. Equation (3.2.10) shows that only the even dispersion orders affect the gain spectrum of an FOPA. $\Delta\beta$ is generally truncated after the fourth order, so it can be expressed as

$$\Delta\beta = \beta_2(\omega_p)(\omega_s-\omega_p)^2 + \frac{1}{12}\beta_4(\omega_p)(\omega_s-\omega_p)^4 \tag{3.2.11}$$

The solution to Eqs. (3.2.5) and (3.2.6) are

$$B_s(z) = \left(\left[\cosh(gz) + i\frac{k}{g}\sinh(gz)\right]B_s(0) + i\frac{\gamma P_p}{g}\sinh(gz)\,B_i^*(0)\right)\exp(-ikz) \tag{3.2.12}$$

$$B_i^*(z) = \left(-i\frac{\gamma P_p}{g}\sinh(gz)\,B_s(0) + \left[\cosh(gz) - i\frac{k}{g}\sinh(gz)\right]B_i^*(0)\right)\exp(ikz) \tag{3.2.13}$$

where the parametric gain coefficient g is introduced as

$$g = \sqrt{(\gamma P_p)^2 - k^2} \tag{3.2.14}$$

When only the pump and signal are launched into the fiber, by setting $B_i^*(0) = 0$ in Eq. (3.2.12), one can find the signal power, $P_s(z) = |B_s|^2$, as

$$\begin{aligned} P_s(z) &= \left[1 + (1+\frac{k^2}{g^2})\sinh^2(gz)\right]P_s(0) \\ &= (1 + \left[\frac{\gamma P_p}{g}\sinh(gz)\right]^2)P_s(0) \end{aligned} \tag{3.2.15}$$

Therefore the amplification factor for a fiber with length L is:

$$G_s = \frac{P_s(L)}{P_s(0)} = 1 + \left[\frac{\gamma P_p}{g}\sinh(gL)\right]^2 \tag{3.2.16}$$

The idler power, $P_i(z) = |B_i|^2$, and gain can be found using (3.2.13) in the same way, resulting in:

$$P_i(z) = \left[\frac{\gamma P_p}{g}\sinh(gz)\right]^2 P_s(0) \tag{3.2.17}$$

$$G_i = \frac{P_i(L)}{P_s(0)} = \left[\frac{\gamma P_p}{g}\sinh(gL)\right]^2 = G_s - 1 \tag{3.2.18}$$

Equation (3.2.17) shows that almost immediately after the signal is launched into the fiber, the idler wave is generated. The idler has the same properties as the signal except for its phase which is the conjugate of that of the signal.

For a complete description of parametric amplification, pump depletion effects should be considered, which requires a numerical approach for solving (2.4.5)-(2.4.7). However, in order to get a physical insight we can assume the pump isn't depleted much and use the approximate analytical solutions in (3.2.12) and (3.2.13).

3.2.3 The Extrema of the FOPA Gain Spectrum

The extrema points of the gain (G_s) in (3.2.16) are the zeros of the derivative of G_s with respect to Ω [84], so:

$$\frac{\partial G_s}{\partial \Omega} = -\frac{1}{2}(\gamma P_p)^2 \frac{\sinh(gL)}{g^4}[gLcosh(gL) - \sinh(gL)]k\frac{\partial \Delta\beta}{\partial \Omega} = 0 \tag{3.2.19}$$

when g is real, $f(x) = \frac{\sinh(gL)}{g^4}[gLcosh(gL) - \sinh(gL)]$ is always positive therefore the extrema are obtained from $\partial\Delta\beta/\partial\Omega = 0$ and $k = 0$. The zeros of $\partial\Delta\beta/\partial\Omega$ are

$$\Omega = 0 \tag{3.2.20}$$

$$\Omega = \pm\sqrt{-6\beta_2/\beta_4} \tag{3.2.21}$$

while $k = 0$ leads to

$$\Omega = \pm\frac{\sqrt{2}}{\beta_4}\sqrt{\beta_4(-3\beta_2 \pm \sqrt{9\beta_2^2 - 6\gamma P_p \beta_4})} \tag{3.2.22}$$

Therefore the gain spectrum can have up to seven extrema. The extremum at $\Omega = 0$ always exists while the existence of the other extrema depends on the FOPA parameters β_2, β_4 and γP_p. Four cases can be considered:

1. $\beta_4 < 0$ and $\beta_2 > 0$

For this configuration as the second and fourth order dispersions have opposite signs the extrema at $\Omega = \pm\sqrt{-6\beta_2/\beta_4}$ will exist. In these conditions only two of the four possible solutions in (3.2.22) exist, therefore along with $\Omega = 0$, the gain spectrum has totally five extrema points.

2. $\beta_4 < 0$ and $\beta_2 < 0$

This arrangement will lead to two maxima obtained from Eq. (3.2.22) and one minimum ($\Omega = 0$).

3. $\beta_4 > 0$ and $\beta_2 > 0$

For all values of β_2 and β_4 which fulfill this condition, there won't be any signal wavelength which satisfies Eq. (3.2.22). Since both of these parameters have the same sign the only extremum will be in $\Omega = 0$.

4. $\beta_4 > 0$ and $\beta_2 < 0$

For this case the three extrema obtained from $\partial\Delta\beta/\partial\Omega = 0$ exist; meanwhile the four points from $k = 0$ only exist if $\beta_2 < -\sqrt{2\gamma P_p \beta_4/3}$. Hence, this configuration can have up to seven extrema.

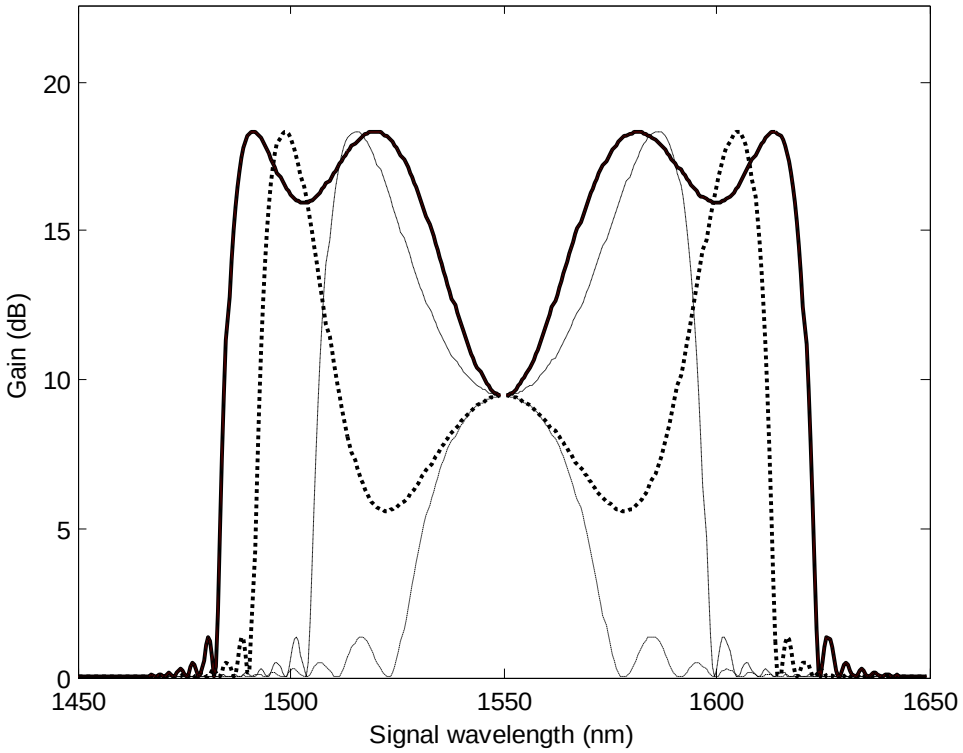

Fig. 3.2 Signal gain spectra for $\boldsymbol{\gamma = 2\ km^{-1}W^{-1}}$, $\boldsymbol{P_p = 7\ W}$ and $\boldsymbol{L = 200\ m}$. Solid line: $\boldsymbol{\beta_4 = 2.5 \times 10^{-4}\ ps^4km^{-1}}$, $\boldsymbol{\beta_2 = -0.06\ ps^2km^{-1}}$; broken and dotted line: $\boldsymbol{\beta_4 = 2.5 \times 10^{-4}\ ps^4km^{-1}}$, $\boldsymbol{\beta_2 = 0.02\ ps^2km^{-1}}$; dotted line: $\boldsymbol{\beta_4 = -2.5 \times 10^{-4}\ ps^4km^{-1}}$, $\boldsymbol{\beta_2 = 0.02\ ps^2km^{-1}}$; broken line: $\boldsymbol{\beta_4 = -2.5 \times 10^{-4}\ ps^4km^{-1}}$, $\boldsymbol{\beta_2 = -0.02\ ps^2km^{-1}}$.

In Fig. 3.2 the gain spectra of all four conditions are shown which are found by using Eq. (3.2.16). It can be seen that the gain spectrum with seven extrema is more likely to have a flat gain. By using the approximation $\sinh^2 gL \approx e^{2gL}/4$, the gain in decibel units can be written as:

$$G_{dB} = 8.7gL - 20\log\left(\frac{g}{\gamma P_p}\right) - 6 \tag{3.2.23}$$

Therefore the gain ripple in the low ripple region of the gain spectrum in this configuration ($\beta_4 > 0$ and $\beta_2 < 0$) can be obtained by:

$$\Delta G = G_{max} - G_{min} = 8.7\left(\gamma P_p - \sqrt{\frac{3\gamma P_p {\beta_2}^2}{\beta_4} - \frac{9{\beta_2}^4}{4{\beta_4}^2}}\right)L + 10\log\frac{\left(\frac{3\gamma P_p {\beta_2}^2}{\beta_4} - \frac{9{\beta_2}^4}{4{\beta_4}^2}\right)}{(\gamma P_p)^2} \quad (3.2.24)$$

From the equation above it can be observed that if $\beta_2 = -\sqrt{2\gamma P_p \beta_4/3}$, the gain ripple will be zero in this region which is the same result as the one mentioned by Florida *et al.* in [85]. However in practice up to now observing such an ideal spectrum hasn't been possible. Therefore in the next chapter another method for obtaining a flat gain spectrum in a single pump FOPA is investigated.

3.3 Gain Spectrum of a Single Pump FOPA

The gain spectrum of a FOPA can be tailored by changing different fiber properties. In order to have a better understanding of the parametric amplifier, in this section the gain characteristics of FOPAs as a function of fiber length (L), second order dispersion (β_2), fourth order dispersion (β_4), pump power (P_p) and nonlinear coefficient (γ) are studied. The simulations are performed by using Eq. (3.2.16), assuming that the pump is much more intense than the signal and that all waves are continuous waves. The FOPA parameters used in the simulations are given in Table 3.1 which are based on the parameters in Ref. [86] . The obtained gain spectra are plotted by tuning the signal wavelength in steps of 2 nm.

Table 3.1 FOPA parameters used in the simulations

L [m]	γ $[km^{-1}W^{-1}]$	β_2 [$\mathrm{ps^2km^{-1}}$]	β_4 [$\mathrm{ps^4km^{-1}}$]	P_p $[W]$	λ_p $[nm]$	$P_s(0)$ $[dBm]$
100	$20\ km^{-1}W^{-1}$	0	-2.85×10^{-4}	1	1550	-30

The gain spectra of a FOPA with different fiber lengths are shown in Fig. 3.3. As expected from Eq. (3.2.16), it can be seen that an increase in the fiber length will increase the signal gain, while the wavelength of the peak gain remains unchanged.

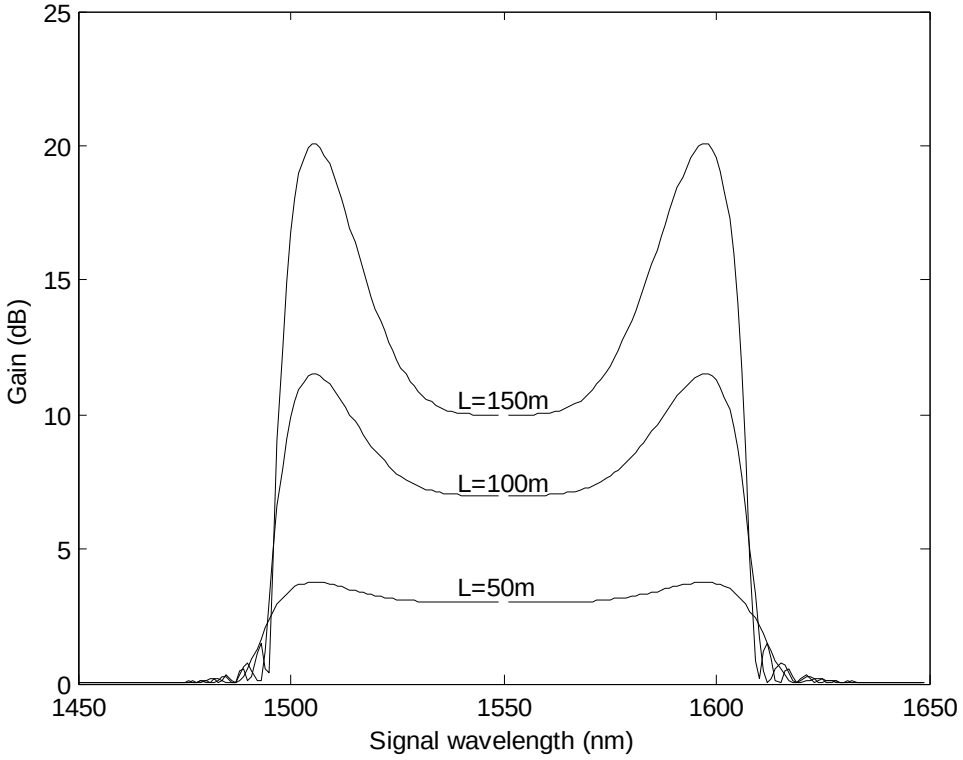

Fig. 3.3 Small signal gain spectra of a FOPA with different fiber lengths.

The effect of β_2 on the gain spectrum is shown in Fig. 3.4. A positive β_2 will have a gain peak in the center of the gain spectrum [87], while a negative one will have a dip. A fiber with $\beta_2 = 0$ has a broader gain spectrum than others.

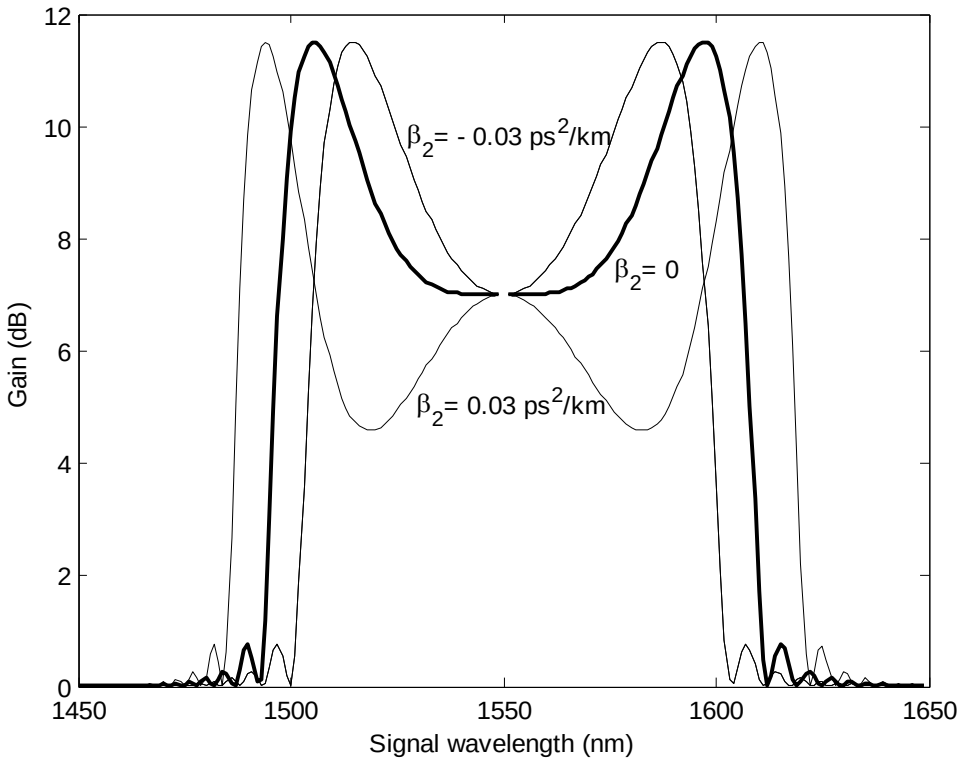

Fig. 3.4 Small signal gain spectra of a FOPA with different second order dispersions.

In Fig. 3.5 the gain spectra of the FOPA are demonstrated for different β_4 values. As shown, a positive and negative β_4 will cause a bell-like and a dual-hump curve, respectively [88]. The smaller the absolute value of β_4 is, the broader the gain bandwidth will become.

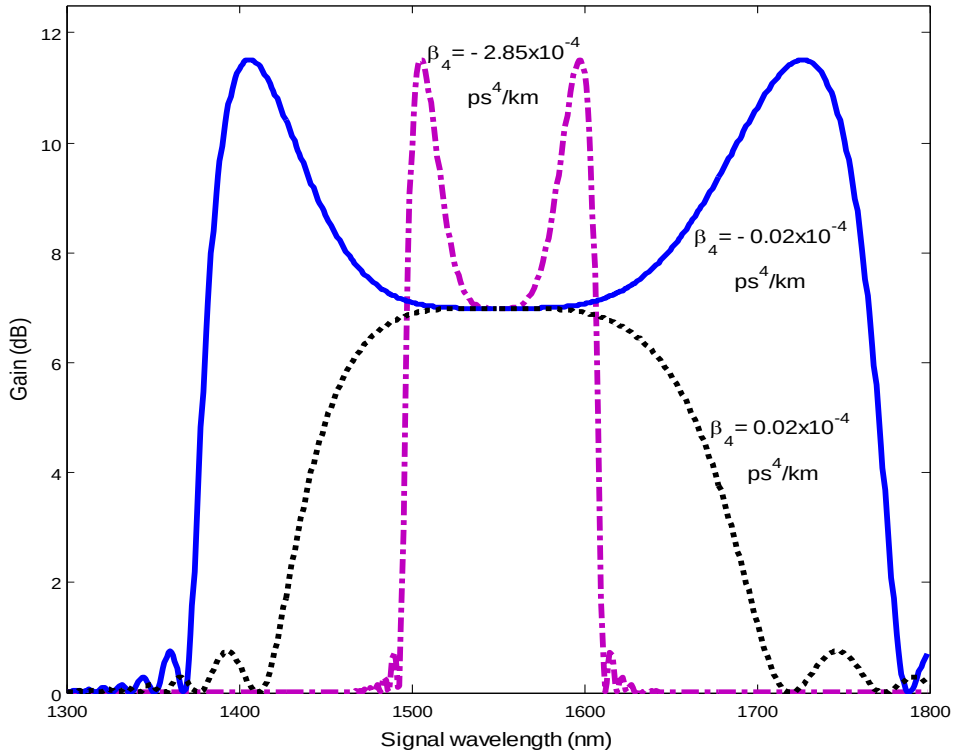

Fig. 3.5 Small signal gain spectra of a FOPA with different fourth order dispersions.

Other parameters which affect the gain spectrum are the nonlinear coefficient of the fiber and the pump power. Figures 3.6 and 3.7 show the effect of these two parameters in the gain spectrum, respectively. The gain grows by increasing γ or pump power. The wavelength of the peak gain will shift away from the pump wavelength with the increase of pump power.

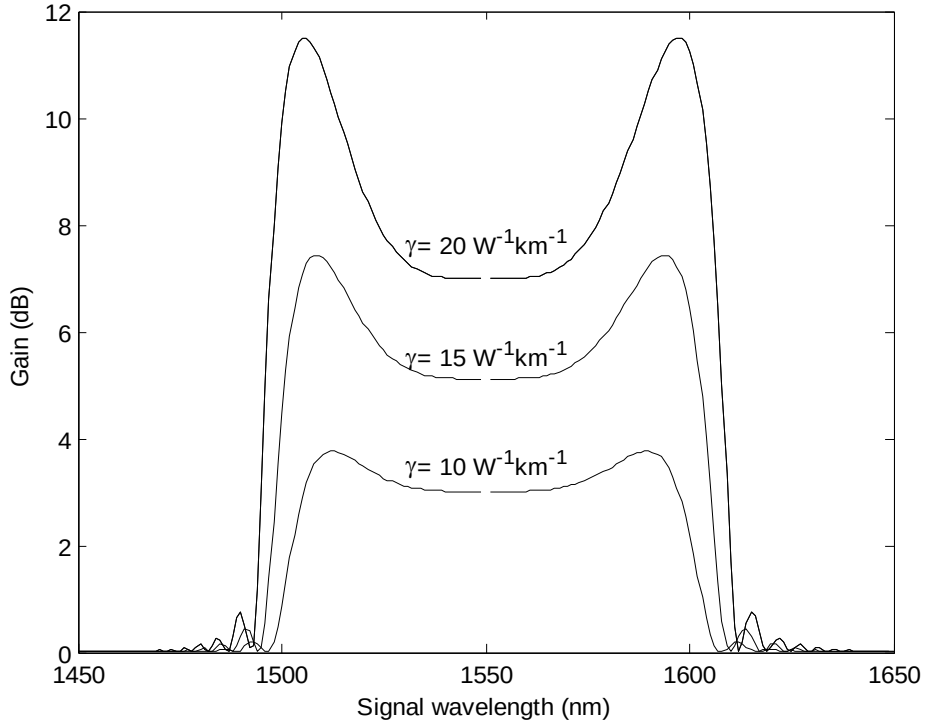

Fig. 3.6 Small signal gain spectra of a FOPA with different nonlinear coefficients.

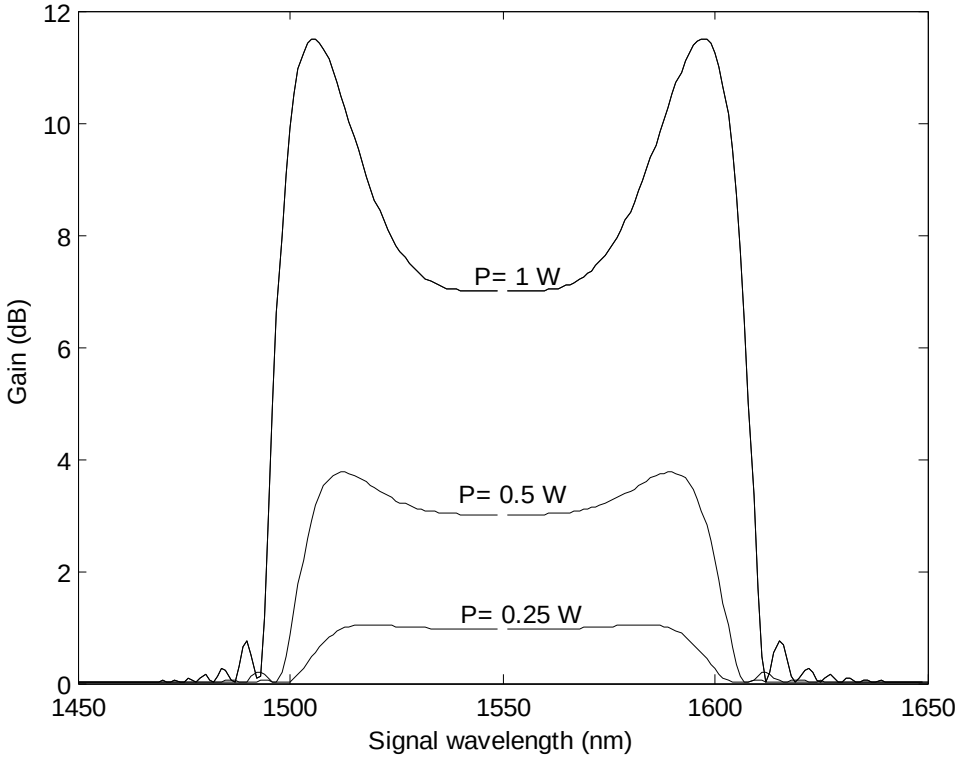

Fig. 3.7 Small signal gain spectra of a FOPA with different pump powers.

3.4 Summary

In this chapter basic concepts of optical amplifiers followed by a brief overview of current optical amplifiers are provided. The theory behind parametric amplification and the characteristics of FOPAs are mentioned. Based on the second and fourth order dispersion of the highly nonlinear fiber, the gain spectrum of an FOPA can have different shapes and consequently different numbers of extrema points which are explained in this chapter. In the end the dependence of the FOPA performance on different fiber parameters, such as length, dispersion parameters and also pump power are presented.

Chapter 4

Optimization and Characteristics of Single Pump Fiber Optical Parametric Amplifiers

4.1 Single Pump FOPA Gain Flattening

One of the necessities for an optical amplifier to be practically used in a DWDM system is to have a flat gain spectrum over a wide range of wavelengths [85]. However, in a single pump FOPA the gain spectrum is far from uniform over the entire bandwidth due to the phase matching condition of the underlying FWM process. For signal wavelengths close to the pump wavelength we have:

$$\Omega = \omega_p - \omega_s \to 0 \qquad \Longrightarrow \qquad \Delta\beta = \beta_2\Omega^2 + \frac{1}{12}\beta_4\Omega^4 \to 0$$

Therefore in the pump vicinity

$$k = \frac{\Delta\beta}{2} + \gamma P_p \approx \gamma P_p$$

Since the phase mismatch value is quite large the gain spectrum exhibits a dip near the pump wavelength. One of the proposed ways for overcoming this problem is to cascade a number of highly nonlinear fiber (HNLF) sections with different parameters [86]. A broad non-uniform gain spectrum is generated by the first piece of HNLF; then by properly tuning the parameters of the following HNLF sections they will gradually flatten the gain curve of the first HNLF segment. The challenge of this method lies in how to

determine the parameters of the fiber segments. Zhang *et al.* have proven that a genetic algorithm (GA) can be successful in finding each segment's parameters in order to obtain a flat gain spectrum [89]. In their design, they considered the second order dispersion at the pump wavelength ($\beta_2(\omega_p)$) and length (L) of each fiber section in the optimization scheme while the fourth order dispersion (β_4) was assumed to be constant throughout the different fiber segments. However, according to the expression of linear propagation constant mismatch, $\left(\Delta\beta = \beta_2\Omega^2 + \frac{1}{12}\beta_4\Omega^4\right)$, β_4 also plays a great role in the performance of the FOPA. This can also be seen in Figures 3.2 and 3.5. Therefore it is reasonable to consider a different β_4 for each fiber section. Hence, in this work to understand the effect of β_4 in flattening the gain spectrum, besides β_2 and L, β_4 is also included in the optimization scheme.

In the recent years, researchers have designed index profiles of HNLFs with optimized higher order dispersion, and have actually fabricated them as well [65, 90-93]. The refractive index profile of these fabricated HNLFs is W-shaped type, which has a highly GeO_2 doped core surrounded by a fluorine doped cladding area called the depressed cladding which has a lower refractive index than that of the outer cladding area as seen in Fig. 4.1. Although the W-shape profile is relatively complex, however it is employed due to its flexibilities in designing chromatic dispersion characteristics of the fiber [94]. By precisely adjusting the relative refractive index difference of the outer cladding and the core (Δn^+) and that of the depressed cladding (Δn^-), the chromatic dispersion of the HNLF can be tailored. These efforts in fabricating HNLF demonstrate that by controlling the value of the dispersion slope (a parameter which can be measured with good accuracy), the value of β_4 can be adjusted [95]. β_4 is expected to approach zero when the dispersion slope approaches $0.025\, ps/(nm^2 km)$. HNLFs with higher or lower slopes have a negative or positive β_4 respectively. By this method, HNLFs with small

$(0.2 \times 10^{-4}\ \mathrm{ps^4km^{-1}})$ [90] ,moderate $(1 \times 10^{-4}\ \mathrm{ps^4km^{-1}})$ [65] and also large β_4 values $(\pm 2 \times 10^{-4}\ \mathrm{ps^4km^{-1}})$ [91, 92] have been reported. Thus, fabricating a HNLF with a β_4 close to our desired value isn't an out of reach issue.

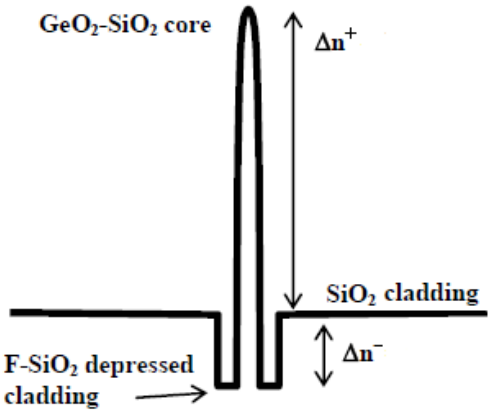

Fig 4.1 Refractive index profile of fabricated HNLFs **[93]**

4.1.1 Multi-Section FOPA

The schematic configuration of a single pump FOPA with multiple section HNLFs is shown in Fig. 4.2. Based on the theory of multi-section FOPA given in [86], for a FOPA composed of N highly nonlinear fiber sections, the amplitude of the signal and idler at the output of the N-th fiber section are given by

$$Y_N(z_N, \Omega) = [u_s(z, \Omega), u_i^*(z, \Omega)]^T = \prod_{k=1}^{N} \psi(z_k) \times Y(0, \Omega) \tag{4.1.1}$$

where u_s and u_i are the signal and idler amplitudes, respectively. The frequency detuning between the signal and pump is $\Omega = \omega_p - \omega_s$ and z is the propagation distance. The transfer matrix, $\psi(z)$, for a single pump FOPA is:

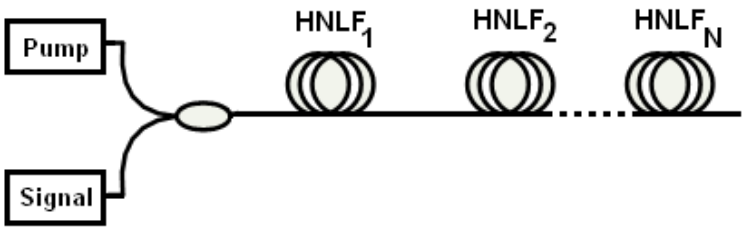

Fig 4.2 Schematic configuration of one pump FOPA with *N*-section HNLFs

$$\psi(z) = \frac{1}{1-\xi^2}\begin{bmatrix} e^{gz} - \xi^2 e^{-gz} & -\xi(e^{gz} - e^{-gz}) \\ \xi(e^{gz} - e^{-gz}) & -\xi^2 e^{gz} + e^{-gz} \end{bmatrix} \tag{4.1.2}$$

where $\xi = -(k + ig)/\gamma P_p$,while k and g can be found by Eqs. (3.2.7) and (3.2.14), respectively. The transfer matrix can also be written in the form of

$$\psi(z) = \begin{bmatrix} \cosh(gz) + \frac{ik}{g}\sinh(gz) & \frac{i\gamma P_p}{g}\sinh(gz) \\ -\frac{i\gamma P_p}{g}\sinh(gz) & \cosh(gz) - \frac{ik}{g}\sinh(gz) \end{bmatrix} \tag{4.1.3}$$

which is equivalent to Eqs. (3.3.8) and (3.3.9). The parameters are the same as the ones defined in chapter 3. The small signal power gain at the output of the *k*-th fiber section, is calculated using:

$$G_k = 10\log[|u_s^k(L_n, \Omega)|^2] \tag{4.1.4}$$

The gain spectrum of the first fiber section determines the approximate required bandwidth and gain, so its parameters are chosen in advance based on the system requirements. In order to expand the available bandwidth, β_2 of the first section is normally chosen close to zero. For *N* fiber sections, there will be $3(N-1)$ parameters to optimize simultaneously; the length, second order and fourth order dispersion at the pump wavelength for the ith fiber section ($i = 2 - N$).

It should be noted that there is a tradeoff between gain and flat bandwidth in FOPAs. They either have a high gain spanning over a small bandwidth or low gain over a large bandwidth. Thus achieving a flat gain over a large bandwidth in FOPAs is difficult [19].

In the next section the operating process of the GA for optimizing multiple parameters will be discussed in detail. Finding the optimum values using a GA has been carried out in MATLAB environment.

4.1.2 Genetic Algorithm Optimization Process

A genetic algorithm (GA) [96] is a multivariate stochastic optimization scheme which mimics the process of natural evolution. The GA operates on a population of potential solutions, where the fittest solution is more likely to survive in the selection process in order to produce better approximations to a solution.

Since the optimization scheme used in this research is the GA, a brief explanation of its different steps is provided [97].

1. Coding

Each possible solution of a problem solved by GA, is an "individual" which is described by "chromosomes". First, reasonable upper and lower bounds are set for each of the variables, and based on this range the length of each chromosome is defined. In the optimization for FOPA, each individual (pop_i) is made of $3(N-1)$ chromosomes; $\{L_2, L_3, \dots L_N, \beta_{2,1}, \beta_{2,2}, \dots, \beta_{2,N}, \beta_{4,1}, \dots, \beta_{4,N}\}$ where L_i , $\beta_{2,i}$ and $\beta_{4,i}$ represent the length, second order and fourth order dispersion of the ith HNLF segment, respectively ($i = 2$ to N).

2. Initialization

At the first generation, an initial population of the individuals is randomly generated. The population size is an important matter to determine. Choosing a larger population on one hand increases the probability of obtaining the best solution, whilst on the other hand a longer time will be consumed to find the optimum solution. After several trials the size of the population was chosen to be 100.

3. Evaluating Fitness

A fitness function is an objective function which prescribes the optimality of an individual in a GA. Each individual is ranked by the fitness function and the most optimal individuals are allowed to mix their data for creating a new generation. In the optimization process of FOPAs, the fitness function is related to the degree of satisfaction with the amplifier performance. Since uniformity of the FOPA gain spectrum is the objective, the fitness function ($f_i = \text{fitness}(pop_i)$) is defined as obtaining the widest bandwidth with maximum 0.3 dB gain ripple.

4. Selection

A series of operations are performed on the initial population, in order to create the next generation. The selection of appropriate individuals plays an important role in GA for producing successive generations. A probabilistic selection based on the individual's fitness is carried out such that the larger the fitness value (f_i) of an individual is, the more chance it has for being selected for reproduction. Hence, the fittest individuals of any population are more likely to reproduce and survive into the next generation. The selection method used in this work is the roulette wheel. In roulette wheel selection, individuals are given a probability of being selected that is directly

proportionate to their fitness. The probability for an individual to be selected is:

$$p_i = \frac{f_i}{\sum_{j=1}^{popsize} f_i} \tag{4.1.5}$$

Two individuals are then chosen randomly based on these probabilities to produce offspring.

5. Crossover and Mutation

Genetic operators are required to create new solutions based on the existing individuals in the population. These operators are known as crossover and mutation, which are implemented at each generation.

The selected chromosomes (parent chromosomes) are sorted in pairs, and crossover is implemented on each pair to generate offspring. The idea behind crossover is that the newly generated offspring might be better than both of the parents if it takes the best characteristics from each of the parents. In single point crossover, a locus is chosen at which from that point on, the genes of the two parent chromosomes are swapped to produce two offspring. The single point crossover is shown in Fig. 4.3. As seen, the children take one section of the chromosome from each parent. The point at which the crossover occurs is randomly selected.

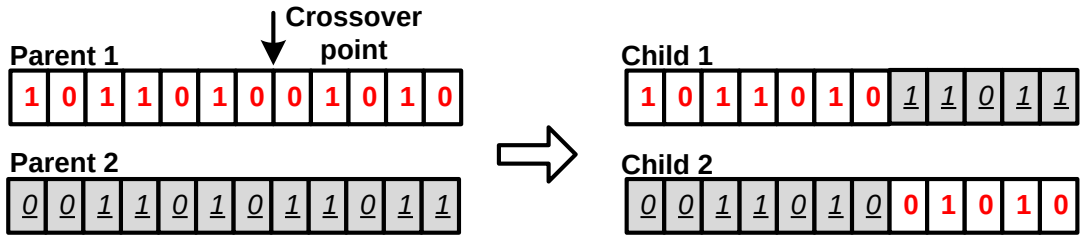

Fig. 4.3 Basic structure of single point crossover

Sometimes crossover doesn't occur and the parents survive to the next generation. The probability of crossover occurrence is usually 65% to 85%. The crossover rate in this work is considered 70%.

If only the crossover operator is used for producing offspring, one potential problem which may arise is that if all the chromosomes in the initial population have the same value at a particular gene, then all future offspring will inherit the same value at that gene as well. Therefore, a mutation operator is required to overcome this situation. Mutation operator alters the value of one or more genes in a chromosome from its initial state. In the case of bit representation, if a gene is one it will be changed to zero and vice versa. Mutation occurs during evolution according to a user-defined mutation probability known as the mutation rate. Each gene in each chromosome will be checked for possible mutation by generating a random number between zero and one, if this number is less than or equal to the mutation rate then the gene value will be changed. Hence, the mutation rate should be set fairly low so that the search doesn't turn into a random one. The mutation rate is set to 8% in the FOPA optimization program.

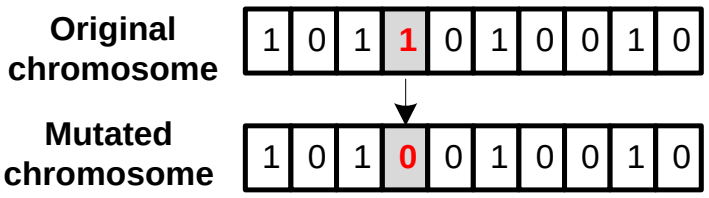

Fig. 4.4 Mutation operator in GA

6. Termination Criteria

New chromosomes are created in each generation until the termination condition is satisfied. The most frequently used final point is a specified number of generations. By properly setting the upper and lower bounds for

each of the variables it was found that 50 generations are sufficient to obtain the optimum solution.

The different steps of a genetic algorithm are summarized in the following flowchart.

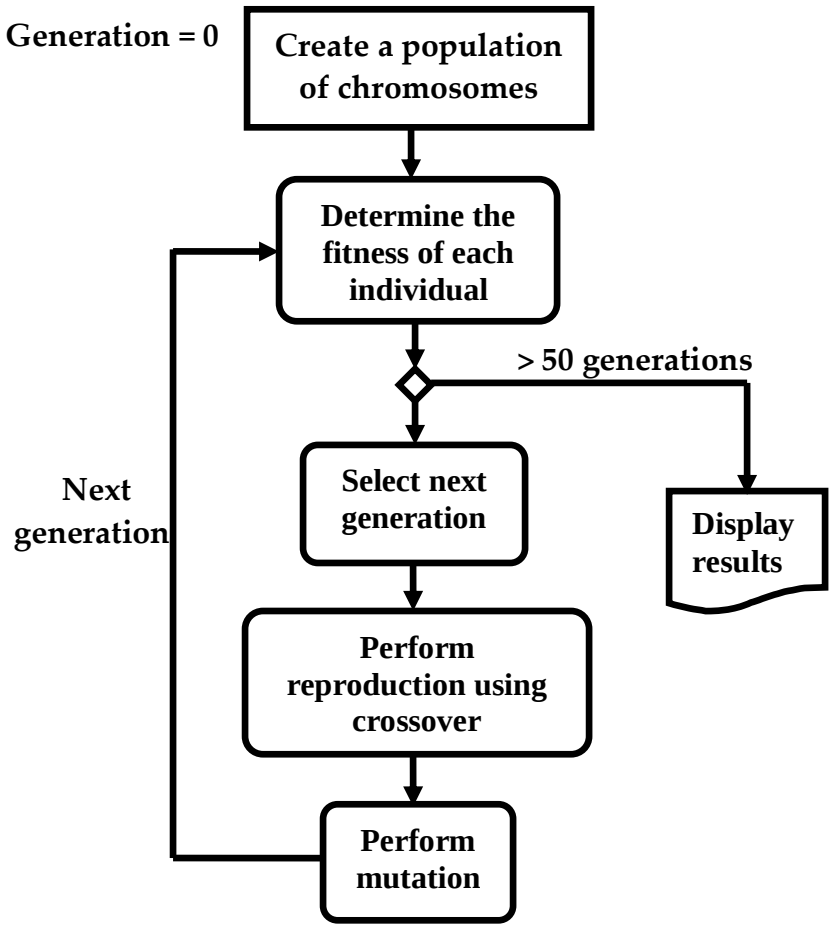

Fig. 4.5 Flowchart of genetic algorithm

4.1.3 Results and Discussion

In practice it is difficult to set β_2 precisely equal to zero, so in our analysis the second order dispersion of the first segment is set to $10^{-3}\ ps^2 km^{-1}$. The fourth order dispersion and length of this segment are $\beta_4 = -2.85 \times 10^{-4} \mathrm{ps}^4\mathrm{km}^{-1}$ and $L = 100\ m$, respectively. By considering the splicing loss, the pump power at the input of the kth fiber section is $P_k = P_p \alpha^{(k-1)}$ with $\alpha = 0.87$, where P_p is the input pump power.

After trials it was found that at least three fiber sections (N=3) are needed to generate a flat gain spectrum for a bandwidth close to 100 nm. For finding the optimum parameters of the next segments the following three cases are considered:

Case I

In this case three parameters - length, β_2 and β_4 - of the second and third sections are optimized using GA. The optimum parameters are given in Table 4.1. The nonlinear coefficient is considered $\gamma = 20\ km^{-1}W^{-1}$ for all segments.

Table 4.1

Section	1	2	3
Length (m)	100	36	62
β_2 ($\times 10^{-2}$ ps^{2}km^{-1})	0.1	6.48	-8.25
β_4 ($\times 10^{-4}$ ps^{4}km^{-1})	-2.85	0.53	0.15

$P_p = 1\ W, \lambda_p = 1550\ nm$

These parameters lead to a FOPA with a maximum parametric gain of 11.09 dB with 0.15 dB peak to peak gain ripple over 95 nm flat bandwidth covering

the wavelength range 1504 to 1599 nm. Fig. 4.6 illustrates the signal gain at the output of each fiber section.

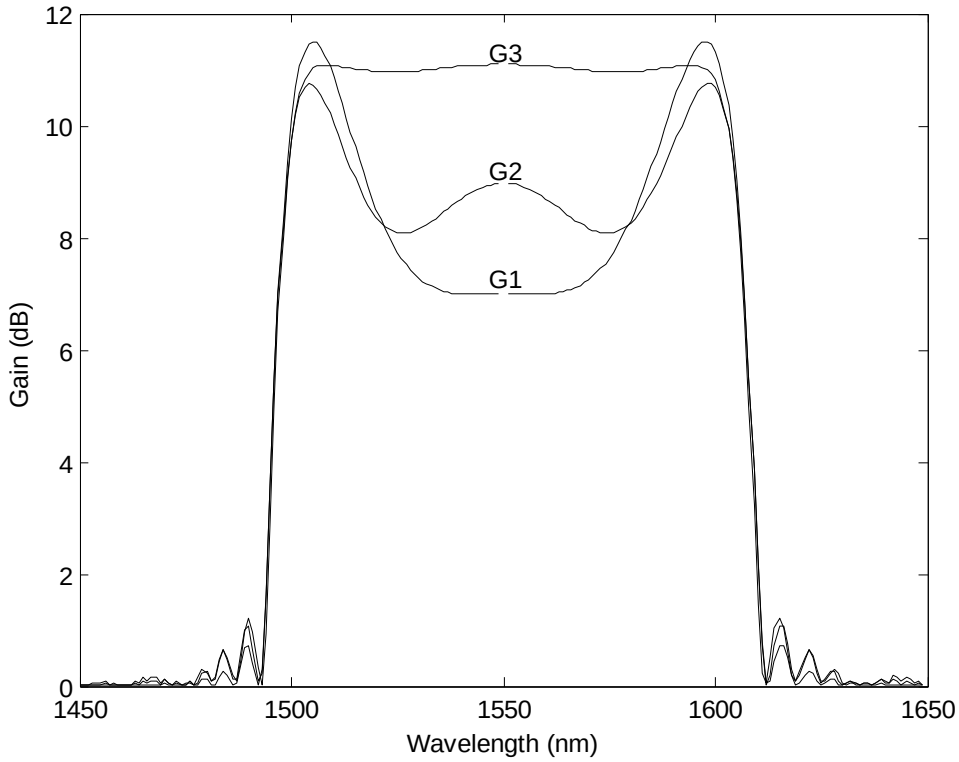

Fig. 4.6 Gain spectra of single pump FOPA with three optimized parameters . G*i* (*i*=1,2,3) represents the signal gain at the output of the *i*th fiber section.

The first segment has a broad gain bandwidth which exhibits a big dip in the center. To flatten the gain spectrum, the gain at the center of the spectrum near the pump wavelength should be increased by the second fiber section. To do so, the second fiber should be chosen such that it has a bell-like gain curve which can be obtained by a fiber with a positive β_2 and β_4. The gain of the third fiber section covers the whole bandwidth, in such a way that the overall gain becomes a square-shaped spectrum.

At some wavelengths the energy might be transferred from the signal to the pump because of the phase matching conditions. This is shown in Fig. 4.7, where the differential gain between two consecutive sections is

demonstrated. It can be seen that at some wavelengths the differential gain is negative which means the signal is absorbed by the pump at that certain wavelength. This might occur in any of the segments except the first segment because the idler isn't present at the input of the first segment therefore phase sensitive amplification isn't provided in this segment.

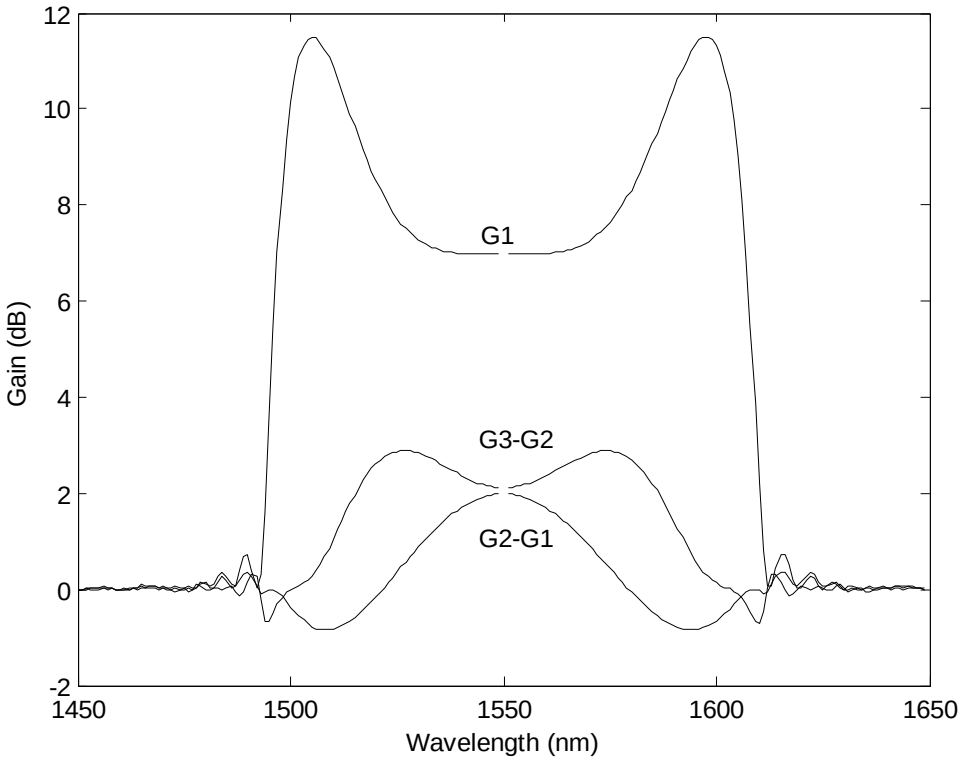

Fig. 4.7 Differential gain between two consecutive sections.

To see the tolerance of the optimal dispersion parameters found by the genetic algorithm, the second order and fourth order parameters of the fiber segments are modeled as:

$$\beta_2 = \beta_{2c} + \delta\beta_{2r} \tag{4.1.5}$$

$$\beta_4 = \beta_{4c} + \delta\beta_{4r} \tag{4.1.6}$$

where the first terms are the optimal dispersion parameters found by the genetic algorithm and the second terms are the deviation from these optimal amounts. As can be seen in Fig. 4.8 for $\delta\beta_{2r} = \pm 0.12$ ($\times 10^{-2} \frac{ps^2}{km}$) and $\delta\beta_{4r} =$

$\pm 0.5\ (\times 10^{-5}\frac{ps^2}{km})$, a peak-to-peak gain ripple of less than 0.5 dB can be achieved.

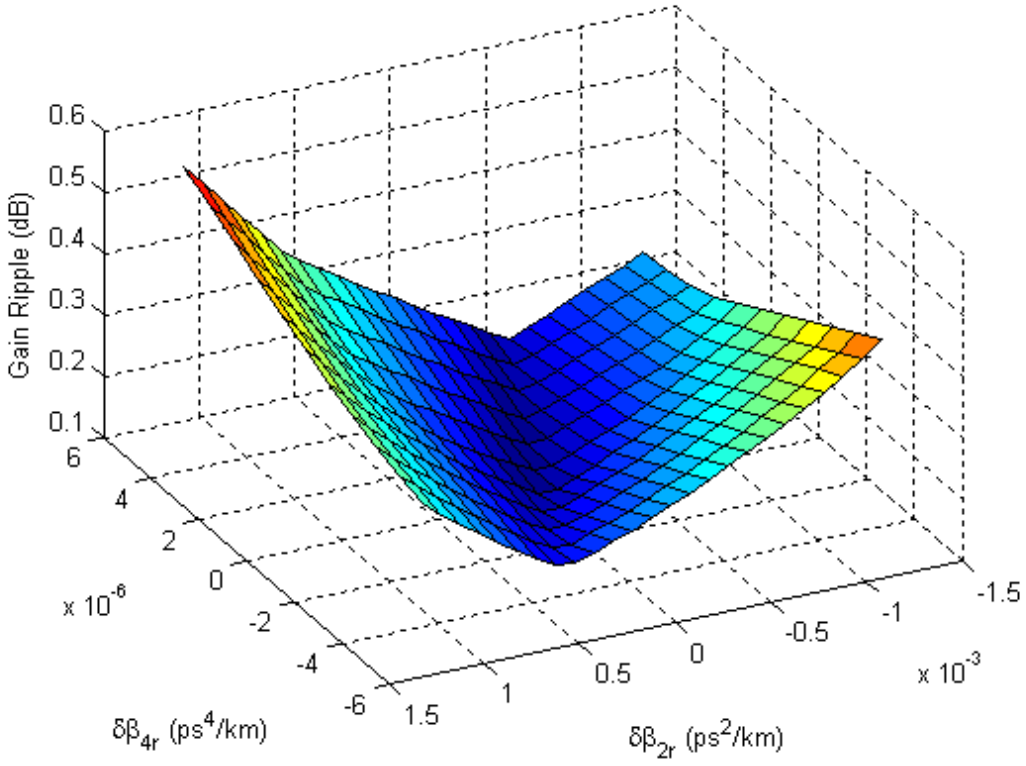

Fig. 4.8 FOPA gain ripple versus the deviations in the fiber dispersion parameters.

Case II

In the second case only two fiber properties, L and β_2 , are optimized and β_4 is -2.85×10^{-4} ps^{4}km^{-1} in all segments. By keeping all the other conditions the same as case I, as seen in Fig. 4.9 the flatness of the gain spectrum will vary considerably compared to the preceding case. The optimized parameters found by GA for this FOPA are given in Table 4.2.

Table 4.2

Section	1	2	3
Length (m)	100	41	59
β_2 (×10^{-2} ps^{2}km^{-1})	0.1	6.8	-9.73

$P_p = 1\ W, \lambda_p = 1550\ nm, \beta_4 = -2.85 \times 10^{-4}$ ps^{4}km^{-1}

The flat bandwidth is 46 nm with 0.29 dB peak to peak gain ripple. This means that the flat bandwidth and gain ripple are half and twice the bandwidth and gain ripple of the previous case, respectively.

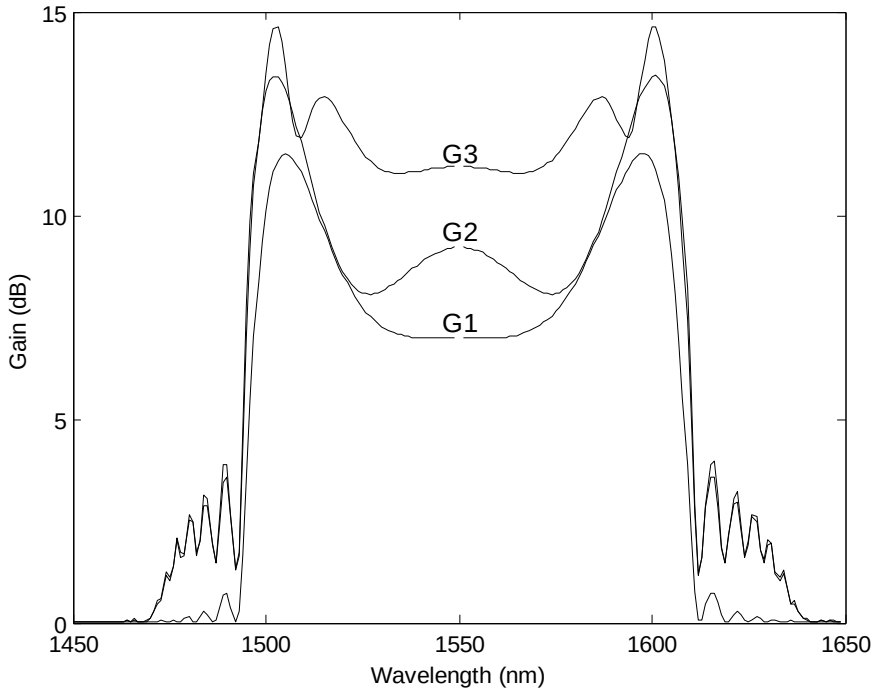

Fig. 4.9 Gain spectra of single pump FOPA with two optimized parameters . $\boldsymbol{G_i}$ $(\boldsymbol{i = 1, 2, 3})$ represents the signal gain at the output of the *i*th fiber section.

By applying the same program of genetic algorithm to other FOPAs with different configurations, the same results are obtained. For example, the parameters of another FOPA are given in the following tables and the resulting gain spectra are illustrated in Fig. 4.10.

Table 4.3

Section	1	2	3
Length (m)	150	37	95
β_2 ($\times 10^{-2}$ ps^{2}km^{-1})	0.1	5.42	-4.47
β_4 ($\times 10^{-4}$ ps^{4}km^{-1})	-1.5	0.01	0.31

$P_p = 1\ W, \lambda_p = 1550\ nm, \gamma = 20\ km^{-1}W^{-1}$

Table 4.4

Section	1	2	3
Length (m)	150	49	109
β_2 ($\times 10^{-2}$ ps^{2}km^{-1})	0.1	5.79	-5.94

$P_p = 1\ W, \lambda_p = 1550\ nm, \beta_4$ = -1.5×10^{-4} ps^{4}km^{-1}, $\gamma = 20\ km^{-1}W^{-1}$

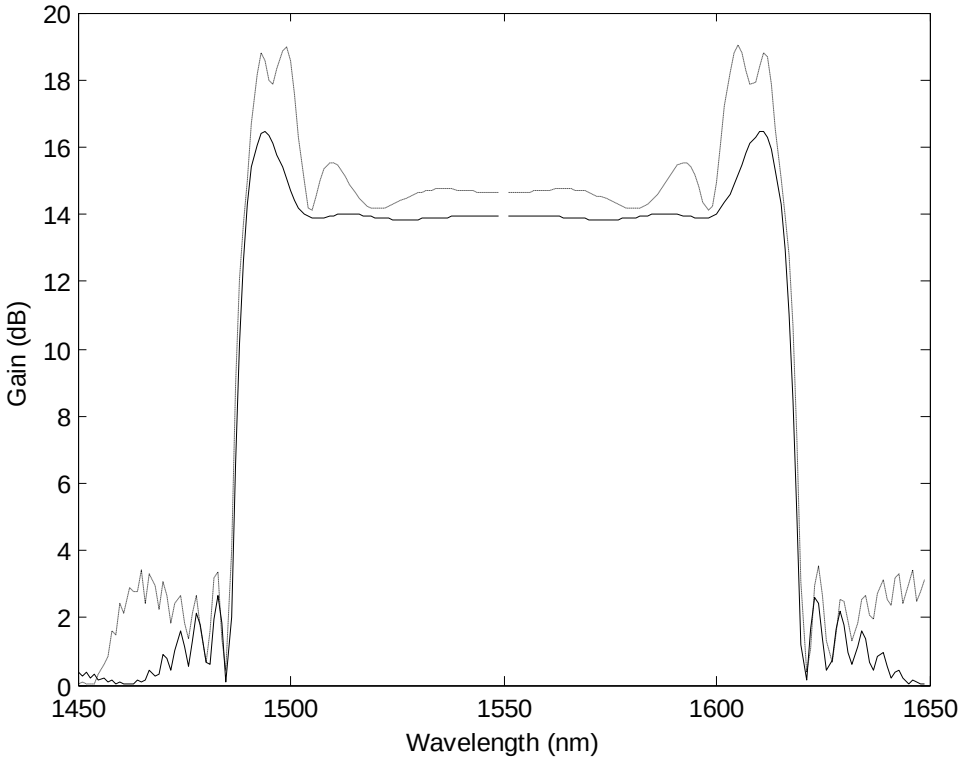

Fig. 4.10 Gain spectra of an FOPA with (solid curve) and without (dotted curve) its fourth order dispersion optimized.

Therefore, by controlling β_4 of each fiber segment, the flatness of the gain spectrum of a single pump FOPA can significantly be increased.

Case III

In this case it is assumed that β_4 of the second and third fiber sections are the same, whereas they are different from β_4 of the first section. Hence, β_2 and length of the second and third fiber segments along with only one β_4 for these two segments are optimized. The parameters of the first fiber section

are considered the same as that of the FOPA mentioned in Fig. 4.6. The rest of the FOPA's parameters can be seen in Table 4.5.

Table 4.5

Section	1	2	3
Length (m)	100	37	61
β_2 ($\times 10^{-2}$ ps^{2}km^{-1})	0.1	6.26	-8.17
β_4 ($\times 10^{-4}$ ps^{4}km^{-1})	-2.85	-0.03	-0.03

$P_p = 1\ W, \lambda_p = 1550\ nm$

In Fig. 4.11 it is shown that the gain spectrum will be flatter if each section has a different β_4 (case I) rather than the second and third fiber section having the same β_4 (case III). As mentioned before, the gain ripple in case I is 0.15 dB pick to pick over 95 nm bandwidth , while in case III the ripple is 0.17 dB over a 55 nm bandwidth. Therefore, by comparing the gain ripple and bandwidth of case I and case III, it is seen that the gain ripple doesn't change much while the flat bandwidth increases considerably in the first case.

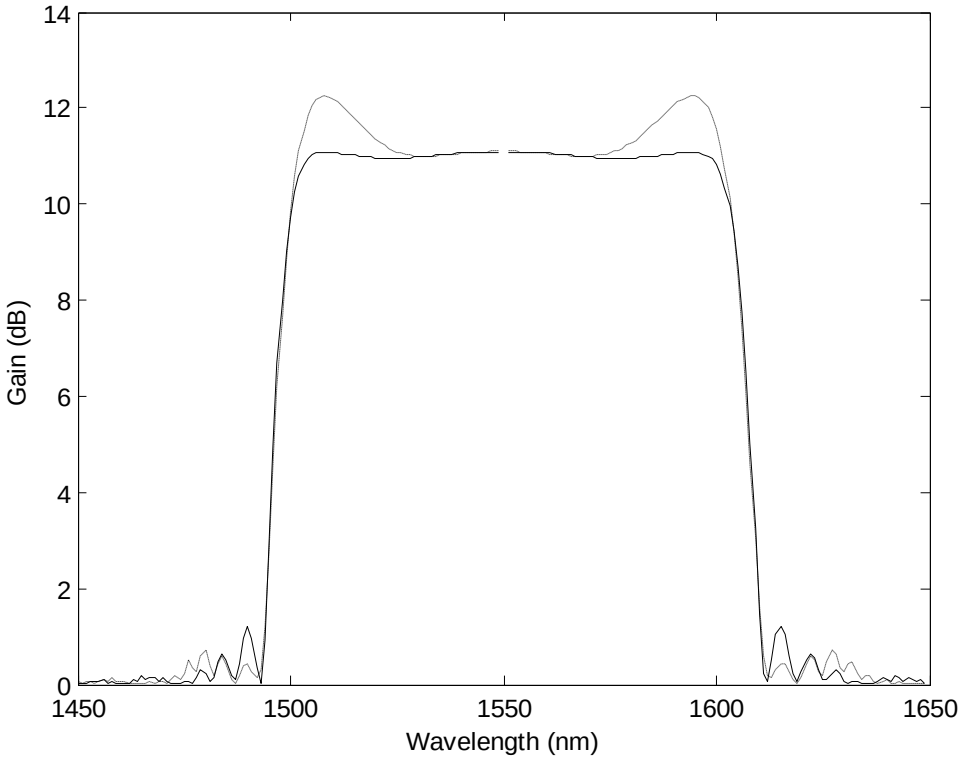

Fig. 4.11 Difference between the gain spectrums of case I (solid curve) and case III (dotted curve).

By comparing the gain spectrums of the first and second abovementioned cases, it can be seen that by controlling β_4 of the fiber segments, the flat gain bandwidth of the amplifier becomes much broader, while its ripple is decreased. The gain ripple in the third case doesn't change much compared to the first one, but its flat bandwidth becomes narrower. So overall if β_4 of each fiber section is optimized, a flat gain spectrum with a broader bandwidth can be achieved.

4.2 Phase Mismatch

Some factors such as fourth order dispersion, fiber losses and ZDW fluctuations cause a phase mismatch [98]. When the pump wavelength is

chosen close to the ZDW, the influence of the second order dispersion on the gain characteristics of the FOPA becomes less significant while the effect of the fourth order dispersion increases and can't be neglected. In the previous section the phase mismatch caused by β_4 was taken into account. The effect of fiber losses and ZDW fluctuations on the gain spectrum of a single pump FOPA with optimized β_4 will be discussed in the next two sections.

4.2.1 Fiber Losses

While considering the loss, the term $-{}^{\alpha}/_{2}\, A_j$, $(j = p, s, i)$ should be added to the right hand side of Eqs. (2.2.16)-(2.2.18), where α is the attenuation constant. In this case (3.3.1) changes to

$$A_p(z) = \sqrt{P_p(z)}\exp[i\gamma P_p(z)z] \tag{4.2.1}$$

where

$$P_p(z) = |A_p(0)|^2 \exp(-\alpha z) = P_{p0}\exp(-\alpha z) \tag{4.2.2}$$

The phase mismatch and gain coefficient will depend on the propagation distant and change to:

$$k(z) = \Delta\beta/2 + \gamma P_p(z) \tag{4.2.3}$$

$$g(z) = \sqrt{[\gamma P_p(z)]^2 - [k(z)]^2} \tag{4.2.4}$$

The gain will be:

$$G_s = \frac{P_s(z)}{P_s(0)} = 1 + [\frac{\gamma P_p(z)}{g(z)}\sinh(g(z)z)]^2 \tag{4.2.5}$$

Fiber losses will reduce the pump power which will lead to a fall in the parametric gain. The bandwidth of a FOPA depends on the pump power[83], thus its bandwidth will become narrower due to fiber losses. In Fig. 4.12 it is shown that as a result of fiber losses the signal wavelength with peak gain will shift towards the pump wavelength. For signal wavelengths close to the pump wavelength $\Delta\beta \to 0$; thus in the pump vicinity $k(z) \approx \gamma P_p(z)$. As a result by the reduction of pump power, $k(z)$ decreases and the dip in the gain spectrum becomes smaller.

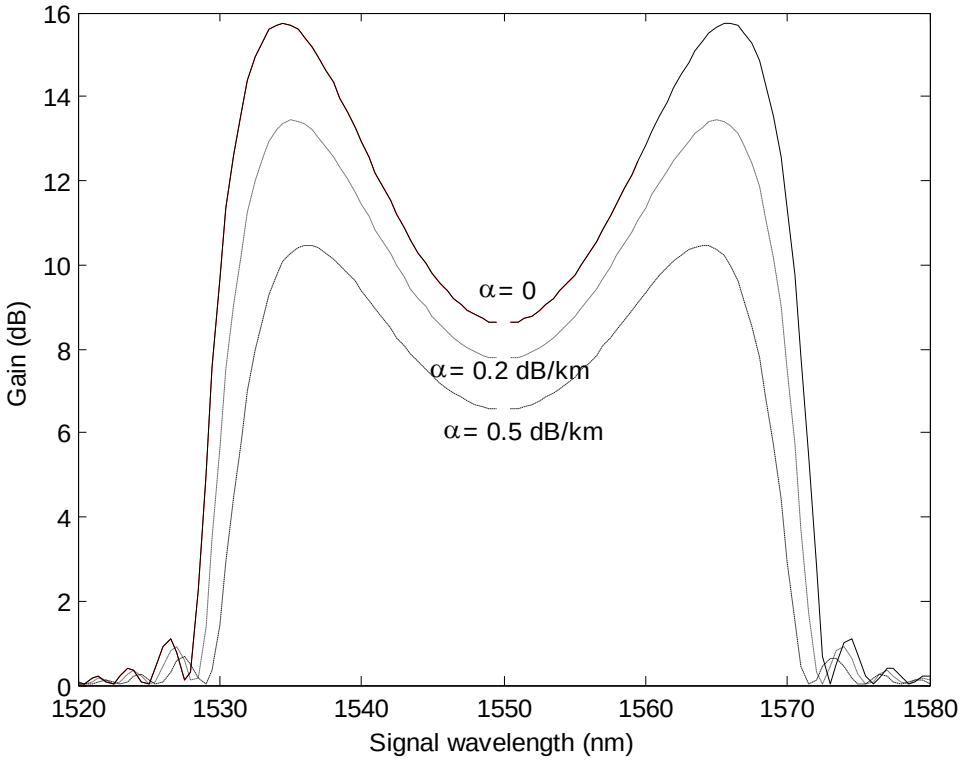

Fig. 4.12 Gain spectra of single pump FOPA with fiber losses of 0, 0.2 and 0.5 dB/km. The other parameters are $\boldsymbol{\lambda_p = 1550\ nm}$, $\boldsymbol{P_p = 0.1\ W}$, $\boldsymbol{L = 2.5\ km}$, $\boldsymbol{\gamma = 10\ km^{-1}W^{-1}}$, $\boldsymbol{\beta_2 = -0.01\ ps^2/km}$, $\boldsymbol{\beta_4 = -2.5 \times 10^{-4}\ ps^4/km}$.

In the design of a multi-section FOPA, short fibers (usually shorter than 200 m) are used. Thus the propagation losses of these short fibers don't have a significant effect on the gain spectrum, and can be neglected. However, the

splicing losses between two consecutive HNLFs were considered in section 4.1.3.

4.2.2 Effects of ZDW Fluctuations

The manufacturing process of fiber is such that the core diameter of any fiber exhibits random variations. These variations will cause changes in the zero dispersion wavelength (ZDW) of the fiber as a function of the fiber length. Fluctuations in the ZDW will cause changes in the linear phase mismatch $\Delta\beta$, which will eventually make the signal gain spectrum become non-uniform. Mechanical perturbations on fibers such as twists and also temperature variations can cause ZDW fluctuations as well. In Fig. 4.13 different ZDW distributions over the fiber length and their corresponding gain spectra are illustrated.

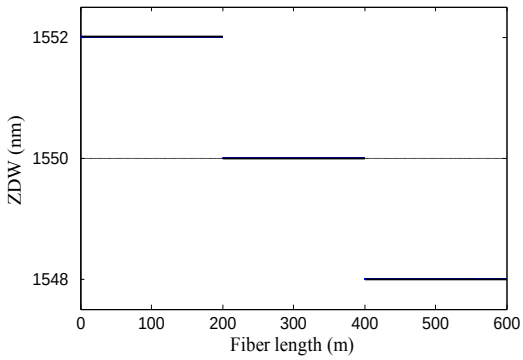

(a)

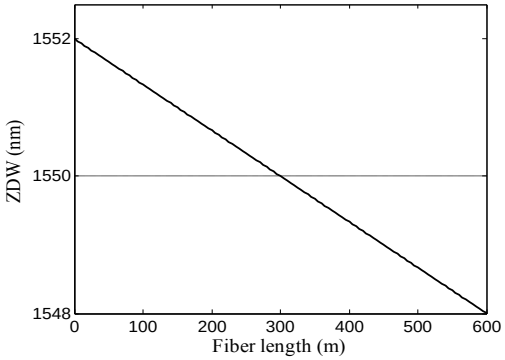

(b)

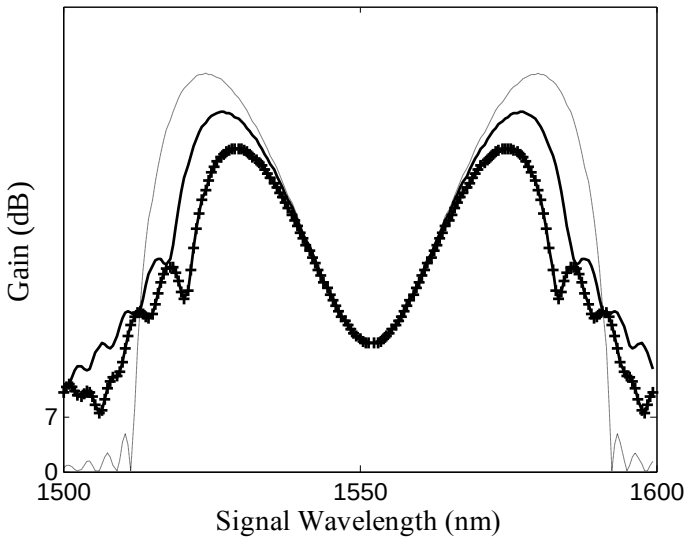

(c)

Fig. 4.13 (a) and (b) are different ZDW distributions, (c) is the corresponding gain spectrum to distributions shown in (a) (curve with + markers) and (b)(solid line). The dashed spectrum is related to a constant ZDW of 1550 nm.

Zero dispersion wavelength variations along the fiber length will change the gain spectrum of a FOPA from the ideal spectrum which is calculated for a perfectly uniform fiber. A common way for investigating the effect of these variations on the gain spectrum is to divide the fiber into a large number of small segments of length l_c and consider the ZDW to be constant in each segment. Therefore the ZDW of each segment is modeled as a summation of a constant part, $\lambda_{0,mean}$, along with a randomly varying part [99-101], i.e.,

$$\lambda_0(z) = \lambda_{0,mean} + \lambda_{0,random}(z) \tag{4.2.6}$$

The randomly varying part which is due to the ZDW fluctuations is a Gaussian process with zero mean and standard deviation equal to σ. The second and fourth order dispersion at the pump wavelength are related to the third order and fourth order dispersion at the fiber's ZDW through[100]

$$\beta_2(\omega_p) \approx \beta_3(\omega_0)(\omega_p - \omega_0) + \beta_4(\omega_0)(\omega_p - \omega_0)^2/2 \tag{4.2.7}$$

$$\beta_4(\omega_p) \approx \beta_4(\omega_0) \tag{4.2.8}$$

By using Eq. (4.2.7) and considering $\omega_0 = \frac{2\pi c}{\lambda_0}$, the constant part of the ZDW, $\lambda_{0,mean}$, can be found from the optimal β_2 obtained by the genetic algorithm. Random variations in the ZDW will cause random variations in β_2 which leads to fluctuations in the total phase mismatch. As a result the gain spectrum becomes considerably non-uniform.

To investigate the effect of ZDW variations in the gain spectrum of the FOPA, Eq. (4.1.2) is used to obtain the signal amplitude at the end of each small fiber segment of length l_c [102, 103]. The overall gain is found by multiplying the matrices of each segment. This model was used to observe how ZDW variations affect the flatness of the gain spectrum of a FOPA. An

FOPA with the same parameters as the one mentioned in case I of section 4.1.3 is considered. The average of 400 gain spectra with ZDW fluctuations with different amounts of standard deviation of are shown in Fig. 4.14. The correlation length is assumed to be $l_c = 4m$. As can be seen in the figure, as the signal-pump wavelength separation increases, the gain spectrum becomes more sensitive to ZDW fluctuations. The reason is that when the signal wavelength is close to that of the pump's, $\Delta\beta$ is small regardless of the ZDW fluctuations. However, as the signal moves away from the pump, the fluctuations of $\Delta\beta$ increase due to ZDW fluctuations. FOPA gain with around 1dB ripple can be achieved when the average ZDW in each fiber segment is maintained close to the optimum value and the standard deviation of the fluctuations is less than 0.7 nm.

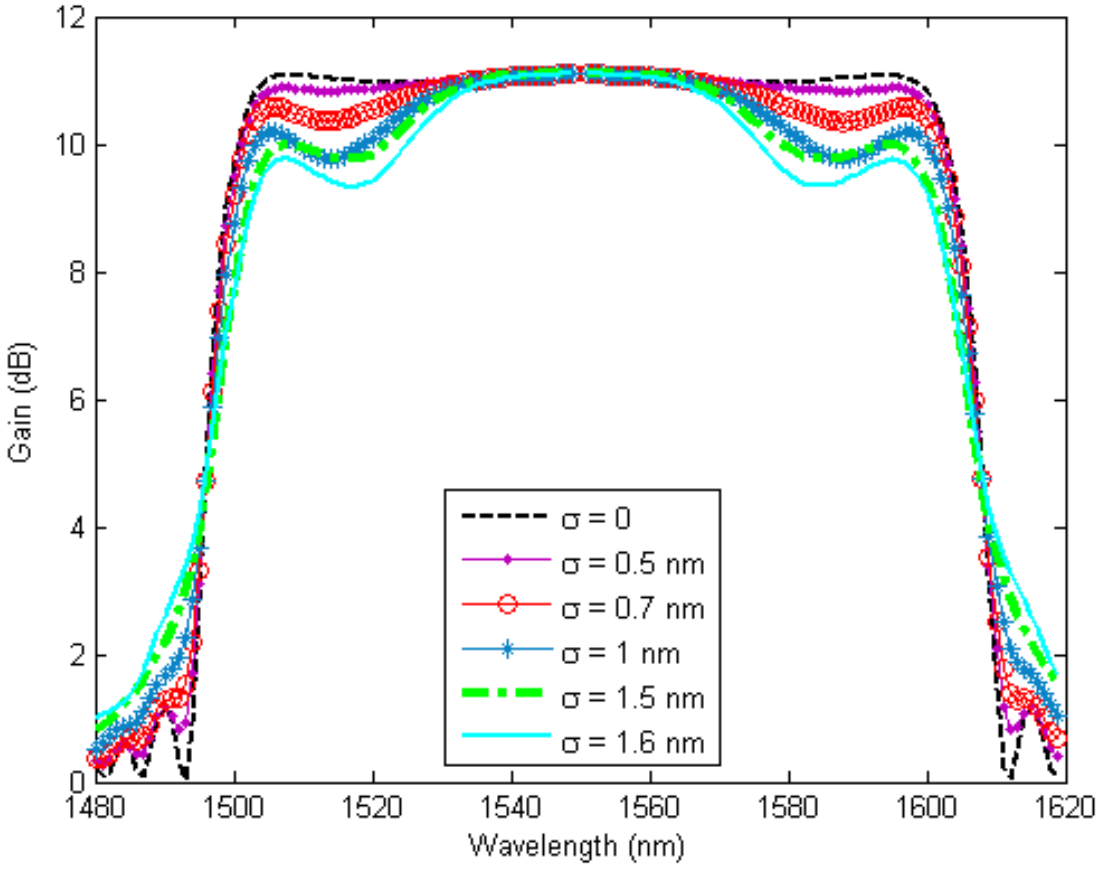

Fig. 4.14 The effect of ZDW fluctuations on the gain spectrum of a FOPA composed of three fiber sections with optimized length, β_2 and β_4.

In order to study the effect of ZDW fluctuations on the flatness of the gain spectrum a measure of flatness is introduced through a degree of flatness defined as $S = G_{min}/G_{max}$, where G_{min} and G_{max} are the minimum and maximum values of the average gain in the gain region of the FOPA. Fig 4.15 shows how the flatness of the FOPA varies as a function of the standard deviation of the ZDW fluctuations σ.

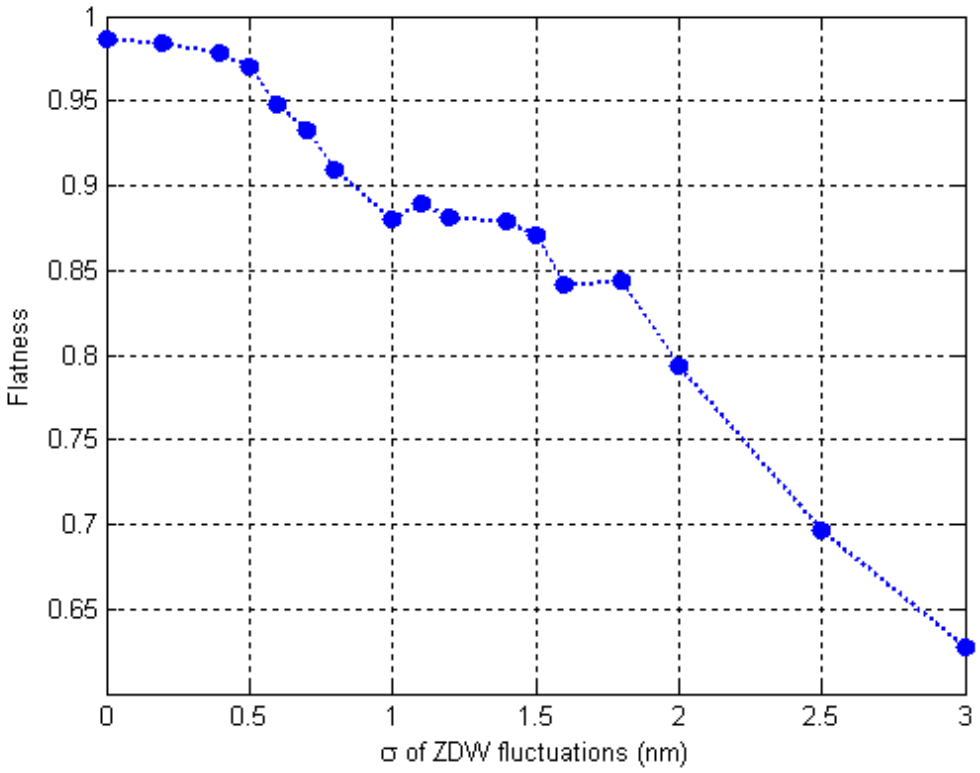

Fig. 4.15 Degree of flatness as a function of standard deviation of ZDW fluctuations

To have parametric amplification the parametric gain coefficient g in Eq. (3.2.14) should be positive over the signal bandwidth. A purely imaginary g corresponds to a phase change in which the signal won't be amplified anymore. Due to the ZDW fluctuations, the amplitude of the total phase mismatch, k, is changed and it might get large enough to cause an imaginary g. If the fluctuations have long correlation lengths, this imaginary g occurs over a long fiber section and thus causes detrimental effects on the gain

profile of the amplifier. This can be seen in Fig. 4.16 where as the correlation length gets longer, the flatness of the gain spectrum is reduced.

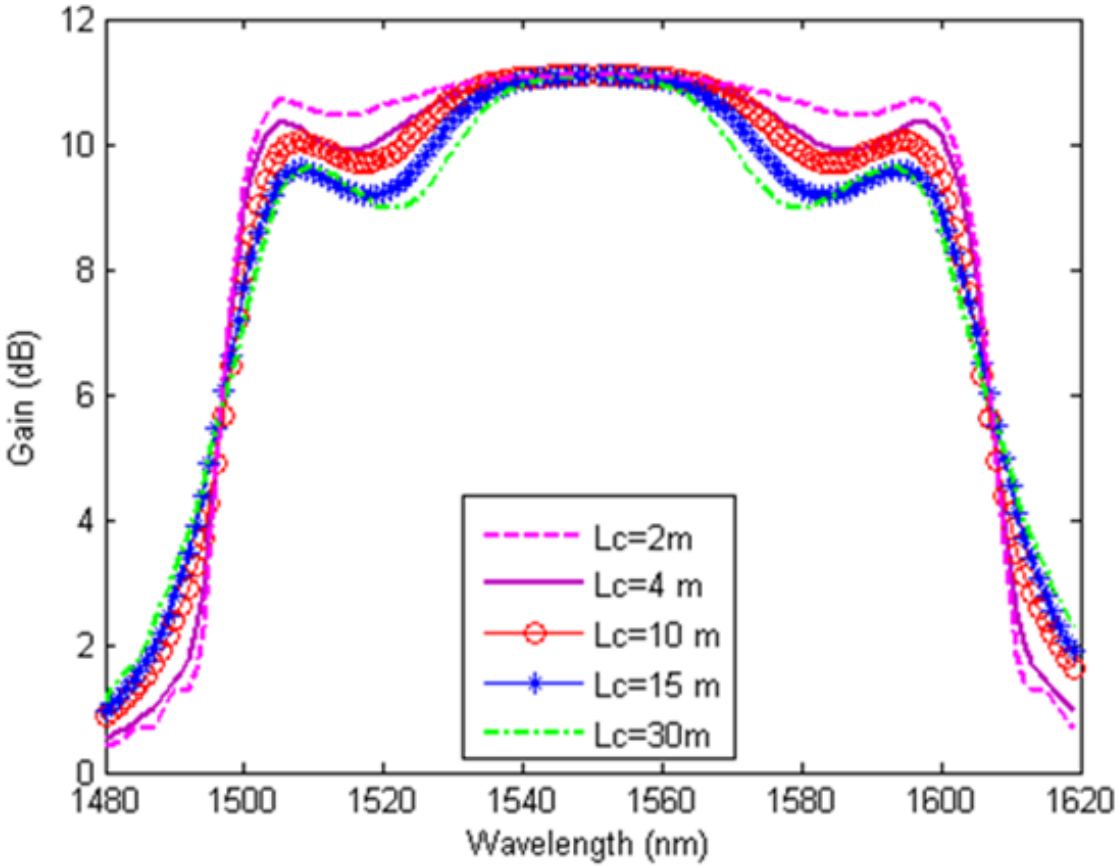

Fig. 4.16 Gain spectra of FOPA with different correlation length**s,** standard deviation for ZDW fluctuations is 1 nm.

4.3 Noise Properties of a Multi-Section FOPA

The main noise sources which affect the performance of the FOPA are the amplified quantum noise (QN) and the excess pump noise [101, 104]. Due to the quantization of the optical field, an optical power will be present in the fiber even though there are no signal photons. These vacuum fluctuations are referred to as QN. The QN spectral density is given by:

$$S_{QN} = {}^{h\upsilon}/_{2} \tag{4.3.1}$$

where h is Plank's constant and υ is the optical signal frequency. The QN spectral density will be amplified by the FOPA. In addition, during the FWM process, the QN around the signal frequency will beat with the QN around the idler frequency, which will result in additional noise at the signal and idler waves. Thus, the total QN spectral density after the parametric amplification is:

$$S_{AQN} = S_{QN}(G_s + G_i) = \frac{h\upsilon}{2}(2G_s - 1) \tag{4.3.2}$$

The intensity variation of the signal after detection, due to the beating between the signal and QN is expressed as:

$$\sigma^2_{s-QN} = 4R_s^2 G_s P_{s0} S_{AQN} \Delta f \tag{4.3.3}$$

where G_s is the FOPA gain, R_s is the responsitivity of the detector, P_{s0} is the input signal power and Δf is the electrical filter bandwidth.

Since the amplifier gain is dependent on the pump power, all intensity variations of the pump will cause gain variations in the signal and idler. The major noise sources affecting the pump are the beating between the amplified spontaneous emission (ASE) and the pump source and also the pump's relative intensity noise (RIN). However, RIN effects are much less compared to ASE. Moreover, although the pump source is also influenced by the QN, but as these variations are small it can be neglected. The pump intensity variation created from the beating of ASE noise with the pump is:

$$\sigma_{Pp-ASE}^2 = 4R_s^2 P_p S_{ASE} \Delta f \tag{4.3.4}$$

where S_{ASE} is the spectral density of the ASE noise. The intensity variation of the signal due to this noise is:

$$\sigma_{S-Pp}^2 = \sigma_{Pp-ASE}^2 (\frac{dG_s}{dP_p} P_s(0))^2 \tag{4.3.5}$$

The noise figure (NF), which is the most common used expression for reporting the noise performance of an amplifier, is the ratio of the input signal to noise ratio (SNR) to output SNR and is written as:

$$NF_s = 10log\ (F_s) \tag{4.3.6}$$

where

$$F_s = \frac{2G_s - 1}{G_s} + \frac{\sigma_{S-Pp}^2}{4G_s^2 R_s^2 S_{QN} P_s(0) \Delta f} \tag{4.3.7}$$

The first term in the noise factor (F_s) in Eq. (4.3.7) is related to amplified QN, while the second term is due to the excess pump noise.

In a multiple section FOPA the total noise factor can be found by using Frii's formula [105]:

$$F_s = F_{s1} + \frac{F_{s2} - 1}{G_{s1}} + \frac{F_{s3} - 1}{G_{s1} G_{s2}} + \cdots + \frac{F_{sn} - 1}{G_{s1} G_{s2} \ldots G_{s(n-1)}} \tag{4.3.8}$$

where F_{sn} and G_{sn} are the noise factor and power gain of the n-th fiber section, respectively.

In order to see the noise properties of a multi-section FOPA with optimized fourth order dispersion, the noise figure of such an amplifier is shown in Fig. 4.17. The FOPA parameters are the same as the ones mentioned earlier in Fig. 4.6. The input signal power is considered 0.1 mW. It can be realized that in the FOPA gain region, the NF is less than 4dB. The proposed multi-section FOPA has a broad bandwidth with >10 dB gain and an acceptable noise figure

compared to other reported FOPAs. The method can be used to obtain bandwidths larger than 100 nm, however in that case more fiber sections (N>3) should be cascaded. Considering the fact that, there is a tradeoff between gain and flat bandwidth in FOPAs, for achieving a higher gain we should compromise the bandwidth.

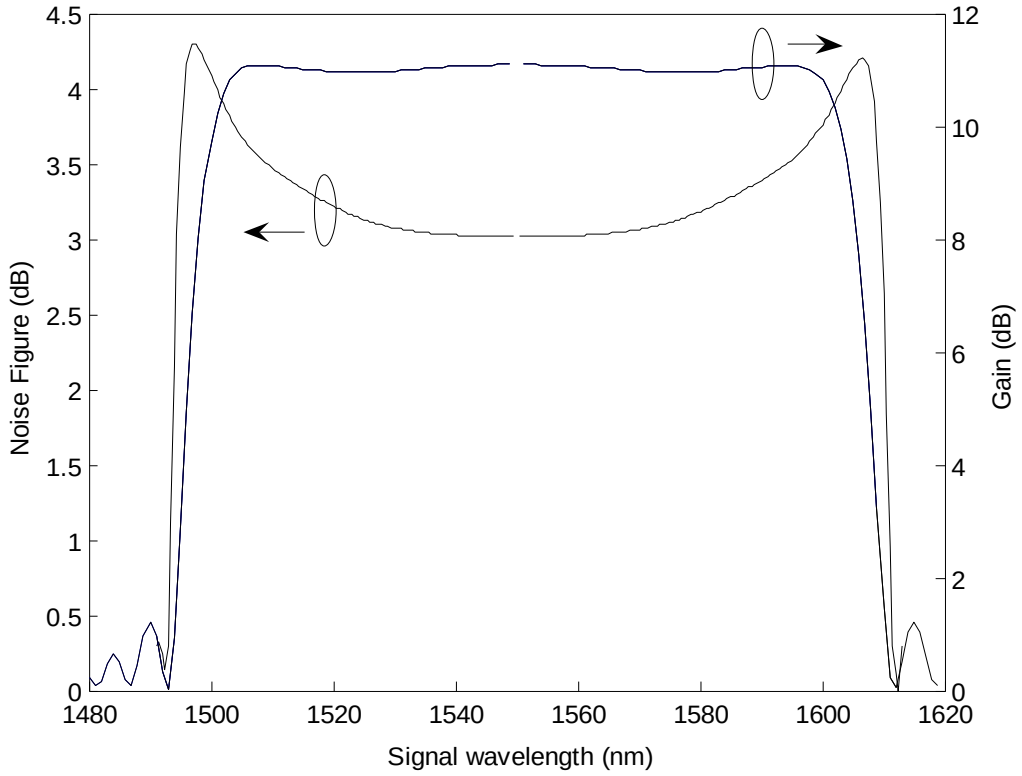

Fig. 4.17 Gain and noise figure of a FOPA composed of three fiber sections with optimized length, $\boldsymbol{\beta_2}$ and $\boldsymbol{\beta_4}$.

4.4 Pump Depletion

The preceding sections focused on the gain spectra of the FOPA in the small signal gain regime, where there is no pump depletion. This regime leads to a gain spectrum which is independent of the input signal power. In practice, however, pump depletion and signal power limit the maximum achievable gain. With the increase of input signal power (P_{s0}) the pump is

depleted and the signal gain drops. The condition for complete pump depletion is that $\Delta\beta$ should be close to $\Delta\beta_0 = \gamma(P_{s0} - P_{p0}/2)$ [106], which is different from the phase matching condition in the small signal regime; $\Delta\beta_0 = -2\gamma P_{p0}$. This indicates that the gain spectrum optimization in these two regimes have different results. The output gain spectra of a multi-section FOPA with different input signal powers are shown in Fig. 4.18 where the coupled equations are solved numerically using the Runge-Kutta approach.

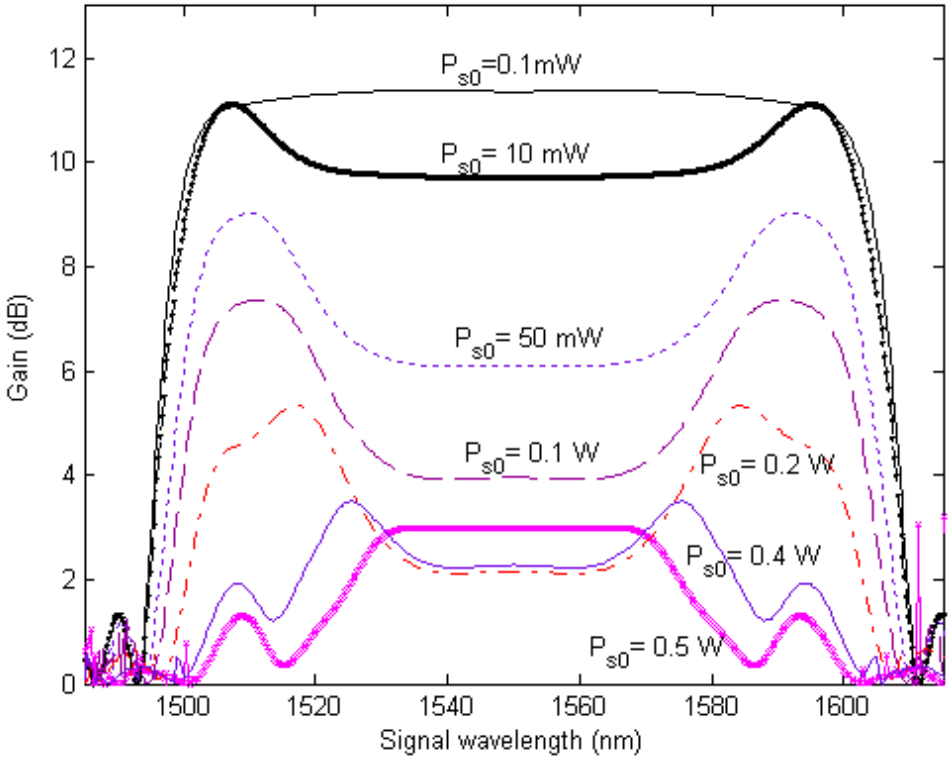

Fig. 4.18 Gain spectra of a FOPA composed of three fiber sections for different input signal powers.

The parameters are the same as the ones in Fig. 4.6 except for the input signal power. As can be seen, the signal gain drops significantly when the input signal is increased, therefore as mentioned above the optimization results obtained for the small signal regime aren't suitable for the pump depletion regime.

The frequency relation $2\omega_p = \omega_s + \omega_i$ indicates that when the pump releases two photons, both signal and idler get one photon. Therefore, if the pump is completely depleted the signal and idler powers increase by $P_{p0}/2$ which is the maximum power the idler can have. Hence, in the pump depletion regime the conversion efficiency increases with increasing P_{s0} up to a certain amount and increasing P_{s0} further on will lead to a drop in the conversion efficiency. The conversion efficiency is defined as the output idler power to the total input power, which is given by:

$$\eta = P_i / (P_{p0} + P_{s0}) \tag{4.4.1}$$

Figure 4.19 which has the same parameters as Fig. 4.6, shows the conversion efficiencies of a FOPA with different input signal powers. It can be seen that with the increase of P_{s0}, the conversion efficiency rises and when the signal power increases to more than about 50 mW, the conversion efficiency decreases.

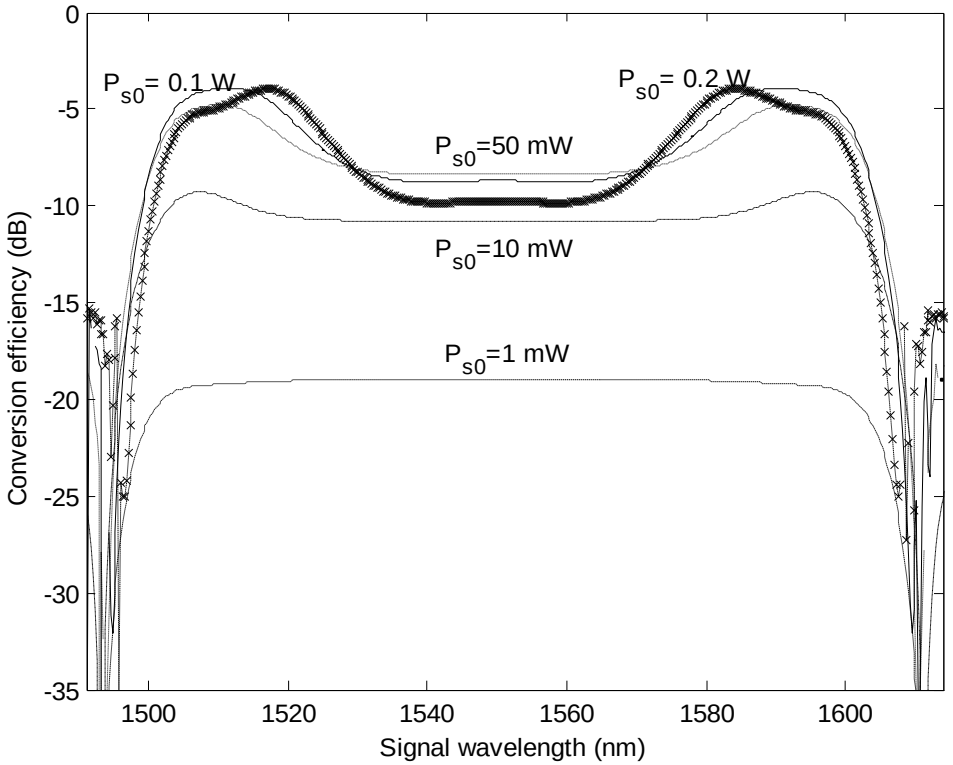

Fig. 4.19 Conversion efficiency of a FOPA composed of three fiber sections for different input signal powers.

The input signal power affects the noise figure as well. For a small signal input power, the parametric amplifier will be quantum limited. But with the rise of input signal power the noise figure increases as well. This is illustrated in Fig. 4.18. The rest of the FOPA parameters are the same as Fig. 4.6.

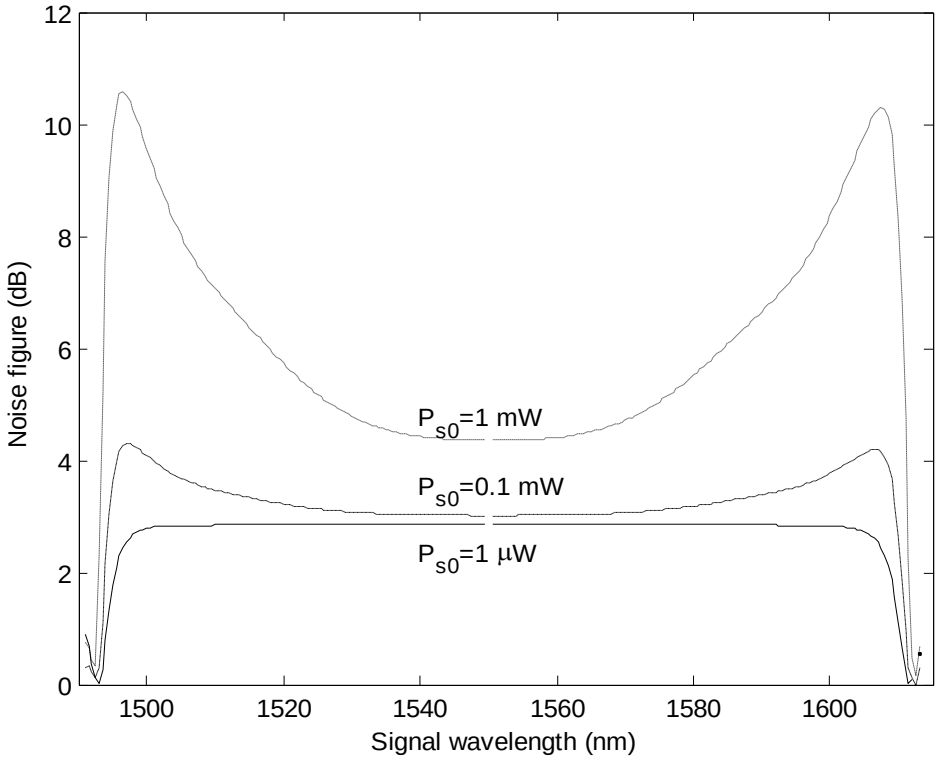

Fig. 4.20 Noise figure of a FOPA composed of three fiber sections for different input signal powers.

4.5 Summary

The parameters of a FOPA composed of three cascaded HNLF sections are optimized using genetic algorithm. Different from previously reported methods, in this work the fourth order dispersion of each fiber section is also optimized as well as the second order dispersion and length. It is shown that optimizing the fourth order dispersion will lead to a wider flat bandwidth which is required for using the amplifier in WDM systems. The effect of zero dispersion wavelength fluctuations on the performance of the FOPA is studied. The noise figure for such a multi-section FOPA and also its performance in the depleted pump regime are investigated.

Chapter 5

Four-Wave Mixing in a Fiber Loop Mirror

5.1 Parametric Loop Mirror

Two common issues which arise in most four wave mixing processes are (1) separating the generated idler wave from the input beams when the optical frequency of the idler is close to those of the input waves, and (2) suppressing the amplified spontaneous emission (ASE) which is injected into the fiber along with the amplified input waves. Mori *et al.* proposed a solution to these problems which was the optical parametric loop mirror (PALM) [107]. This device can intrinsically separate the generated idler from the input pump and signal and also suppress their background ASE without the need of optical filtering. The basic configuration of the PALM is made up of a nonlinear medium and a dispersive element connected through a 3-dB coupler to make a Sagnac interferometer loop which is shown in Fig. 5.1. The pump and signal waves are injected into the loop from port 1 and divided by the 3-dB coupler to ports 3 and 4. The clockwise pump and signal generate a FWM signal in the nonlinear medium after propagating through the dispersive element while the counterclockwise beams first pass through the nonlinear medium and then along with the generated idler, all three waves propagate in the dispersive element.

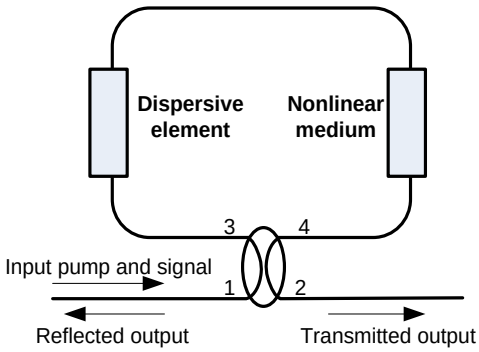

Fig. 5.1 Basic configuration of the PALM.

After propagating in the loop the two input waves will be reflected back to the input port (port 1), which is where the name loop mirror comes from. Meanwhile the output port for the idler depends on the phase difference between the counter-propagating idler waves in the loop. The complex amplitudes of the idler waves after propagating through the loop, at ports 3 and 4 are:

$$A_{i3} = -i\sqrt{\frac{\eta}{8}}\, A_p^2 A_s^* \exp(-i\beta(\omega_i)L) \tag{5.1.1}$$

$$A_{i4} = \sqrt{\frac{\eta}{8}}\, A_p^2 A_s^* \exp(-i[2\beta(\omega_p) - \beta(\omega_s)]L) \tag{5.1.2}$$

where A_p and A_s are the complex amplitudes of the input pump and signal at port 1, respectively, L is the length of the dispersive element and $\beta(\omega)$ is its propagation constant. These two counter-propagating FWM waves interfere at the coupler; the output idler powers at ports 1 (P_1) and 2 (P_2) are given by:

$$P_1 = (|A_{i3}|^2 + |A_{i4}|^2)(\frac{1 + cos\Delta\beta L}{2}) \tag{5.1.3}$$

$$P_2 = (|A_{i3}|^2 + |A_{i4}|^2)(\frac{1 - cos\Delta\beta L}{2}) \tag{5.1.4}$$

where $\Delta\beta = \beta(\omega_s) - \beta(\omega_i) - 2\beta(\omega_p)$. If $\Delta\beta L = \pi(2n-1)$ (n an integer) the whole FWM power will be output to port 2, therefore the idler wave can be separated from the pump and signal waves without using a filter. This feature of the PALM has been used for spectral inversion [108], wavelength conversion [109] and all optical de-multiplexing [110].

He *et al.* proposed a fiber loop mirror referred to as TDFLM, constructed from two polarization maintaining dispersion shifted fibers (DSF) [111]. While in the PALM four-wave mixing can only happen in the nonlinear medium, it occurs in both DSFs of the TDFLM. It is shown that the conversion efficiency in TDFLM is higher than the PALM especially for higher levels of input pump power. This difference is apparent when the pump signal wavelength separation is small. Placing a single mode fiber (SMF) between the two DSFs changes the phase relationship between the pump, signal and idler at the input of the second DSF in the clockwise branch while in the counter-clockwise direction the phase relation at the input of the other DSF is changed. Thus, the SMF will act as a wavelength-dependent phase shifter, where the phase shift will affect the gain and conversion efficiency of the loop mirror. This effect is studied in this section.

5.1.1 Theory

As seen in Fig. 5.2 the input pump (A_{p0}) is split into A_{p1} and A_{p2} by the 3-dB coupler, while the input signal (A_{s0}) is split into A_{s1} and A_{s2}. It is assumed that the input beams are continuous waves and that the pump is un-depleted.

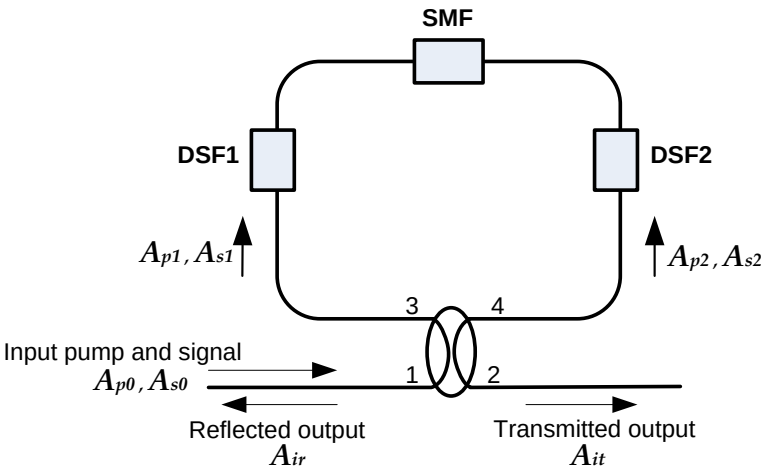

Fig. 5.2 Dispersion imbalanced fiber loop mirror.

In the clockwise branch the signal is amplified in the DSF and an idler is generated. The relative phase relationship between the three waves at the output of DSF1 depends on the gain and phase matching properties of DSF1. Then the waves propagate through the SMF where they experience a wavelength-dependent phase shift. For $|\omega_s - \omega_p| \ll \omega_p$, we have $\Delta\beta \cong \beta_2(\omega_s - \omega_p)^2$, where β_2 is the GVD parameter of the SMF. The phase shift introduced by the SMF is

$$\Delta\phi = \Delta\beta L_{SMF} = -2\pi c(\frac{\lambda_p - \lambda_s}{\lambda_s})^2 D L_{SMF} \tag{5.1.5}$$

where c is the vacuum speed of light, D is the dispersion coefficient of the SMF at the pump wavelength and L_{SMF} is the length of the SMF. λ_p and λ_s are the pump and signal wavelengths, respectively. The three waves then propagate in the second DSF. After propagating through the loop the amplitudes of the two counter-propagating generated idlers at ports 4 and 3 are A_{i1} and A_{i2}, respectively. The interference between the two idlers in the coupler, causes the reflected (A_{ir}) and transmitted (A_{it}) idler amplitudes at ports 1 and 2, respectively, which are derived from the following equations:

$$A_{ir} = i\sqrt{0.5}A_{i1} + \sqrt{0.5}A_{i2}$$
$$= \{\frac{A_{p0}^2}{g_1 g_2}\sinh(g_1 L_1)\sinh(g_2 L_2)(\gamma_2 k_1 + \gamma_1 k_2)\sin\left(\frac{\Delta\phi}{2}\right)$$
$$- A_{p0}^2\cos\left(\frac{\Delta\phi}{2}\right)\left[\frac{\gamma_2}{g_2}\cosh(g_1 L_1)\sinh(g_2 L_2)\right.$$
$$\left.+\frac{\gamma_1}{g_1}\sinh(g_1 L_1)\cosh(g_2 L_2)\right]\}A_{s0}^*/2 \quad (5.1.6)$$

$$A_{it} = \sqrt{0.5}A_{i1} + i\sqrt{0.5}A_{i2}$$
$$= \{\frac{A_{p0}^2}{g_1 g_2}\sinh(g_1 L_1)\sinh(g_2 L_2)(\gamma_2 k_1 - \gamma_1 k_2)\cos\left(\frac{\Delta\phi}{2}\right)$$
$$+ A_{p0}^2\sin\left(\frac{\Delta\phi}{2}\right)\left[\frac{\gamma_2}{g_2}\cosh(g_1 L_1)\sinh(g_2 L_2)\right.$$
$$\left.-\frac{\gamma_1}{g_1}\sinh(g_1 L_1)\cosh(g_2 L_2)\right]\}A_{s0}^*/2 \quad (5.1.7)$$

where L_i, γ_i, g_i and k_i $(i = 1,2)$ are the length, nonlinear coefficient, parametric gain coefficient and total phase mismatch for DSF1 and DSF2, respectively. When there is no SMF in the loop ($\Delta\phi = 0$), the second term in Eq. (5.1.7) which is multiplied by $\sin(\Delta\phi/2)$ will be deleted. However, when the SMF is available and the phase shift isn't zero, this term will also be included in A_{it}, which will increase A_{it} at certain wavelengths. Thus the conversion efficiency for the transmitted idler increases at some wavelengths compared to the PALM and TDFLM.

The conversion efficiency for the transmitted idler wave is:

$$\eta = \frac{|A_{it}|^2}{|A_{s0}|^2} \quad (5.1.8)$$

The transmitted signal to output port 2 is zero; hence the idler wave can be transmitted while the signal can't. Therefore this configuration can be used to suppress the pump and signal waves without the need of optical filtering.

5.1.2 Results and Discussion

For the simulations, the length and zero dispersion wavelength (ZDW) of DSF1 and DSF2 are 1km and 1550 nm, 300 m and 1552 nm, respectively. A pump power of 40 mW at $\lambda_p = 1550\,nm$ is considered. The nonlinear coefficient and dispersion slope of the two DSFs are $\gamma = 9\,km^{-1}W^{-1}$ and S = 0.03 $ps/nm^2/km$. Due to its large dispersion even a few meters of SMF can cause large changes in the relative phase relation between the waves. The SMF is chosen 8 m long. Since in [111] it is shown that the conversion efficiency in TDFLM is higher than the PALM, we compare the conversion efficiency of our design with the TDFLM in Fig. 5.3. The difference between the conversion efficiency of the two designs can get as high as 14 dB at wavelengths close to the pump wavelength, meaning that the conversion efficiency of this design is more than the TDFLM and also the PALM. Since the two DSFs have different dispersion properties, the phase matching conditions can be satisfied in only one of the DSFs by setting the pump wavelength at the ZDW of that DSF. In the region where pump-signal wavelength separation is large enough, the FWM contribution in DSF2 whose ZDW is away from the pump wavelength isn't considerable; therefore, for this range of wavelengths this design becomes similar to the TDFLM and PALM. But for signals placed close to the pump this configuration results in a higher conversion efficiency compared to the previous designs of PALM and TDFLM, due to the phase shift which the SMF will induce in the waves.

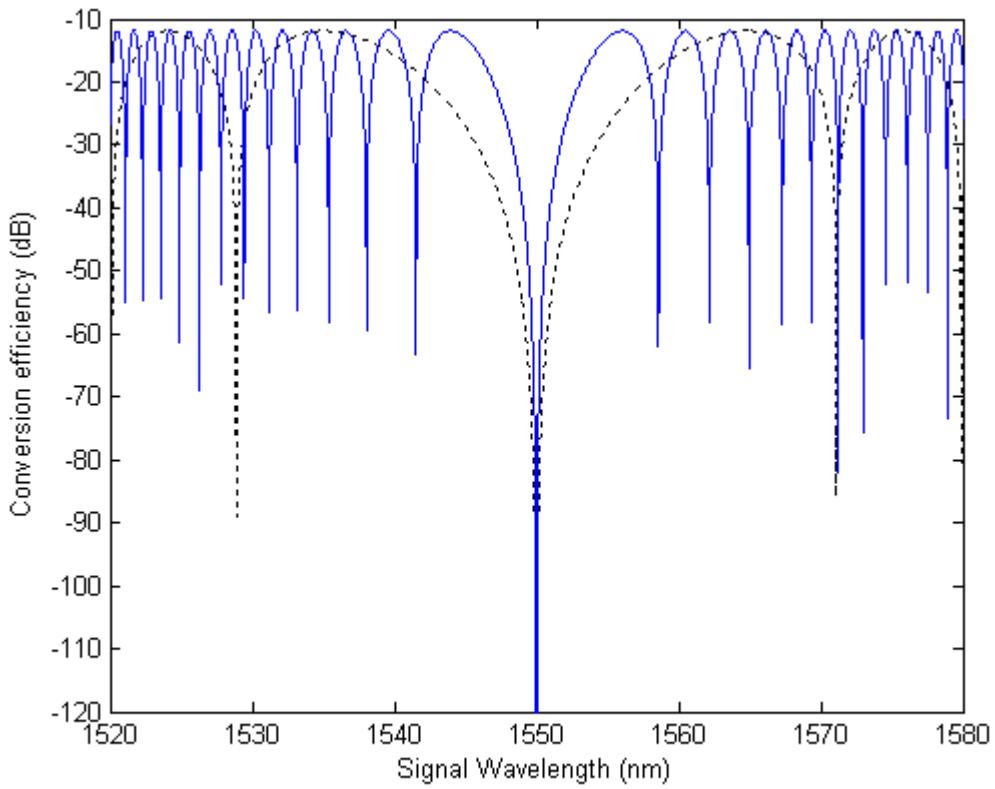

Fig. 5.3 Conversion efficiency of transmitted idler wave, with (solid line) and without (dotted line) the SMF in the loop.

The conversion efficiency for different SMF lengths are shown in Fig. 5.4. By changing the length of the SMF, the amount of the phase shift changes and consequently the wavelengths in which the conversion efficiency is higher than the case with no SMF will change.

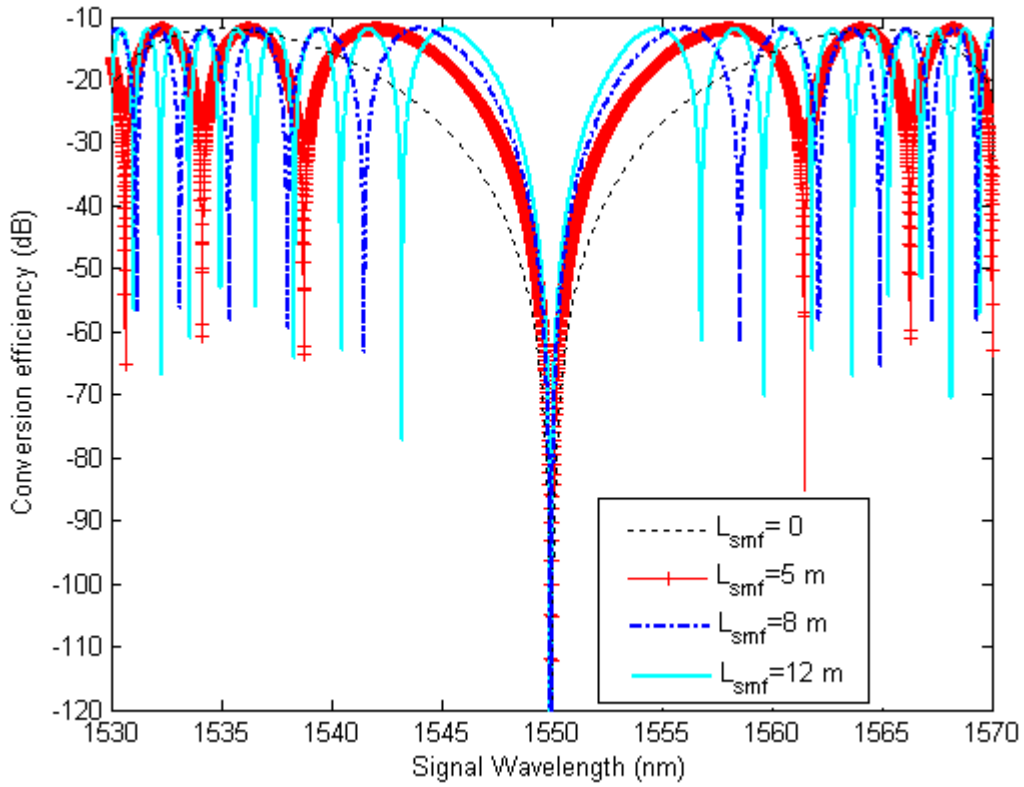

Fig 5.4 Conversion efficiency of transmitted idler wave for different SMF lengths

The power of the transmitted idler for this design and TDFLM are displayed in Fig. 5.5. It can be seen that there is a significant difference between the transmitted idler powers at the output of the loop for these two designs. Figure 5.6 shows that the conversion efficiency of the reflected idler ($\eta = |A_{ir}|^2/|A_{s0}|^2$) for wavelengths in the vicinity of the pump is basically lower in our design, which is desirable.

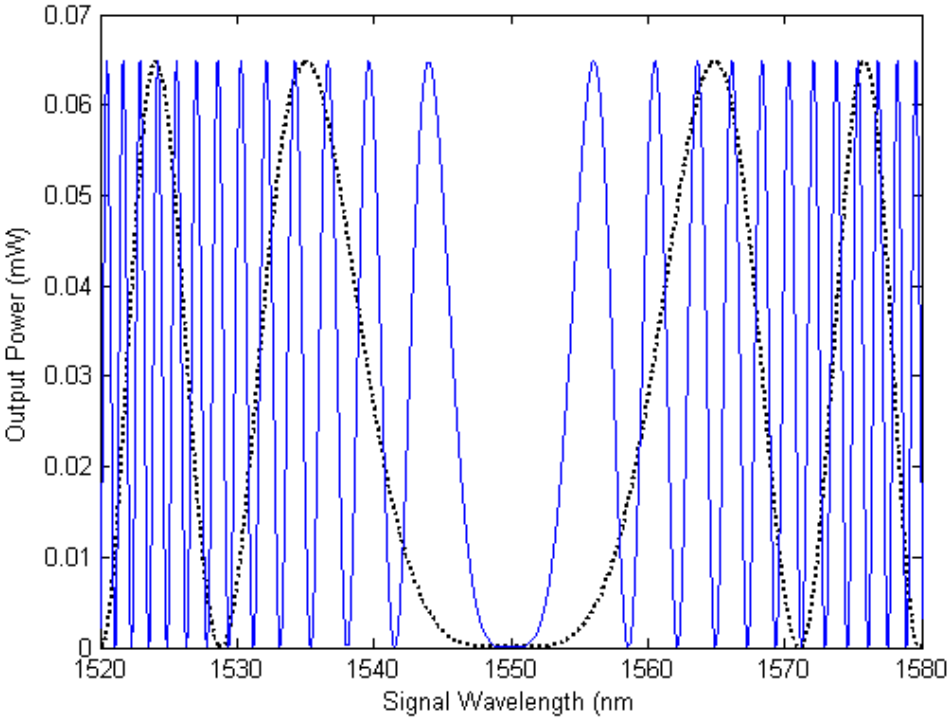

Fig. 5.5 The transmitted idler power with (solid line) and without (dotted line) the SMF in the loop.

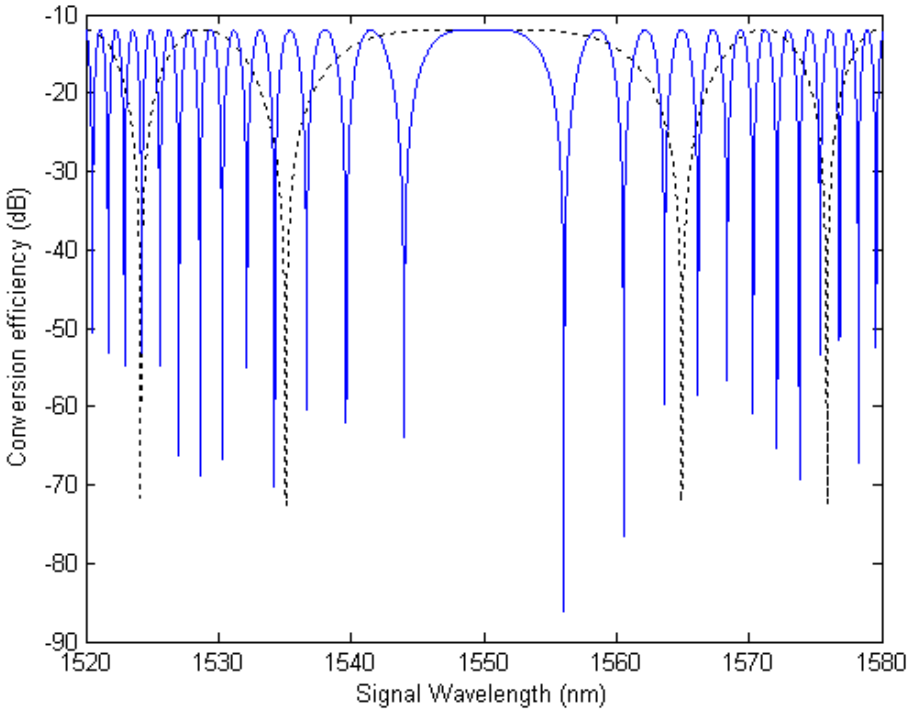

Fig. 5.6 Conversion efficiency of reflected idler wave power with (solid line) and without (dotted line) the SMF in the loop.

5.2 All-Optical Simultaneous De-multiplexing and Demodulation of RZ-DPSK OTDM Signals

Optical time-domain multiplexing (OTDM) is a promising technology to deal with the increasing demand for higher transmission capacity in optical fiber networks. An OTDM signal is a high-speed data stream composed of several lower bit rate channels interleaved together in a periodic pattern [112]. Thus in OTDM, N channels are interwoven in time-domain and grouped in frames of N pulses, where the nth pulse in each frame belongs to the nth channel.

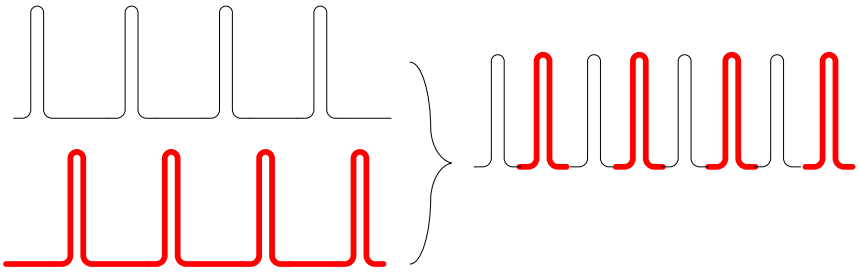

Fig. 5.7 Optical time-domain multiplexing of two channels.

To recover the data of a certain channel of an OTDM signal at the receiver, a de-multiplexer is required to select and separate only the pulses associated with that specific channel from all the frames.

5.2.1 OTDM De-multiplexing Techniques

Several approaches for OTDM de-multiplexing based on XPM and FWM in highly nonlinear fibers [47, 113], XPM and FWM in semiconductor optical amplifiers [114, 115] and also electro-absorption modulators [116] have been studied and experimentally demonstrated.

De-multiplexing can be realized by using FWM wavelength conversion in a FOPA. In this case, an optical pulse train referred to as an optical clock is required. The optical clock should only have one pulse per frame; in other words its bit rate must be the same as an individual channel. The duration of the clock pulses shouldn't be more than that of one bit of the OTDM signal. For de-multiplexing the nth channel, the clock pulses should coincide with the nth slot in each frame. When the clock pulses and the OTDM signal propagate inside a HNLF, idler pulses will be generated through FWM only at times when the signal and clock pulses are present simultaneously and overlap in the time domain. Hence, the idler will have the same bit pattern as the nth channel, making it suitable for being used as the output of the OTDM de-multiplexer (DMUX). This technique was first used in 1997 for de-multiplexing a 20 Gb/s OTDM bit stream [46].

Most of the reported OTDM de-multiplexers are for return-to-zero on-off keying (RZ-OOK) modulation format. However, differential phase shift keying (DPSK) modulation format is capable of improving the performance of long haul transmission systems; thus, it is reasonable to investigate de-multiplexing schemes for RZ-DPSK OTDM systems [117, 118].

In the following sections first the DPSK modulation format will be explained and then de-multiplexing of RZ-DPSK OTDM bit streams will be studied.

5.2.2 Return-to-Zero Differential Phase Shift Keying (RZ-DPSK)

In addition to optical intensity modulation where the digital signal is represented by the optical power level of the carrier, a signal can also be represented by the phase of an optical carrier, which is referred to as optical phase shift keying (PSK). For using PSK modulation the phase of the optical carrier should remain stable so that at the receiver the phase information can

be extracted without ambiguity. This requirement puts a stringent condition on the tolerable linewidth of the transmitter laser. To overcome this requirement a variant of the PSK format, known as differential phase shift keying (DPSK) is mostly used.

In DPSK the information is transmitted through the differential phase of the optical carrier. A binary "1" results in a π phase change between consecutive data bits in the optical carrier, while there won't be any phase change between adjacent bits for a binary "0".

The advantage of DPSK over PSK is that as long as the carrier phase remains stable over the duration of two bits, the phase information of the transmitted signal can be retrieved at the receiver end. The main benefit of using DPSK instead of OOK is the 3-dB improvement in the receiver sensitivity which can be understood from Fig. 5.8. For a fixed average optical power, the separation between two DPSK symbols when viewed on a complex phase constellation diagram of the optical field is larger than OOK by a factor of $\sqrt{2}$. This increased symbol distance means that for equal bit-error-rate (BER) the DPSK signal can accept a $\sqrt{2}$ larger standard deviation for the optical field noise compared to OOK, which is equivalent to 3-dB reduction in the required optical signal-to-noise ratio (OSNR).

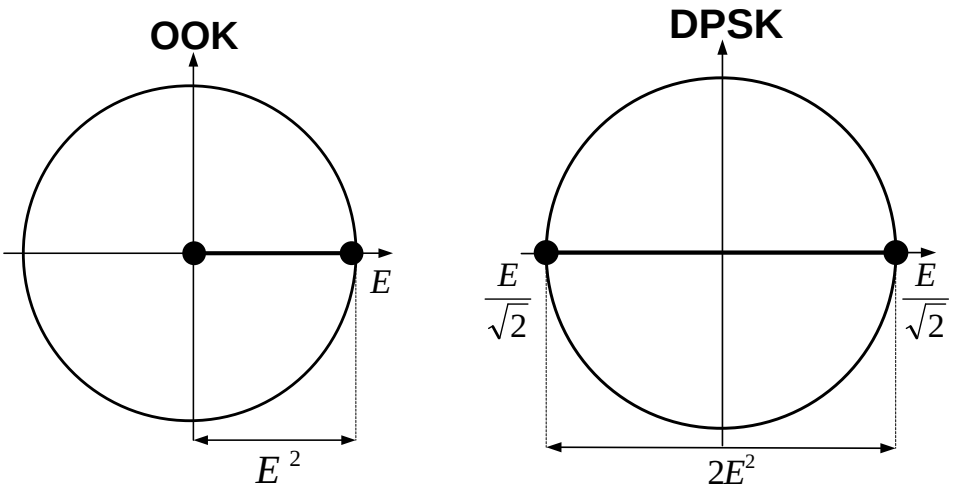

Fig. 5.8 Constellation diagram for on-off keying and DPSK signal.

The block diagram of a typical RZ-DPSK transmitter is shown in Fig. 5.9. As depicted in the figure, before the electrical signal enters the external phase modulator to generate a DPSK optical signal, it should be first pre-encoded by a DPSK encoder. The DPSK encoder contains a XOR gate which combines the non-return-to-zero (NRZ) data with its one-bit delay version. The DPSK encoded electrical signal is then used to drive an electro-optic phase modulator to generate an optical NRZ-DPSK signal. An intensity modulator driven by a clock signal is required to convert the NRZ-DPSK signal to a RZ-DPSK one.

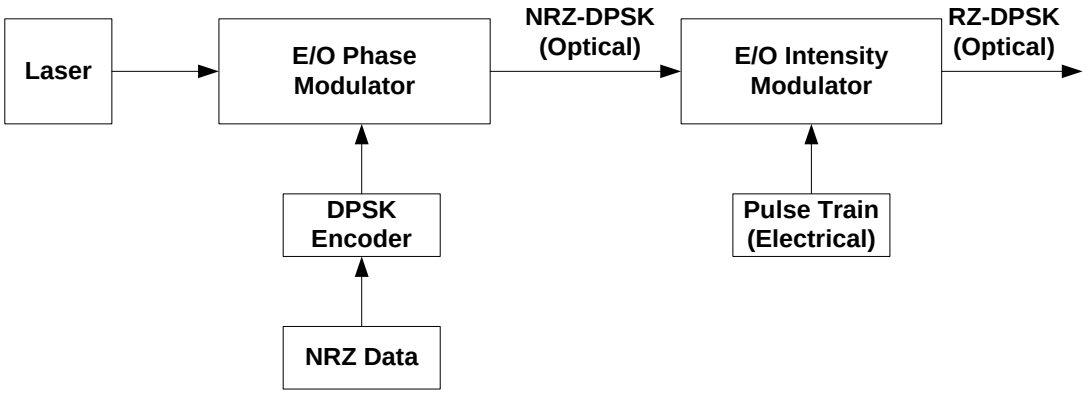

Fig. 5.9 Block diagram of a DPSK transmitter.

5.2.3 DPSK Demodulator

For recovering the binary information carried by OOK signals, a simple photodiode can be used. However, this is not the case for DPSK signals where binary "1" and "0" have the same optical powers. A photodiode can't differentiate the two logic levels, thus a critical element in the receiver end of any system with a phase modulator is a demodulator, which converts the phase modulation into intensity modulation to enable detection by using a photodiode. Decoding a DPSK signal is achieved by comparing the phase of

two sequential bits. A typical DPSK demodulator is shown in Fig. 5.10 which consists of a Mach-Zehnder delay interferometer (MZDI). The incoming DPSK signal is first split into two beams with equal intensities. The beam in one arm of the interferometer is delayed by an optical path difference which introduces a time delay. This length difference between the two arms should be such that the time delay is equivalent to one bit delay. The two beams are then recombined to interfere with each other. As shown in Fig 5.11 the interference turns the phase modulated signal into an intensity modulated one.

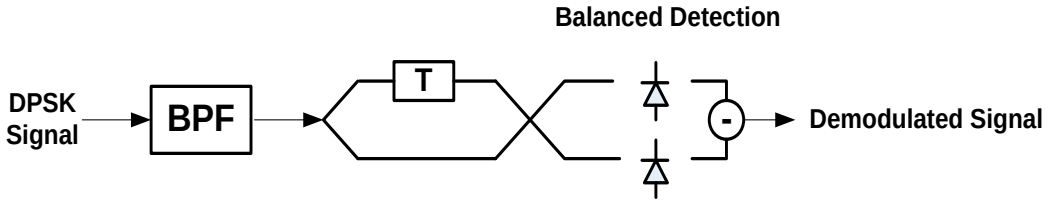

Fig. 5.10 Conventional DPSK demodulator

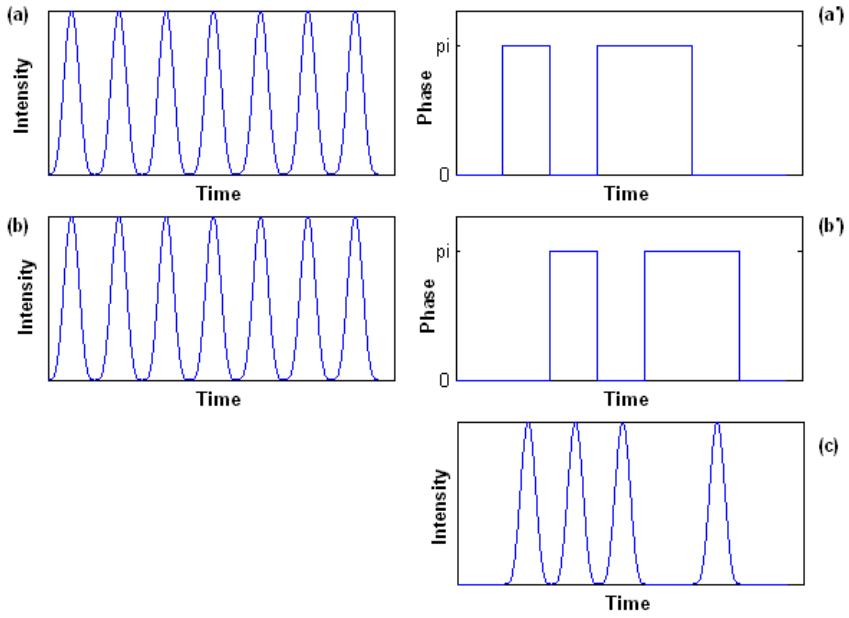

Fig. 5.11 Working principle of optical DPSK demodulation, (a)-(a') intensity and phase of the incoming DPSK signal , (b)-(b') one bit delay of the incoming

DPSK signal, and (c) demodulated signal after interference between (a)-(a') and (b)-(b').

After de-multiplexing a DPSK channel from a RZ-DPSK OTDM bit stream, a demodulator is required for detection. A scheme which can de-multiplex a RZ-DPSK OTDM signal and meanwhile demodulate the de-multiplexed DPSK channel without the need of an external demodulator hasn't yet been investigated. We propose a design which uses the combination of four wave mixing wavelength conversion and wavelength-dependant group delay, for simultaneous de-multiplexing and demodulation of RZ-DPSK OTDM signals.

5.2.4 Principle of Operation

The proposed scheme used for de-multiplexing an RZ-DPSK OTDM signal and demodulating the de-multiplexed channel simultaneously, is shown in Fig. 5.12. It is composed of a HNLF and a single mode fiber connected through a 3-dB coupler to make a Sagnac interferometer loop. The nonlinear medium is used for de-multiplexing the OTDM signal by FWM wavelength conversion while the dispersive element is required for demodulating the de-multiplexed channel due to its wavelength-dependant delay feature [119].

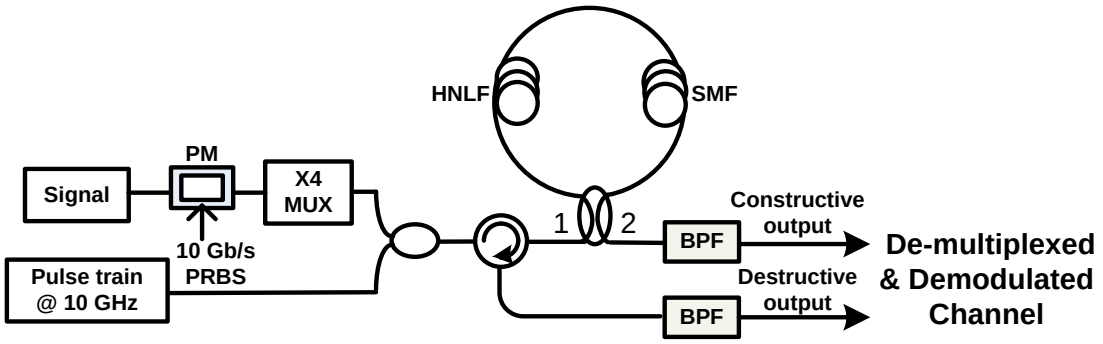

Fig. 5.12 Proposed scheme for RZ-DPSK OTDM de-multiplexer and demodulator.

An RZ-DPSK OTDM data stream at ω_p and a pulse train at ω_s, which has the same bit rate as an individual channel, are injected into the input port of the 3-dB coupler. The pulse train is synchronized with the specific OTDM channel which is intended to be de-multiplexed. After entering the loop, the signal and pump are split into two counter-propagating branches by the coupler. Due to FWM each pair of the counter-propagating pump and signal waves generates a de-multiplexed channel at $\omega_i = 2\omega_p - \omega_s$ in the nonlinear medium. The field of the idler in a FWM process is given by

$$E_i = kA_p^2 A_s \exp[j(2\omega_p - \omega_s)t + (2\phi_p - \phi_s)] \tag{5.2.1}$$

where (A_p, ϕ_p) and (A_s, ϕ_s) are the input field amplitude and phase of the RZ-DPSK OTDM signal and clock pulses, respectively. According to Eq. (5.2.1) the phase of the idler at λ_i is $\phi_i = 2\phi_p - \phi_s$. Since the phase of the pulse train is constant it is considered zero for simplicity. Therefore the phase of the de-multiplexed channel will be twice that of the original input RZ-DPSK OTDM data. Thus in order to preserve the phase information of the input DPSK OTDM signal in the de-multiplexed idler, the modulation depth of the input RZ-DPSK OTDM signal should be set to $\pi/2$ instead of the conventional π

[120, 121]. In this case, the modulation depth of the de-multiplexed channel will be $(0, \pi)$ as seen in Fig. 5.13.

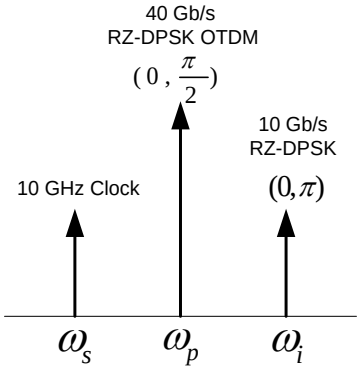

Fig. 5.13 Operation principle of the proposed scheme.

In the clockwise branch of the loop, after the generation of the de-multiplexed channel in the HNLF, the waves are guided to the dispersive medium. Given that the delay of a signal after propagating in the dispersive medium is proportional to its wavelength and considering $\lambda_s = \lambda_p - \Delta\lambda$ and $\lambda_i \cong \lambda_p + \Delta\lambda$, the delay which the clock pulses, OTDM signal and generated de-multiplexed channel experience in the SMF can be expressed by $t_p - \Delta t$, t_p and $t_p + \Delta t$, respectively, where

$$\Delta t = |\lambda_p - \lambda_i| D_{smf} L_{smf} \tag{5.2.2}$$

where D_{smf} and L_{smf} are the dispersion and length of the SMF, respectively.

In the counter-clockwise branch initially the OTDM and clock pulses propagate in the SMF where they will have t_p and $t_p - \Delta t$ delay, respectively, and then these delayed signals enter the HNLF to de-multiplex the OTDM signal. Since it is required to de-multiplex the same OTDM channel as the one in the clockwise branch, the differential time delay, Δt, between the clock and OTDM pulses should be equivalent to one bit period of the clock signal. In this case due to the periodicity of the clock signal, its bit pattern in time domain with $t_p - \Delta t$ delay is the same as it is with t_p delay;

hence, its delay can be considered t_p. This amount of delay will also be transferred to the counter-clockwise de-multiplexed channel through FWM.

The two counter-propagating de-multiplexed RZ-DPSK channels meet at the coupler and interfere. As shown in Fig. 5.14 the differential time delay between these two waves ($ti_{cw} - ti_{ccw} = \Delta t$), is equal to one bit period of each of the time multiplexed RZ-DPSK channels which is the required amount of delay for demodulating the RZ-DPSK de-multiplexed signal. Hence by properly adjusting Δt through tuning the SMF length , the input RZ-DPSK OTDM signal can be simultaneously de-multiplexed and demodulated without the need of a conventional DPSK demodulator. The destructive and constructive demodulated channels can be obtained at the outputs of the loop mirror, making it possible to have balanced detection.

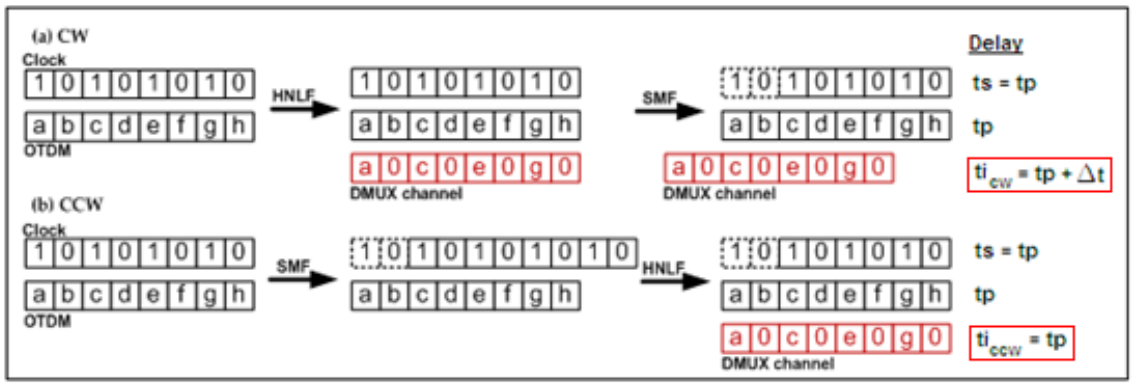

Fig. 5.14 Schematic illustration of the amount of delay which the de-multiplexed channel experiences in (a) the clockwise branch and (b) counter-clockwise branch of the loop mirror. ts: clock delay , tp: OTDM delay , ticw: clockwise branch de-multiplexed channel delay, ticcw: counter-clockwise branch de-multiplexed channel delay.

5.2.5 Numerical Results

The proposed method is simulated based on solving the well-known nonlinear Schrödinger equation using the split-step Fourier method. 40 Gb/s RZ-DPSK OTDM pulses are first amplified by an EDFA with 27 dB gain and 4.5 dB noise figure and then passed through a band pass filter for ASE noise suppression. 10 GHz repetition rate clock pulses placed at 1535.3 nm are synchronized with the RZ-DPSK OTDM pulses with average peak power of 26 dBm, placed at 1550 nm and launched into the loop mirror. A 200 m HNLF with a zero dispersion wavelength of 1549.4 nm, a nonlinear coefficient equal to $\gamma = 20W^{-1}km^{-1}$ and loss of $0.25\,dB/km$ is used for de-multiplexing the OTDM signal to 10 Gb/s tributaries at 1565 nm. The required SMF length for demodulating each of the 10 Gb/s tributaries which is found from Eq. (5.2.2) is 400 m.

The phase and waveform of the input OTDM signal are shown in Fig. 5.15(a) and (b), respectively, while Fig. 5.15(c) shows the clock pulses. The two counter-propagating de-multiplexed signals are displayed in Fig. 5.15(d) and (e), where it can be seen that the differential time delay between these two waves is 100 ps which is the required amount of delay for demodulating the 10 Gb/s RZ-DPSK de-multiplexed channel. The interference between these two waves at the coupler results in a de-multiplexed and demodulated signal as shown in Fig. 5.15(f).

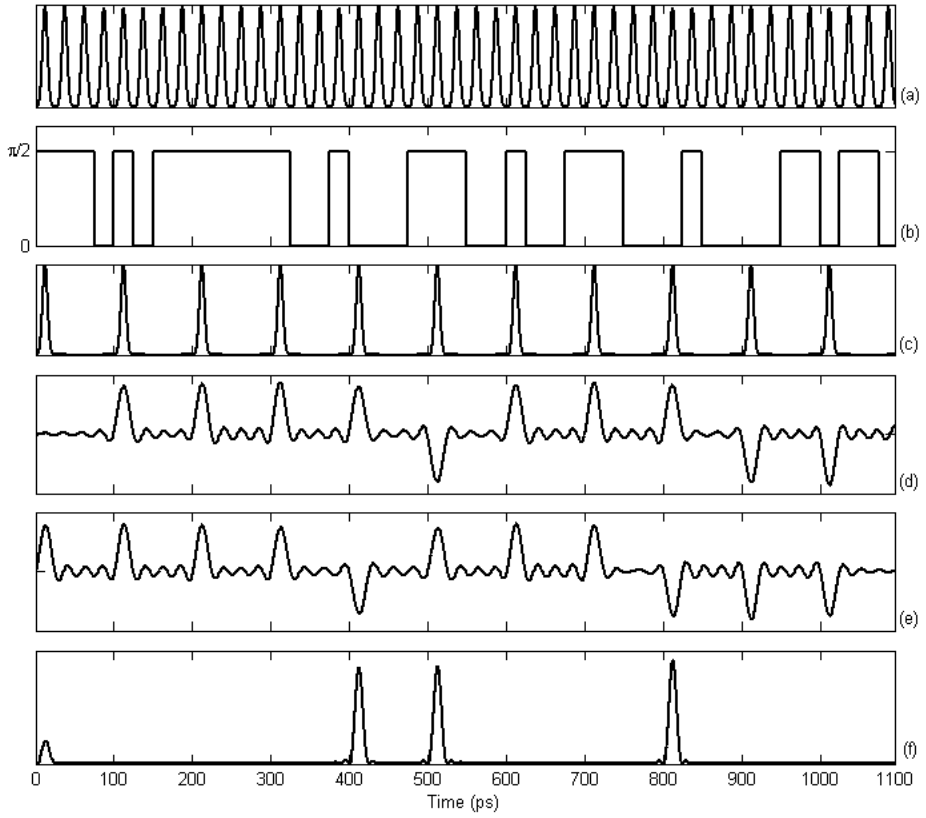

Fig. 5.15 (a), (b) Phase and waveform of the input OTDM signal, (c) clock pulse train synchronized with channel 1, (d) amplitude of the clockwise de-multiplexed signal, (e) amplitude of the counter-clockwise de-multiplexed signal, (f) power of the de-multiplexed and demodulated channel 1 at output port 2.

5.3 Summary

FWM in a loop mirror composed of two DSF fibers with a single mode fiber in between them is analyzed. Due to the phase shift which the SMF induces in the waves propagating through it, the signal to idler conversion efficiency for this design is higher than previously published configurations [107, 111].

An all-optical method for de-multiplexing RZ-DPSK OTDM signals and demodulating the de-multiplexed channels without the help of an external demodulator has been proposed and numerically investigated. This scheme is based on FWM wavelength conversion and wavelength-dependant group delay in a parametric loop mirror.

Using this approach for demodulating DPSK signals at low bit rates will require a large delay, which can be achieved either by increasing the wavelength conversion bandwidth or by increasing the dispersion. Since the wavelength conversion bandwidth of a single pump FOPA is limited and on the other hand increasing the dispersion degrades the signal, thus this scheme isn't suitable for de-multiplexing OTDM data to low bit rate channels. An alternative approach is using a dual pump FOPA design in which the wavelength conversion bandwidth is broader.

Chapter 6

Optical Signal Processing

Nonlinear optics can be used to make all-optical devices which can process high-speed optical signals in a lightwave system. For example as mentioned before, stimulated Raman scattering is used for making Raman amplifiers while four-wave mixing (FWM) is used in fiber optical parametric amplifiers. In this chapter signal processing devices which work based on nonlinear effects, namely cross phase modulation (XPM) and FWM are discussed. In the first section a multiple format conversion module using FWM will be described. An exclusive-OR logic gate which works based on XPM is explained in the second section. An all-optical method for generating 8 level return-to-zero amplitude and phase shift keying (RZ-8-APSK) signals based on FWM and XPM is proposed in the last part.

6.1 All-Optical NRZ/RZ-OOK to CSRZ-OOK and NRZ/RZ-DPSK to CSRZ-DPSK Format Conversion

In response to the system requirements, different modulation formats are expected to be used in different parts of future optical networks [122]. Therefore all-optical format conversions will be desired to maintain high transparency between different network regions. The carrier suppressed return-to-zero (CSRZ) modulation format has attracted interest due to its narrow spectral bandwidth and relatively high tolerance to nonlinearity and residual chromatic dispersion [123]. Several format conversion techniques between non-return-to-zero (NRZ) or RZ with either intensity or phase

modulation, to CSRZ have been reported [124-126]. In this research work we propose a multiple format conversion module based on FWM for converting NRZ/RZ-OOK to CSRZ-OOK and NRZ/RZ-DPSK to CSRZ-DPSK which can also be used for CSRZ-OOK to RZ-OOK with a slight change. In our proposed scheme the format conversion can be obtained with the advantage that the required number of input signals is reduced, which reduces the implementation complexity of the format conversion module.

6.1.1 Carrier Suppressed Return-to-Zero (CSRZ) Modulation

Carrier suppressed return-to-zero (CSRZ) [123] is a pseudo-multilevel modulation format in which the sign of the optical field is reversed at each bit transition [127]. Therefore there is π phase shift between adjacent bits in a CSRZ signal as demonstrated in Fig. 6.2(b). This phase alteration in the optical domain implies that on average, the optical field of half of the "1" bits have a positive sign, while the other half have a negative sign, leading to a zero-mean optical field envelope. This leads to the suppression of the strong frequency component in the optical spectrum of the carrier, giving the format its name. It should be noted that the information is encoded in the intensity of the carrier and this phase alternation is completely independent of the information carrying part of the signal.

A typical CSRZ transmitter setup is illustrated in Fig. 6.1. As can be seen, the generation of CSRZ signals requires two electro-optic modulators. The NRZ data is encoded by the first modulator. The output optical NRZ signal is then modulated in the second modulator to generate a CSRZ signal.

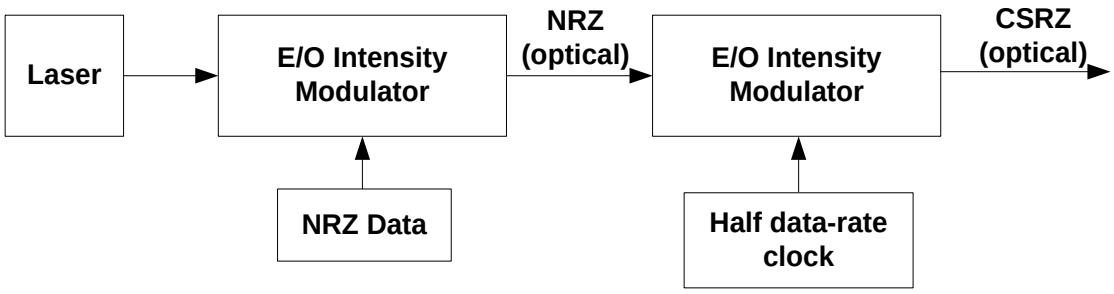

Fig. 6.1 CSRZ transmitter

The second modulator should be driven by a sinusoidal clock at half the bit-rate of the NRZ electrical data signal. CSRZ (67% RZ) will be generated if the the Mach-Zehnder modulator (MZM) is biased at its minimum power transmission point and driven between its transmission maxima, as presented in Fig 6.2 (a). In these conditions the data-rate of the signal at the output of the modulator will be twice the data-rate of the input modulating signal. The phase is periodically modulated between '0' and 'π' for each successive bit, because the optical field transfer function of the MZM changes its sign at the transmission minimum.

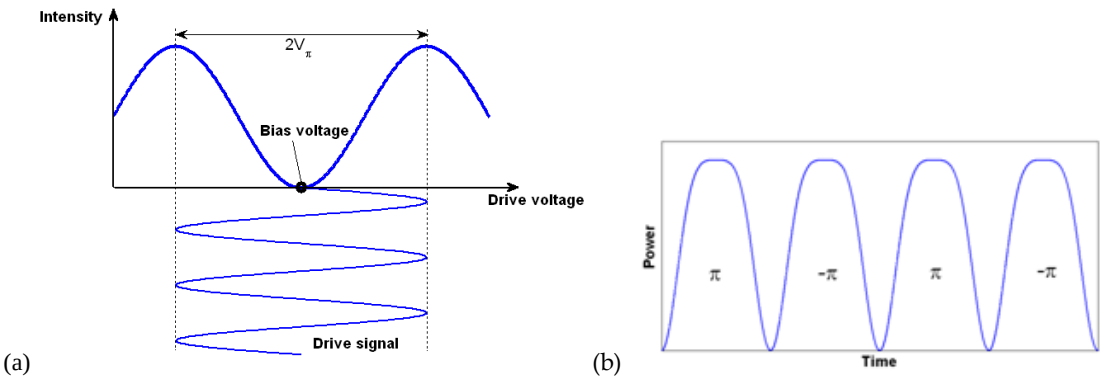

Fig 6.2 (a) The Mach-Zehnder modulator (MZM) biased at the minimum of the transmission curve for CSRZ generation (b) 67% duty cycle CSRZ signal

6.1.2 Principle of Operation

The operation principle of the FWM based all-optical NRZ/RZ-OOK to CSRZ-OOK and NRZ/RZ-DPSK to CSRZ-DPSK modulation format conversions are schematically illustrated in Fig. 6.3.

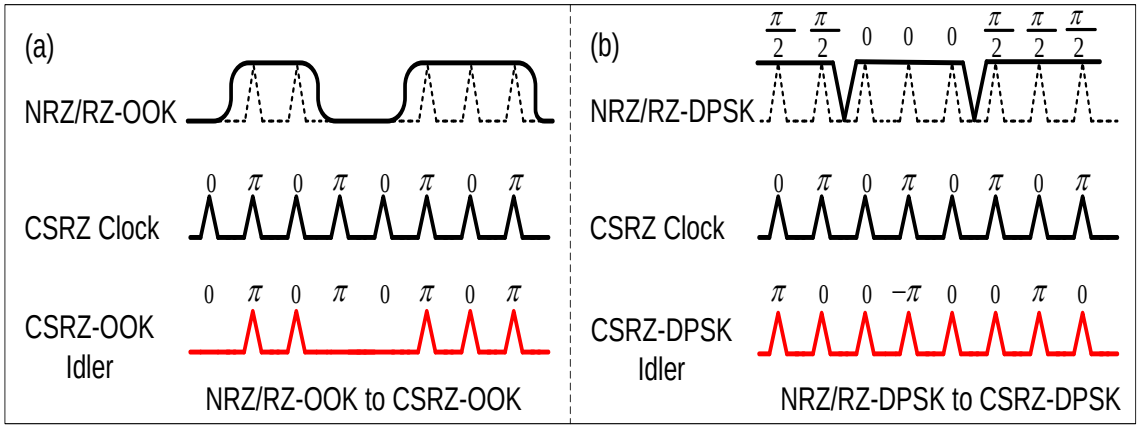

Fig. 6.3 Schematic illustration of FWM based all-optical (a) NRZ/RZ-OOK to CSRZ-OOK, (b) NRZ/RZ-DPSK to CSRZ-DPSK.

As shown in Fig. 6.4 a carrier-suppressed clock pulse train at ω_s along with the input data at ω_p, are launched into a highly nonlinear fiber. Degenerate FWM occurs between these two waves and an idler is generated at $\omega_i = 2\omega_p - \omega_s$.

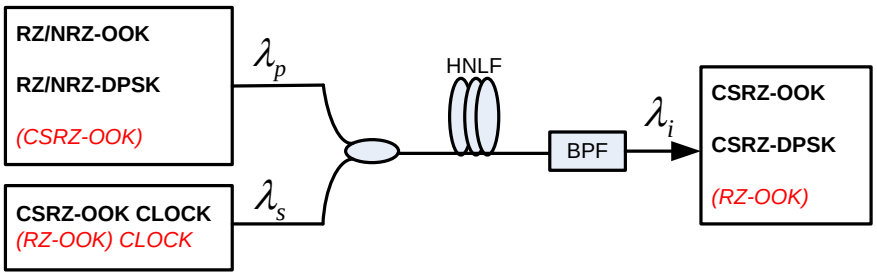

Fig. 6.4 Schematic diagram of the proposed all-optical modulation format converter.

As can be seen in Eq. (5.2.2), the idler phase is expressed as

$$\phi_i = 2\phi_p - \phi_s \tag{6.1.1}$$

For the case of NRZ/RZ-OOK to CSRZ-OOK format conversion the phase of the input NRZ/RZ signal which is located at the pump wavelength is zero, therefore the generated idler will preserve the phase information of the CSRZ clock, resulting in a CSRZ-OOK signal. Whereas, in the NRZ/RZ-DPSK to CSRZ-DPSK format conversion scheme by setting the modulation depth of the DPSK signal to $\left(0,\frac{\pi}{2}\right)$, its phase information will be maintained and transferred to the idler in addition to the phase of the CSRZ clock. Thus the idler will be a DPSK signal with modulation depth of $(0,\pi)$ and it will also have periodic π phase alteration between adjacent bits, which leads to the CSRZ-DPSK modulation format. This scheme can be also used for converting CSRZ-OOK to RZ-OOK if a RZ clock is used instead of the CSRZ one.

6.1.3 Results and Discussion

Numerical studies based on the nonlinear Schrödinger equation using the split-step Fourier method have been carried out for the proposed modulation format conversions. A 200 m long HNLF with a nonlinear coefficient of $= 20W^{-1}km^{-1}$, ZDW of 1550 nm and $0.5\,dB/km$ loss, is assumed. All the optical waves are assumed to be co-polarized. 40 Gb/s, $2^7 - 1$ pseudorandom binary sequence (PRBS) NRZ/RZ-OOK and DPSK signals at 1550 nm along with a synchronized 40 GHz CSRZ clock at 1545 nm are considered. The signal and clock peak powers are 250 mW and 100 mW, respectively. In Fig. 6.5 the gain spectra of the pump and idler related to the FWM based RZ-OOK to CSRZ-OOK format conversion along with the waveforms of the signal,

pump and idler are illustrated. The conversion efficiency defined as the ratio of output idler peak power to the input data peak power is -5.86 dB.

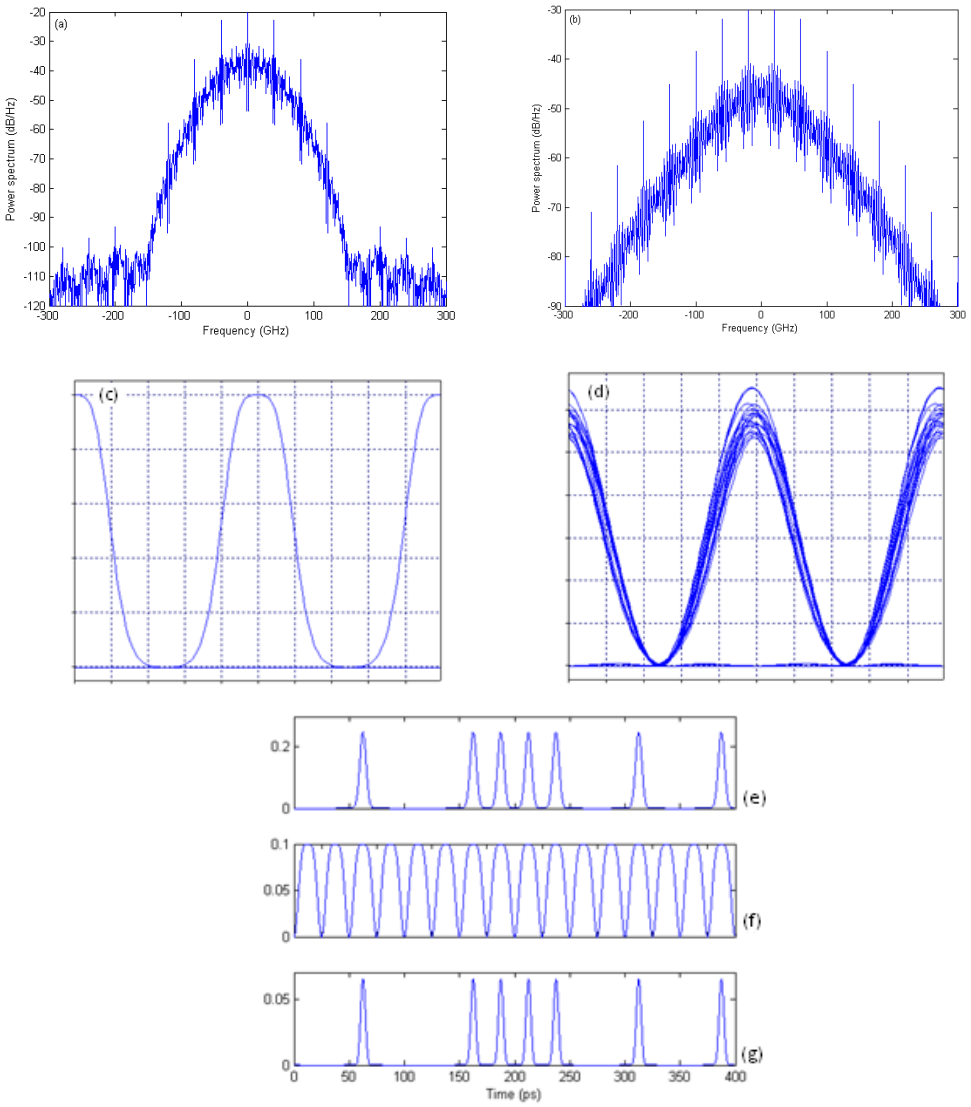

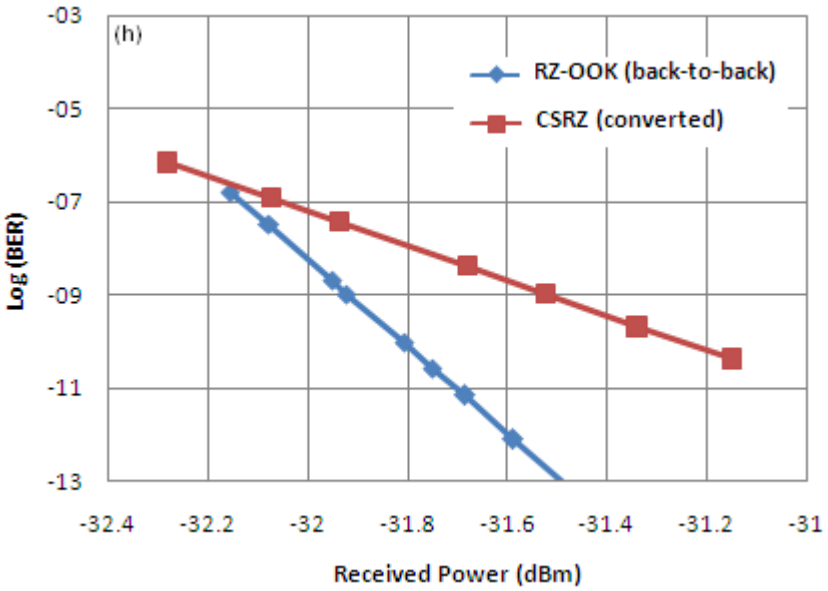

Fig. 6.5 FWM-based 40 Gb/s RZ-OOK to CSRZ-OOK format conversion. Spectrum and eye diagram of (a),(c)RZ-OOK, (b),(d) CSRZ-OOK idler, respectively.(e) Power of the input RZ-OOK signal (f) CSRZ clock (g) generated CSRZ-OOK idler power (h) BER curves for the input and converted signals.

As can be seen in Fig. 6.5 (b) the strong frequency component in the optical spectrum is suppressed leading to CSRZ spectrum. Based on Fig. 6.5(h) there is a 0.33 dB power penalty for the conversion at the bit error rate (BER) level of 10^{-9}. Figure 6.6 shows the gain spectra and waveforms of the waves associated with the NRZ-OOK to CSRZ-OOK format conversion, where the power penalty obtained for the format conversion is 0.7 dB , while Fig. 6.7 contains the data of RZ-DPSK to CSRZ-DPSK showing 0.76 dB power penalty. The spectra and waveforms in Fig. 6.8 are related to the NRZ-DPSK to CSRZ-DPSK format conversion, where it is shown that the power penalty at the BER level of 10^{-9} is 0.93 dB.

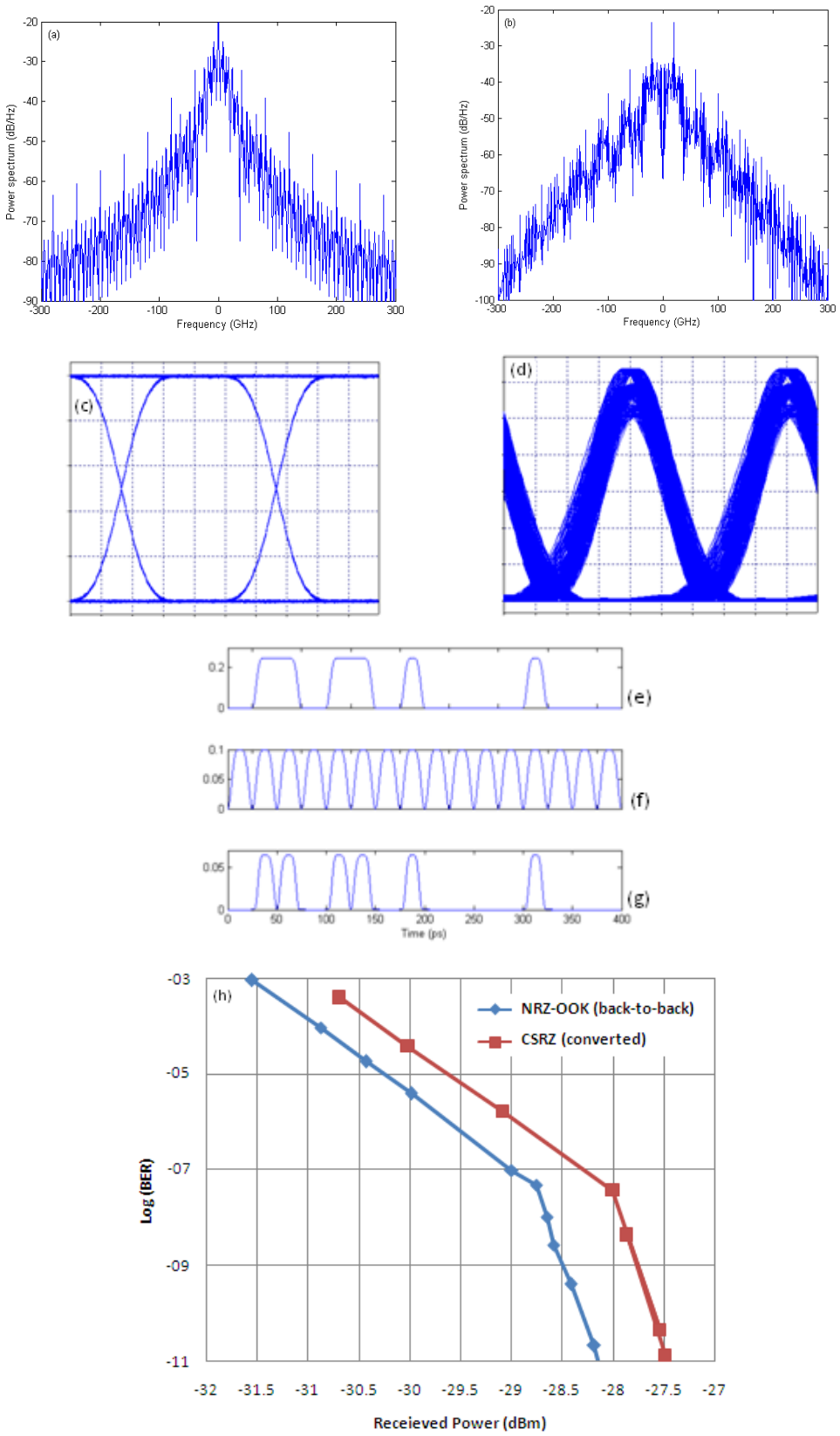

Fig. 6.6 FWM-based 40 Gb/s NRZ-OOK to CSRZ-OOK format conversion (a),(c)NRZ-OOK, (b),(d) CSRZ-OOK idler, respectively.(e) Power of the input

NRZ-OOK signal (f) CSRZ clock (g) generated CSRZ-OOK idler power (h) BER curves for the input and converted signals.

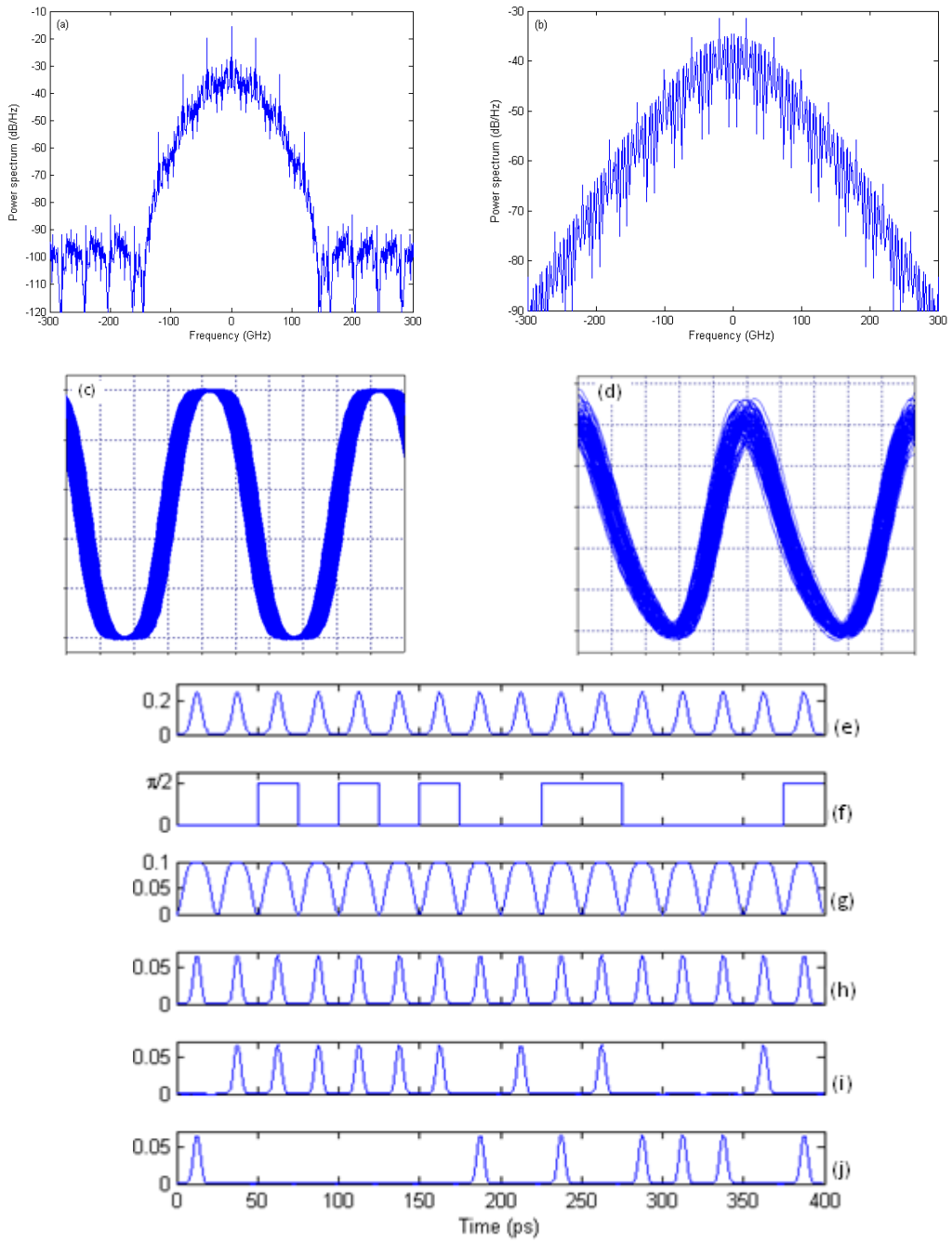

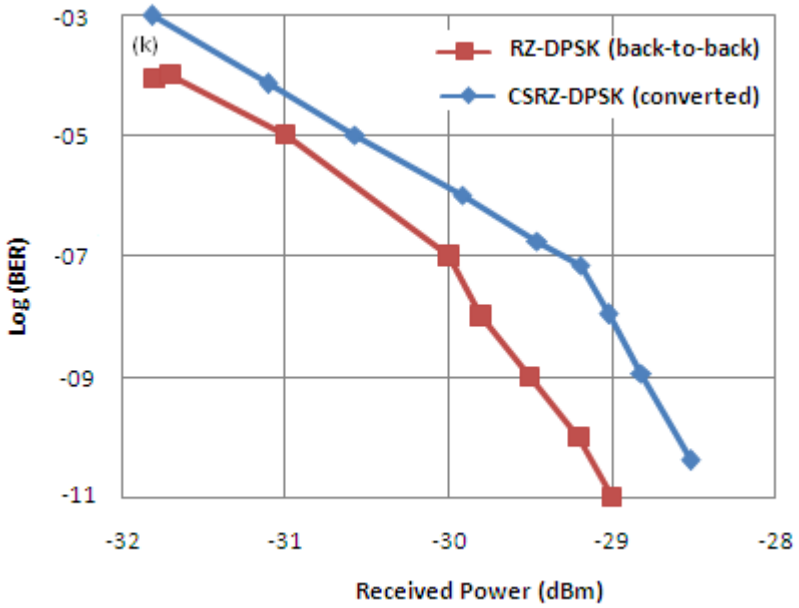

Fig. 6.7 FWM-based 40 Gb/s RZ-DPSK to CSRZ-DPSK format conversion. Spectrum and eye diagram of (a),(c) RZ-DPSK with $(\mathbf{0}, \frac{\pi}{2})$ modulation depth, (b)(d) CSRZ-DPSK idler (e),(f) Power and phase of the input RZ-DPSK signal (g) CSRZ clock (h) generated CSRZ-DPSK idler power (i),(j) Constructive and destructive demodulation outputs. (k) BER curves for the input and converted signals.

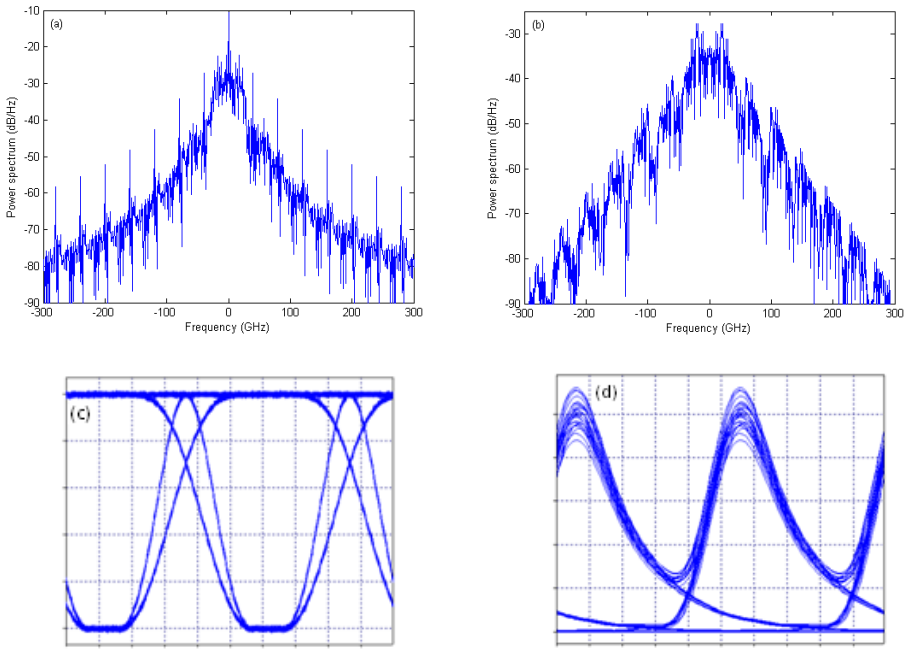

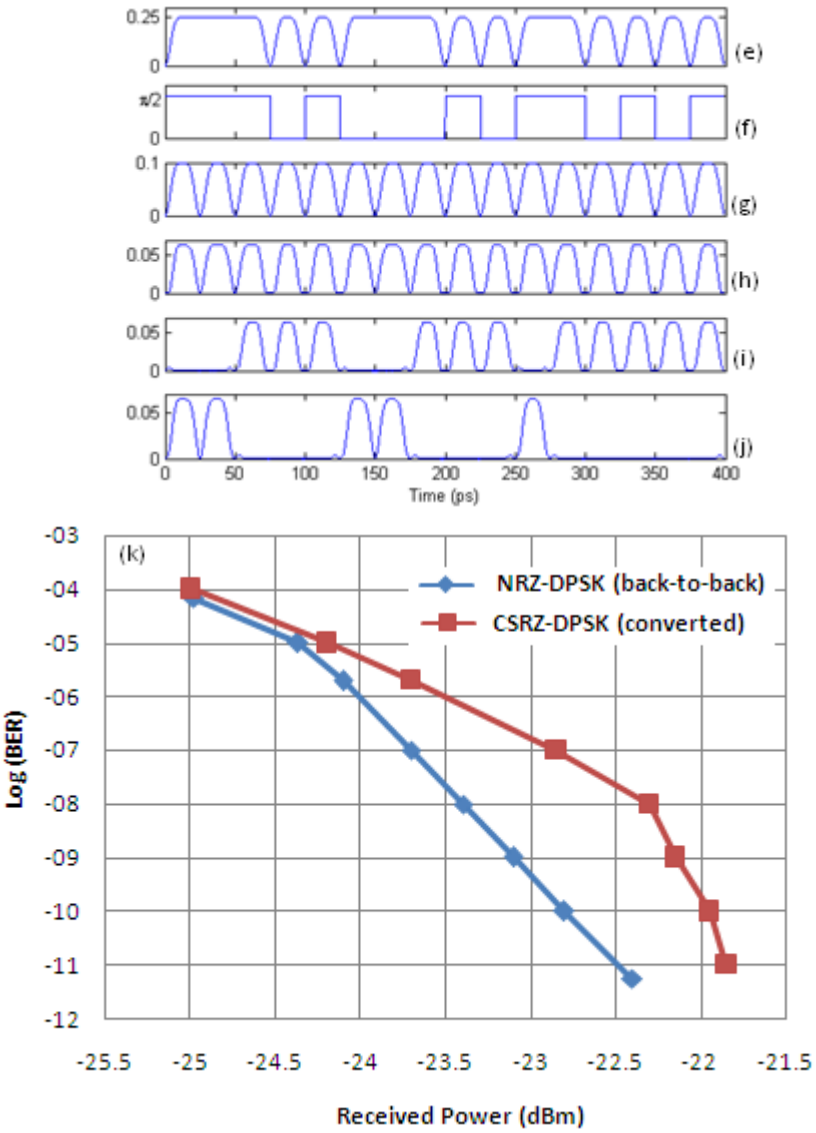

Fig. 6.8 FWM-based 40 Gb/s NRZ-DPSK to CSRZ-DPSK format conversion. Spectrum and eye diagram of (a),(c) NRZ-DPSK with $(\mathbf{0}, \frac{\pi}{2})$ modulation depth, (b)(d) CSRZ-DPSK idler (e),(f) Power and phase of the input NRZ-DPSK signal (g) CSRZ clock (h) generated CSRZ-DPSK idler power (i),(j) Constructive and destructive demodulation outputs. (k) BER curves for the input and converted signals.

6.2 XOR Logic Gate with Intensity and Phase Modulated Inputs

With the speed increase of telecommunication systems going beyond the limit of electronic devices, demands for all-optical logic operations have been rapidly increasing as well. All-optical logic plays an essential role in all-optical signal processing since it can be used for de-multiplexing, addressing, switching and regeneration [128]. Among the logic gates, all-optical exclusive-OR (XOR) can perform some critical functions such as all-optical data comparison for packet address recognition [129], pseudorandom number generation [130], parity checking [131] and packet switching [132].

Semiconductor optical amplifiers (SOAs) are attractive nonlinear elements which have been extensively used for realizing all-optical logic gates, as they exhibit high nonlinearity and can be integrated easily [120, 128, 133, 134]. However setups using SOAs are limited by the gain recovery velocity of SOAs. This issue can be solved by using nonlinearities of optical fibers, owing to the almost instantaneous response of fiber nonlinearity. Recently, optical fibers with relatively high nonlinear coefficient have been manufactured which will help to overcome the limitations caused by the long length of optical fiber-based devices and requirement of high power [135].

In the last few years, several approaches for realizing XOR logic gates for on-off keying (OOK) or phase-shift keying (PSK) input signals have been proposed [56, 120, 136]. Different regions of next generation optical networks are expected to support different modulation formats in order to meet requirements such as bandwidth, spectral efficiency, dispersion and nonlinear tolerance and simplicity [122]; therefore logic gates which can perform logic functions between input signals with different modulation formats will be useful at the interfaces between different network regions. In this case to carry out a logic function between two signals with different modulation formats

there won't be any need to first convert the modulation format of one signal to the same format as the other one and then execute the logic operation. Hence, in this research work a scheme for performing logic XOR between an amplitude modulated signal and a phase modulated one is investigated. This logic gate is based on cross phase modulation (XPM) in a highly nonlinear fiber.

6.2.1 Principle of Operation

When a strong signal pulse at ω_s with peak power P_s propagates through a HNLF along with a weak probe at ω_{pr} with peak power P_{pr} , the phase of the probe pulse is modulated due to the XPM induced by the strong signal. The evolution of the two pulses along the fiber length are described by the following equations

$$\frac{\partial A_s}{\partial z} + \frac{i\beta_{2s}}{2}\frac{\partial^2 A_s}{\partial T^2} = i\gamma(|A_s|^2 + 2|A_{pr}|^2)A_s \tag{6.2.1}$$

$$\frac{\partial A_{pr}}{\partial z} + d\frac{\partial A_{pr}}{\partial T} + \frac{i\beta_{2pr}}{2}\frac{\partial^2 A_{pr}}{\partial T^2} = i\gamma(|A_{pr}|^2 + 2|A_s|^2)A_{pr} \tag{6.2.2}$$

where $\beta_{2x,}(x = pr, s)$ is the second order dispersion parameter at the probe and signal wavelength, respectively. For simplicity, it is assumed that the two signals preserve their polarization during propagation through the fiber and fiber losses are neglected. Parameter d is a measure of group-velocity mismatch between the two pulses known as the walk off parameter which can be obtained by [57]

$$d = \beta_{1pr} - \beta_{1s} \approx \beta_{2s}(\omega_{pr} - \omega_s) + {}^{\beta_{3s}}/_{2}(\omega_{pr} - \omega_s)^2 + {}^{\beta_{4s}}/_{6}(\omega_{pr} - \omega_s)^3 \tag{6.2.3}$$

β_{ix} $(x = s, pr)$ is the ith order dispersion parameter at the signal and probe's frequency. The general solution at $z = L$ is given by

$$A_s(L,T) = A_s(0,T)e^{i\phi_s} \tag{6.2.4}$$

$$A_{pr}(L,T) = A_{pr}(0,T - dL)e^{i\phi_{pr}} \tag{6.2.5}$$

If we assume that the pulses are un-chirped Gaussian pulses of the same width T_0, the initial amplitudes are

$$A_s(0,T) = \sqrt{P_s}\exp(-\frac{T^2}{2T_0^2}) \tag{6.2.6}$$

$$A_{pr}(0,T) = \sqrt{P_{pr}}\exp(-\frac{(T - T_d)^2}{2T_0^2}) \tag{6.2.7}$$

where T_d is the initial time delay between the two pulses. In this case after propagating through a fiber with length L and nonlinear coefficient γ, the time-dependent nonlinear phase shift, $\phi_{pr}(L,T)$, experienced by the probe due to self phase modulation (SPM) and XPM can be found by [63]

$$\phi_{pr}(L,\tau) = \gamma L(P_{pr}e^{-\tau^2} + P_S\frac{\sqrt{\pi}}{\delta}[\mathrm{erf}(\tau - \tau_d) - \mathrm{erf}(\tau - \tau_d - \delta)]) \tag{6.2.8}$$

where $\mathrm{erf}(x)$ is the error function and $\tau = {}^{T}/_{T_0}$, $\tau_d = {}^{T_d}/_{T_0}$ and $\delta = {}^{dL}/_{T_0}$.

Since $P_s \gg P_{Pr}$ the first term in Equation (6.2.8) which is due to SPM can be neglected; hence the induced phase shift experienced by the probe signal will be mainly due to XPM. This nonlinear phase shift leads to frequency chirp which broadens the spectrum. The pump-induced chirp imposed on the probe pulse is obtained from

$$\Delta\nu(\tau) = -\frac{1}{2\pi}\frac{\partial\phi_{pr}}{\partial T} = -sgn(\delta)\frac{\gamma LP_S}{\pi T_0|\delta|}(\mathrm{e}^{-(\tau-\tau_d)^2} - \mathrm{e}^{-(\tau-\tau_d-\delta)^2}) \tag{6.2.9}$$

The induced phase shift due to XPM can be used to realize logic XOR function between an OOK and a binary PSK (BPSK) signal.

The schematic diagram of the proposed logic XOR gate is illustrated in Fig. 6.9, where a strong RZ-OOK data signal at λ_{S1} is launched in to the HNLF with a weak RZ binary phase-shift keying (BPSK) signal at λ_{S2}. The data marks in the OOK signal will induce phase shift on the co-propagating BPSK pulses. The peak power of the OOK pulses are adjusted such that the induced phase shift on the BPSK pulses is "π". Consequently, when an OOK pulse is "1" if the phase of the original BPSK signal is "0" it will change to "π" and if it is "π" it will change to "2π" which is equivalent to "0" due to the periodicity of the phases. This can be seen in the following table

Table 6.1 Truth table of the XOR operation

OOK Power	PSK Phase	XOR	PSK Phase after XPM
0	0 (logic "0")	0	0 (logic "0")
0	π (logic "1")	1	π (logic "1")
1	0 (logic "0")	1	π (logic "1")
1	π (logic "1")	0	2π (logic "0")

As can be seen in table 6.1, after XPM takes place between the two signals, if the resultant PSK signal at the end of the HNLF is de-multiplexed, it will be equivalent to the logic XOR between the two input data signals. The demodulation of the XOR signal can be achieved by using a Mach-Zehnder delay interferometer (MZDI) and a feedback decoder [137]. To avoid parametric interactions, the wavelength of the PSK signal is chosen such that it is not within the optical parametric amplification gain spectrum of the strong OOK signal.

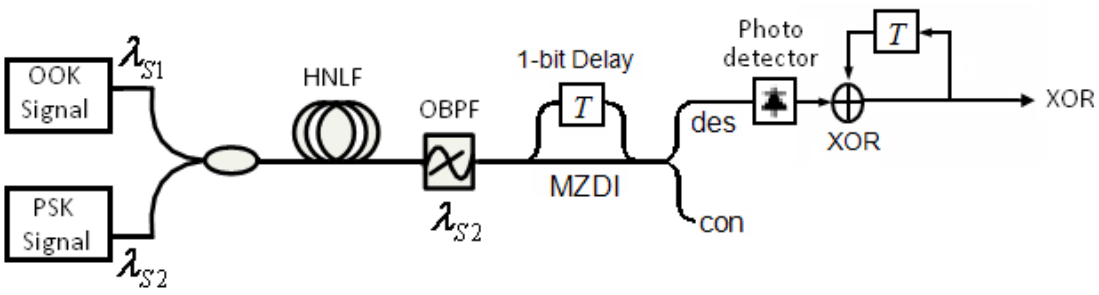

Fig. 6.9 Schematic diagram of the proposed all-optical XOR gate operating between an OOK and a PSK signal.

6.2.2 Results and Discussion

A 200 m HNLF with nonlinear coefficient $\gamma = 20\, W^{-1}Km^{-1}$, zero dispersion wavelength $\lambda_0 = 1550\, nm$, dispersion slope $S = 0.03\, ps/nm^2/km$ and fiber loss α = 0.5 dB/km is considered. Two 40-Gb/s RZ-OOK and RZ-PSK signals placed at 1545 nm and 1565 nm, respectively, are launched in to the HNLF. Both data signals are pseudorandom binary sequences (PRBS) consisting of 1024 pulses. The RZ-OOK signal comes through an optical amplifier with 27 dB gain and a noise figure equal to 5 dB, and a 1 nm bandwidth optical band-pass filter for noise suppression. The peak power of the OOK signal at the fiber input is 26 dBm while that of the BPSK is assumed 3 dBm. A 6nm band-pass filter is used at the output of the HNLF to separate the result of the XPM effect. Numerical simulations based on the nonlinear Schrödinger equation using the split-step Fourier method are carried out. The OOK signal is placed at a wavelength lower than the zero dispersion wavelength so that it's narrow parametric gain spectrum doesn't include the frequency of the BPSK signal as seen in Fig. 6.10.

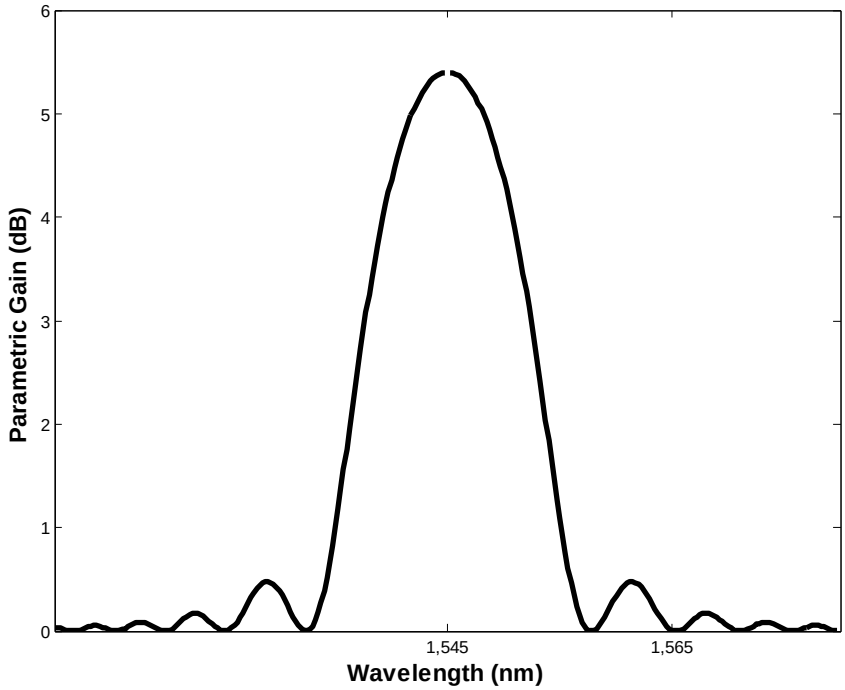

Fig. 6.10 Parametric gain spectrum of the OOK signal.

The simulation results are shown in Fig. 6.11, where the power of the input OOK and BPSK data signals, phase of the input BPSK signal, phase of the BPSK after XPM and its waveform after demodulation are displayed. As can be seen the demodulated BPSK signal (Fig. 6.11 (e)) is equivalent to the XOR operation between the input signals (Fig. 6.11 (a)-(c)). In order to have symmetric spectral broadening of the BPSK spectrum, the initial time delay between the two signals is calculated through Eq. (6.2.9) and set to 0.37 psec. The chirp experienced by the BPSK is shown in Fig. 6.12. The eye pattern of the logic XOR function shown in Fig. 6.13, has a wide eye opening.

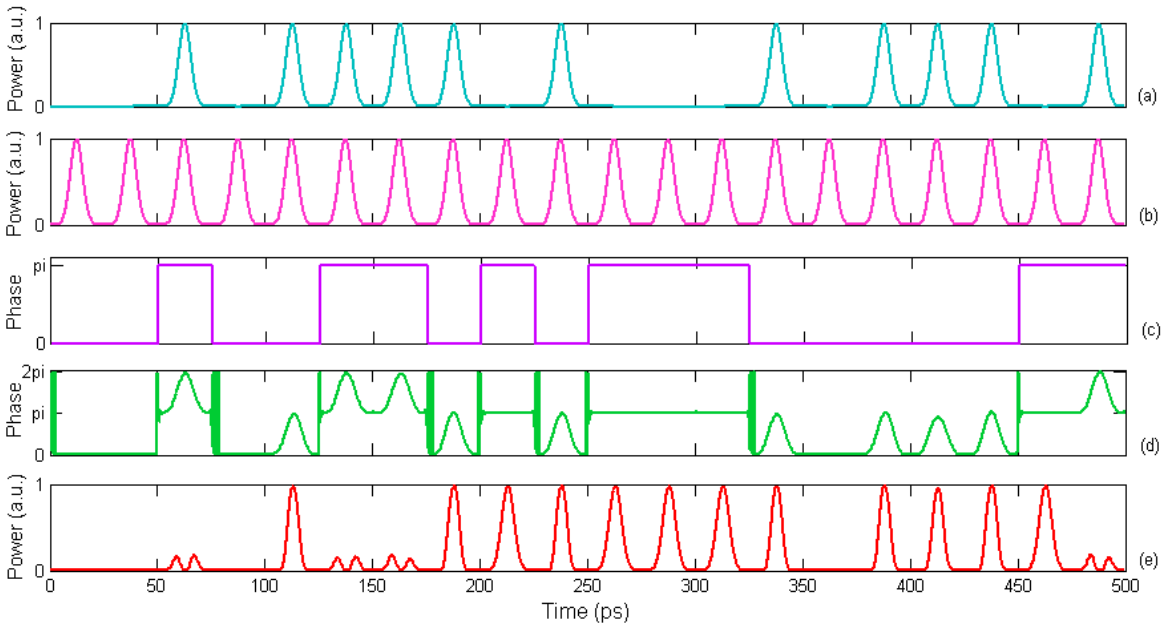

Fig. 6.11 (a),(b) Input OOK and BPSK signal powers, (c) Input BPSK signal phase, (d) BPSK phase after XPM, (e) Demodulated XOR signal.

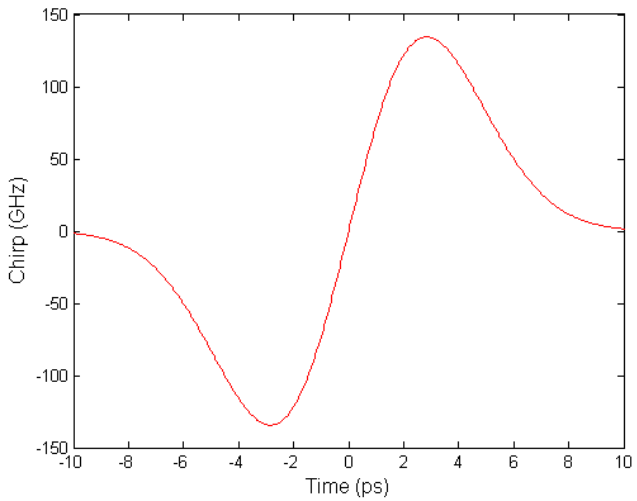

Fig. 6.12 The chirp experienced by the BPSK wave due to XPM

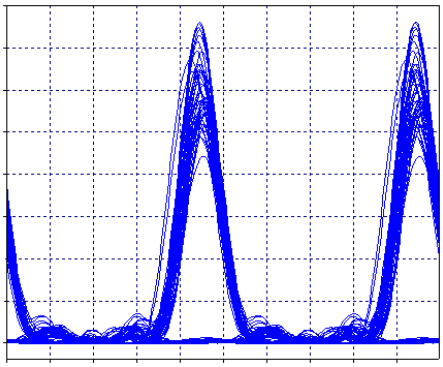

Fig. 6.13 Eye diagram of XOR signal after demodulation (time base: 5 ps/div)

It should be noted that since the XOR gate operates based on XPM in the fiber, the wavelength of the resultant XOR data will not be sufficiently different from that of the probe. Hence the phase of the original data at the probe will not be preserved.

6.3 Numerical Investigation of All-Optical RZ-8-APSK Generation

The capacity of lightwave systems can be increased by increasing the data-rate per channel and also reducing the channel spacing in dense wavelength division multiplexed systems. The distortions caused by linear and nonlinear impairments become worse in high speed DWDM systems. Linear impairments include chromatic dispersion (CD) and polarization mode dispersion (PMD), while self phase modulation, cross phase modulation and four-wave mixing are the nonlinear impairments. In order to reduce these impairments, an optimal modulation format should be chosen. For instance, modulation formats which have a narrow optical spectrum can enhance spectral efficiency and have a higher tolerance to CD distortions and systems which use a modulation format with a constant optical power are less susceptible to SPM and XPM.

The factors which should be taken into account for choosing the modulation format include [138]:

1. Receiver sensitivity
2. Resistance to fiber nonlinearity
3. Tolerance to dispersion accumulation and dispersion map
4. Resistance to polarization mode dispersion (PMD)
5. Achievable spectral efficiency
6. Resistance to concatenated filtering in optically routed networks

7. Complexity and cost of terminal equipment

The importance of each of these items depends on the network types. In metropolitan area networks the dispersion tolerance is the main issue since fiber nonlinearity is often small for such systems. However, in long haul ($\sim 1000\ to\ 3000\ km$) and ultralong-haul ($\gtrsim 3000\ km$) communication systems the receiver sensitivity and mitigating nonlinear impairments are the main factors which should be considered while choosing the modulation format. Spectral efficiency and PMD become important in high speed systems. Moreover, in long-haul networks, modulation formats which are more tolerant to additive amplified spontaneous emission (ASE) noise produced by the EDFAs are of higher interest.

6.3.1 Amplitude and Phase Shift Keying Modulation Format

To realize high capacity optical networks, spectrally efficient modulation formats are of high interest [139]. Multilevel modulation formats, which carry two or more bits in a single symbol, are promising candidates for next generation high-speed high-capacity optical communication systems. By increasing the number of bits transmitted per symbol, the symbol rate can be decreased which in turn reduces the optical bandwidth; thus a greater tolerance to chromatic dispersion will be achieved [140]. The amplitude and phase shift keying (APSK) is one form of multilevel modulation format which has attracted a lot of research recently.

APSK transmitters at 10 Gsymbol/s with up to 32 levels [141] have been experimentally demonstrated by cascading a number of amplitude and phase modulators [142]. However, it should be taken into account that while in

metropolitan networks OOK and PSK formats are used, advanced modulation formats such as APSK are suitable for core networks. Thus, in order to enable flexible cross connections among different networks it is more desirable to perform all-optical format conversion from lower speed signals to a multi-level signal with increased capacity, at the interfaces connecting metropolitan networks to core networks. The elimination of expensive optical-electrical-optical equipment and deployment of all-optical signal processing will help to reduce the implementation cost and re-move the bottleneck for ultrafast signal processing.

Recently all-optical generation of APSK transmitters with 4 levels and 8 levels have been experimentally demonstrated, based on modulation format conversion from NRZ-OOK and through optical amplitude and phase multiplexing, respectively [143, 144].

In this research work another scheme for all-optical generation of 4 levels and 8 levels RZ-APSK modulation format based on four wave mixing and cross phase modulation in a highly nonlinear fiber is presented.

6.3.2 Principle of Operation

The schematic diagram of the proposed multilevel APSK transmitter is shown in Fig. 6.14. Two RZ-OOK signals as control pulses and a RZ-DPSK signal as the probe signal are synchronized and launched into a HNLF. The DPSK signal wavelength is chosen such that it is in the optical parametric amplification gain region of the first OOK signal but not that of the second one. However, both control pulses will induce phase shift on the probe pulse due to XPM. The peak power of the OOK pulses are adjusted such that a mark symbol in the first and second OOK data pulses induces π- and $\pi/2$-phase shift in a probe pulse, respectively. Therefore after propagating in the

fiber, the input DPSK signal gets modulated in its phase and amplitude, leading to a RZ-8-APSK modulation format signal. The 8 different cases are shown in Table 6.2.

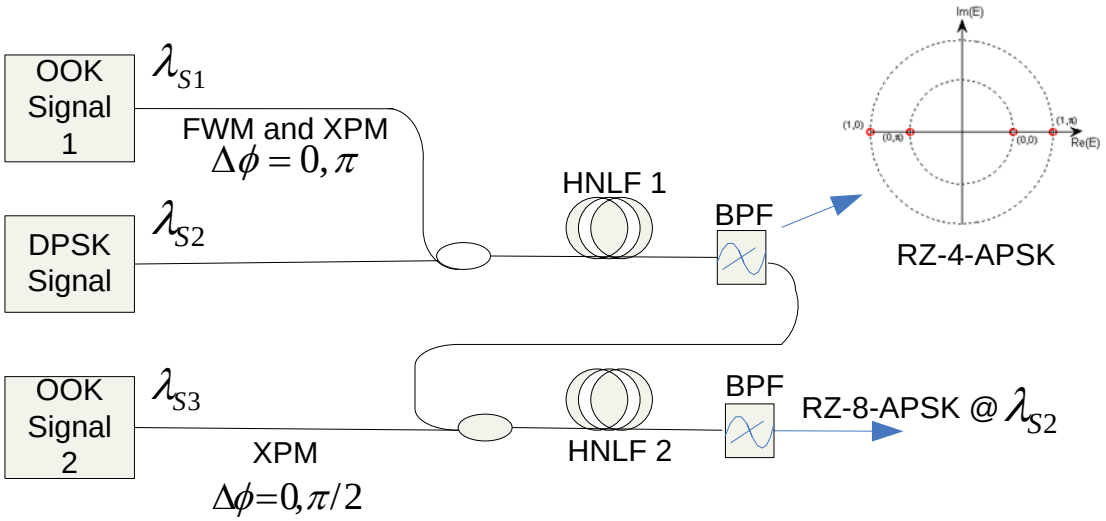

Fig. 6.14 Schematic diagram of the proposed 8 level APSK transmitter.

Table 6.2 The 8 Levels of RZ-8-APSK

OOK 1	OOK 2	DPSK	Gain	Induced Phase
0	0	0	x	0
0	0	π	x	0
0	1	0	x	$\pi/2$
0	1	π	x	$\pi/2$
1	0	0	✓	π
1	0	π	✓	π
1	1	0	✓	$3\pi/2$
1	1	π	✓	$3\pi/2$

6.3.3 Results and Discussion

Two 200 m HNLFs with nonlinear coefficient $\gamma = 20\ W^{-1}Km^{-1}$, zero dispersion wavelength $\lambda_0 = 1550\,nm,$ dispersion slope $S = 0.03\,ps/nm^2/km$ and fiber loss $\alpha = 0.5\,dB/km$ are considered. In practice is better to concatenate fibers with slightly different Brillouin shift to suppress Brillouin scattering. 40 Gb/s RZ-OOK data signals 1 and 2 (control pulses) placed at 1550 and 1520 nm, are each passed through an optical amplifier with 27 and 24 dB gain and 4.5 dB noise figure, respectively, followed by a 1.4 nm optical band-pass filter for noise suppression. The peak powers of OOK signals 1 and 2 at the input of HNLF1 and HNLF2 are 27 dBm and 22.5 dBm correspondingly. The wavelength and peak power of the 40 Gb/s RZ-DPSK probe signal are 1539 nm and 3dBm, correspondingly. All three signals are PRBS data of length $2^9 - 1$. The initial delays between the OOK and DPSK pulses are adjusted such that the spectral broadening of the DPSK spectrum is symmetric. The OOK signal 1 and the DPSK signal are launched in the first fiber, to generate an 80Gb/s RZ-4-APSK signal, which is a result of XPM and optical parametric amplification. As can be seen in Fig. 6.15 the gain which the DPSK signal experiences in HNLF1 is 7 dB. It can also be observed from this figure, that the DPSK probe signal isn't within the parametric gain region of data signal 2, therefore probe pulses won't be amplified in HNLF2.

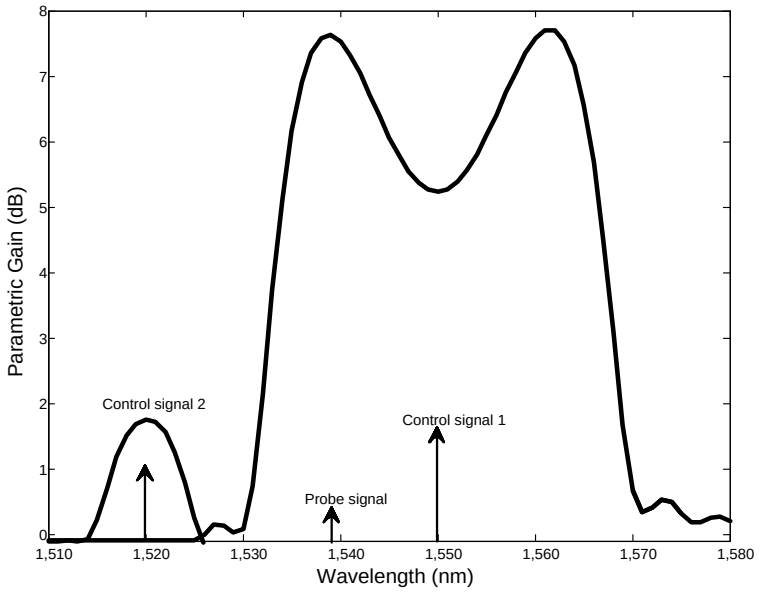

Fig. 6.15 Parametric gain spectrum of the two OOK control signals.

The generated RZ-4-APSK signal in HNLF1 is guided to HNLF2 along with OOK data signal 2. The mark symbols of OOK signal 2 will induce $\pi/2$-phase shift in the RZ-4-APSK pulses; therefore, a 120Gb/s RZ-8-APSK signal is generated. Numerical simulations based on the nonlinear Schrödinger equation using the split-step Fourier method have been carried out. In Fig. 6.16 the power and phase of the input signals and the generated RZ-4APSK and RZ-8-APSK data are displayed.

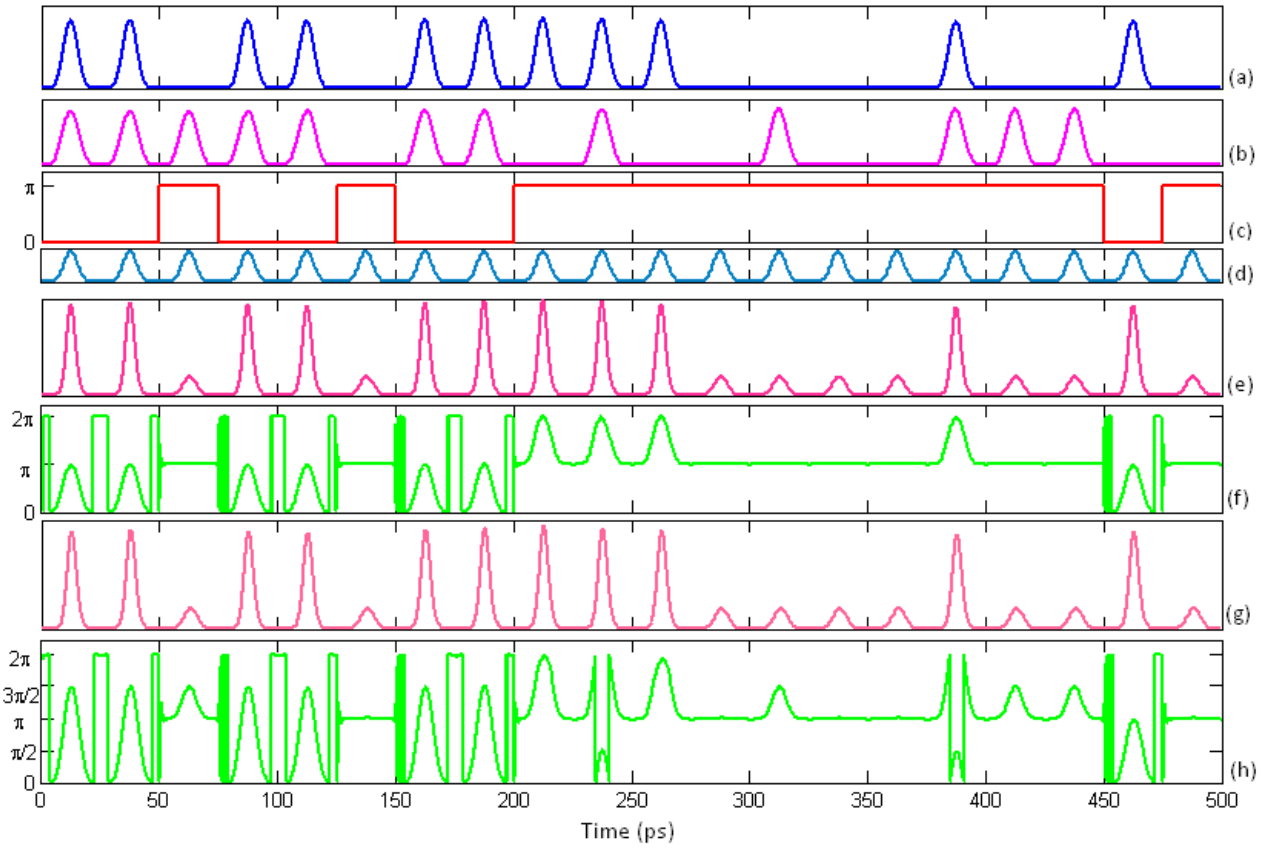

Fig. 6.16 (a) Power of OOK 1 (b)Power of OOK 2, (c) ,(d)Phase and power of DPSK signal , (e) ,(f) Power and phase of RZ-4-APSK at the output of HNLF1, (g) ,(f) Power and phase of RZ-8-APSK at the output of HNLF2.

The obtained constellation map for the generated 8 level APSK signal at the bit centers is demonstrated in Fig. 6.17. Due to the noise fluctuations in the peak power of the OOK pulses, the induced XPM phase shift will have small deviations from π and $\pi/2$.

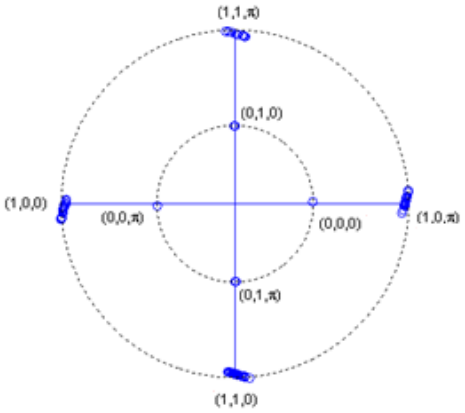

Fig. 6.17 Constellation map for the generatedRZ-8-APSK signal.

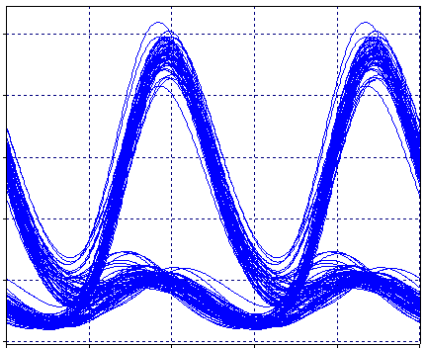

Fig. 6.18 Eye diagram of direct detected RZ-8-APSK (time base:10 ps/div)

The eye diagram of the directly detected RZ-8-APSK signal is shown in Fig. 6.18, where the two amplitude levels of the data can be seen. The BER curves for the input DPSK signal, generated RZ-4-DPSK and RZ-8-DPSK signals are shown in Fig, 6.19. The power penalty for the RZ-4-DPSK is 1.05 dB while that of the RZ-8-DPSK is 1.28 dB.

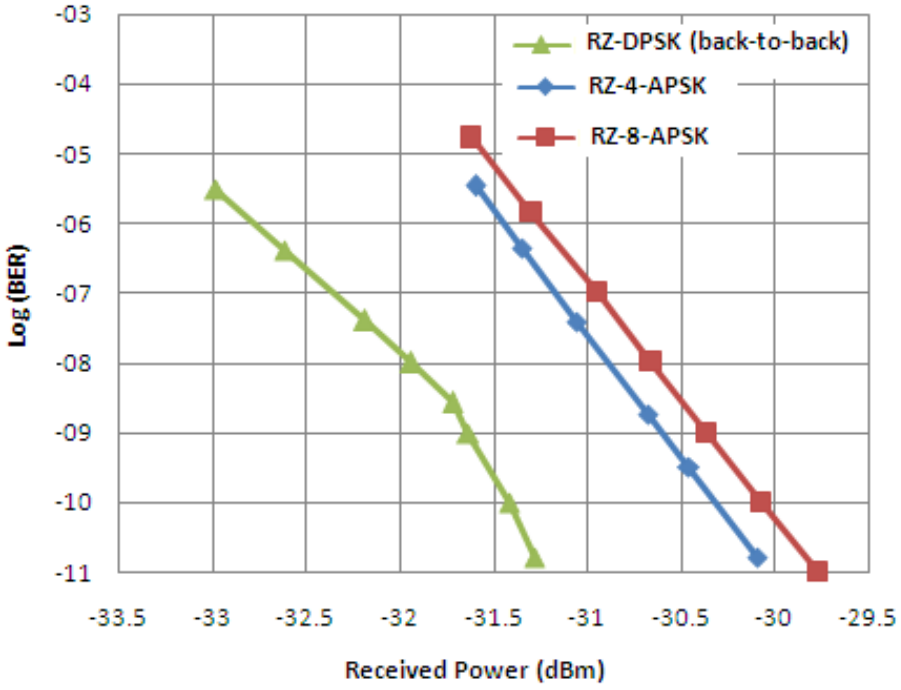

Fig 6.19 BER curves for the input DPSK signal, RZ-4-APSK and RZ-8-APSK signals.

6.4 Summary

Three applications of FWM and XPM in all-optical signal processing are mentioned in this chapter. A format conversion module is presented which can be used for converting NRZ/RZ-OOK to CSRZ-OOK and NRZ/RZ-DPSK to CSRZ-DPSK based on FWM. Compared to other similar methods for format conversion, in this scheme the number of required pumps is less which will make it more cost-effective and simple.

An all-optical logic XOR gate is proposed which operates between a phase modulated and an intensity modulated signal. Thus, to carry out logic XOR function between the two signals with different modulation formats there won't be any need to first convert the modulation format of one signal to the same format as the other one and then execute the logic operation. The working principle of this logic gate is based on XPM in a HNLF.

By using the combination of FWM and XPM it is shown that amplitude and phase shift keying signals can be generated by all-optical means. While the parametric amplification due to FWM provides two levels of amplitude, the induced phase by XPM provides 4 levels of phase. Hence, overall 8 different levels of APSK format are generated.

For the signal processing applications, it is better to concatenate fibers with slightly different Brillouin shift and reduce the launched power into the fibers to suppress Brillouin scattering.

Chapter 7

Conclusions

This research work mainly focuses on the properties and applications of fiber optical parametric amplifiers, which work based on a nonlinear phenomenon in fibers known as the four-wave mixing.

It is desired to have a flat gain spectrum in any amplifier, and this can be achieved in single pump FOPAs by cascading several HNLFs which have different parameters. To find the parameters of each HNLF, in previously reported research work, the second order dispersion at the pump wavelength and the fiber length were optimized for each of the cascaded fiber sections and the fourth order dispersion was assumed constant for all sections. Given that the fourth order dispersion of the fiber also has a great influence on the shape of the gain spectrum, in this work it is optimized along with the other two parameters by the use of a genetic algorithm. The results show improvement in the gain flatness compared to previously reported approaches. Thus by controlling the fourth order dispersion of a HNLF the flat gain bandwidth of the amplifier increases significantly. This is practical, since recent researches in fabricating HNLFs show that it is possible to adjust the fourth order dispersion by controlling the dispersion slope of the HNLF. The effect of ZDW fluctuations on the flatness of the gain spectrum is studied. As long as the average ZDW of the fiber sections are maintained close to the optimum values a relatively flat gain spectrum can be achieved. The noise properties of such a multi-section FOPA are studied and a noise figure less than 4dB in the gain bandwidth is obtained.

The four wave mixing behavior in a fiber loop mirror composed of two dispersion shifted fibers and a single mode fiber is theoretically investigated. Based on the results, the signal to idler conversion efficiency for signal wavelengths close to the pump increases considerably for this design compared to the loop mirror configurations reported earlier. This is due to the SMF which acts as a phase shifter and changes the relative phase relation between the pump, signal and idler generated in the first DSF before entering the second DSF and vice versa. This phase shift will change the gain and conversion efficiency in the second DSF and as a result will change the overall conversion efficiency of the loop mirror.

An all-optical method for simultaneous de-multiplexing and demodulating RZ-DPSK OTDM signals has been proposed and numerically investigated. By using this approach the DPSK OTDM channels which are de-multiplexed can be demodulated at the same time without requiring an external demodulator. This scheme has a loop mirror configuration, where the de-multiplexing is based on FWM wavelength conversion in a HNLF and the demodulation is based on wavelength-dependant group delay in a dispersive element. To use this approach for demodulating DPSK signals at low bit rates a large delay is required which can be achieved either by increasing the wavelength conversion bandwidth or by increasing the dispersion. Since increasing the dispersion will degrade the signal, the better option would be to use a dual pump FOPA instead of a single pump, where it is easier to obtain a larger wavelength conversion bandwidth.

The fast response of nonlinear effects in optical fibers has made HNLF a suitable medium for realizing all-optical signal processing. New schemes based on FWM and XPM for all-optical signal processing have been proposed and investigated.

A modulation format conversion module based on FWM is presented which can be used for converting NRZ/RZ intensity and phase modulated

format to CSRZ-OOK and CSRZ-DPSK, respectively. The number of required input laser beams in this scheme is less than previously reported ones, which makes it more cost-effective and simple.

A Logic gate which can operate between input signals of different modulation formats is useful at the interfaces between different network regions. It is shown that the phase shift which a strong signal induces on a weaker signal due to XPM can be used for realizing an all-optical logic XOR gate which operates between a phase modulated and an intensity modulated signal. In this method, to carry out logic XOR function between the two signals with different modulation formats there won't be any need to first convert the modulation format of one signal to the same as that of the other's and then execute the logic operation.

All-optical generation of multilevel modulation format signals is desired in order to enable flexible cross connections between various networks. Numerical studies show that the combination of FWM and XPM can be used to generate RZ 8 level amplitude and phase shift keying signals. While the two levels of amplitude can be obtained by FWM due to parametric amplification, the different phase levels are achieved by the induced phase by XPM.

The recent advances in nonlinear material, such as photonic crystal structures, silicon and chalcogenide waveguides, has led to the reduction of the powers required for nonlinear optical signal processing and has paved the way for on-chip integration of processing devices. These advances enable the development of novel optical signal processing designs for practical deployment, which should be considered in future studies.

References

[1] T. Miya, Y. Terunuma, T. Hosaka, and T. Miyashita, "Ultimate low-loss single-mode fibre at 1.55 μm," *Electronics Letters*, vol. 15, pp. 106-108, 1979.

[2] S. Kawanishi, H. Takara, K. Uchiyama, M. Saruwatari, and T. Kitoh, "Single polarization completely time-division-multiplexed 100 Gb/s optical transmission experiment," in *Proceedings of European Conference on Optical Communication, ECOC 1993*, pp. 53-56, 1993.

[3] S. Weisser, S. Ferber, L. Raddatz, R. Ludwig, A. Benz, C. Boerner, and H. G. Weber, "Single- and alternating polarization 170 Gb/s transmission up to 4000 km using dispersion-managed fiber and all-Raman amplification," *IEEE Photonics Technology Letters*, vol. 18, pp. 1320-1322, 2006.

[4] H. G. Weber, S. Ferber, M. Kroh, C. Schmidt-Langhorst, R. Ludwig, V. Marembert, C. Boerner, F. Futami, S. Watanabe, and C. Schubert, "Single channel 1.28 T/s and 2.56 Tb/s DQPSK transmission," *Electronics Letters*, vol. 42, pp. 178-179, 2006.

[5] S. Sugimoto, K. Minemura, K. Kobayashi, M. Seki, M. Shikada, A. Ueki, T. Yanase, and T. Miki, "High-speed digital-signal transmission experiments by optical wavelength-division multiplexing," *Electronics Letters*, vol. 13, pp. 680-682, 1977.

[6] D. Qian, M. Huang, E. Ip, Y. Huang, Y. Shao, J. Hu, and T. Wang, "101.7-Tb/s (370×294-Gb/s) PDM-128QAM-OFDM Transmission over 3×55-km SSMF using Pilot-based Phase Noise Mitigation," in *Optical Fiber Communication Conference, OFC 2011*, 2011.

[7] R. J. Mears, L. Reekie, I. M. Jauncey, and D. N. Payne, "Low-noise erbium-doped fibre amplifier operating at 1.54pm," *Electronics Letters*, vol. 23, pp. 1026-1028, 1987.

[8] M. Tachibana, R. I. Laming, P. R. Morkel, and D. N. Payne, "Erbium-doped fiber amplifier with flattened gain spectrum," *IEEE Photonics Technology Letters*, vol. 3, pp. 118-120, 1991.

[9] J. F. Massicott, J. R. Armitage, R. Wyatt, B. J. Ainslie, and S. P. Craig-Ryan, "High Gain, Broadband, 1.6 mμ $Er3^{+}$ Doped Silica Fibre Amplifier," *Electronics Letters*, vol. 26, pp. 1645-1646, 1990.

[10] S. Aozasa, T. Sakamoto, T. Kanamori, K. Hoshino, and M. Shimizu, "Gain-shifted thulium-doped fibre amplifiers employing novel high concentration doping technique," *IET Electronics Letters*, vol. 36, pp. 418-419, 2000.

[11] C. V. Raman and K. S. Krishnan, "A new type of secondary radiation," *Nature*, vol. 121, p. 501, 1928.

[12] C. Lin and R. Stolen, "Backward Raman amplification and pulse steepening in silica fibers," *Applied Physics Letters*, vol. 29, pp. 428-431, 1976.

[13] M. N. Islam, "Raman amplifiers for telecommunications," *IEEE Journal of Selected Topics in Quantum Electronics*, vol. 8, pp. 548-559, 2002.

[14] R. H. Stolen, "Phase-matched-stimulated four-photon mixing in silica-fiber waveguides," *IEEE Journal of Quantum Electronics*, vol. 11, pp. 100-103, 1975.

[15] F. S. Yang, M. E. Marhic, and L. G. Kazovsky, "CW fibre optical parametric amplifier with net gain and wavelength conversion efficiency >1," *Electronics Letters,* vol. 32, pp. 2336 -2338, 1996.
[16] T. Torounidis, P. A. Andrekson, and B.-E. Olsson, "Fiber-Optical Parametric Amplifier With 70-dB Gain," *IEEE Photonics Technology Letters,* vol. 18, pp. 1194-1196, May 15 2006.
[17] M. E. Marhic, K. K. Y. Wong, and L. G. Kazovsky, "Wide-Band Tuning of the Gain Spectra of One-Pump Fiber Optical Parametric Amplifiers," *IEEE Journal of Quantum Electronics,* vol. 10, pp. 1133-1141, 2004.
[18] M. E. Marhic, K. K. Y. Wong, M. C. Ho, and L. G. Kazovsky, "92% pump depletion in a continuous-wave one-pump fiber optical parametric amplifier," *Optics Letters,* vol. 26, pp. 620-622, May 1 2001.
[19] T. Torounidis and P. A. Andrekson, "Broadband Single-Pumped Fiber-Optic Parametric Amplifiers," *IEEE Photonics Technology Letters,* vol. 19, pp. 650-652, May 2007.
[20] G. Kalogerakis, M. E. Marhic, K. K. Y. Wong, and L. G. Kazovsky, "Transmission of optical communication signals by distributed parametric amplification," *Journal of Lightwave Technology,* vol. 23, pp. 2945-2953, 2005.
[21] R. Tang, P. Devgan, P. L. Voss, V. S. Grigoryan, and P. Kumar, "In-Line Frequency-Nondegenerate Phase-Sensitive Fiber-Optical Parametric Amplifier," *IEEE Photonics Technology Letters,* vol. 17, pp. 1845-1847, 2005.
[22] J. Hansryd, P. A. Andrekson, M. Westlund, J. Li, and P. O. Hedekvist, "Fiber-based optical parametric amplifiers and their applications," *IEEE Journal of Selected Topics in Quantum Electronics,* vol. 8, pp. 506-520, 2002.
[23] M. Westlund, J. Hansryd, P. A. Andrekson, and S. N. Knudsen, "Transparent wavelength conversion in fibre with 24 nm pump tuning range," *Electronics Letters,* vol. 38, pp. 85-86, 2002.
[24] J. A. Levenson, I. Abram, T. Rivera, and P. Grangier, "Reduction of quantum noise in optical parametric amplification," *Journal of the Optical Society of America B,* vol. 10, pp. 2233-2238, 1993.
[25] W. Imajuku, A. Takada, and Y. Yamabayashi, "Inline coherent optical amplifier with noise figure lower than 3 dB quantum limit," *IET Electronics Letters,* vol. 36, pp. 63-64, 2000.
[26] R. Stolen, "Polarization effects in fiber Raman and Brillouin lasers," *IEEE Journal of Quantum Electronics,* vol. 15, pp. 1157-1160, 1979.
[27] H. H. Kee, C. R. S. Fludger, and V. Handerek, "Statistical properties of polarisation dependent gain in fibre Raman amplifiers," in *Proceedings of Optical Fiber Communication Conference and Exhibit (OFC 2002)*, pp. 180-181, 2002.
[28] W. Kenneth K.-Y. , M. E. Marhic, K. Uesaka, and L. G. Kazovsky, "Polarization-Independent Two-Pump Fiber Optical Parametric Amplifier," *IEEE Photonics Technology Letters,* vol. 14, pp. 911-913, 2002.
[29] W. Kenneth K.-Y. , M. E. Marhic, K. Uesaka, and L. G. Kazovsky, "Polarization-independent one-pump fiber-optical parametric amplifier," *IEEE Photonics Technology Letters,* vol. 14, pp. 1506-1508, 2002.
[30] T. Torounidis, "Fiber Optical Parametric Amplifiers in Single and Multi Wavelength Applications," PhD Thesis, Department of Microtechnology and Nanoscience, Chalmers University, Goteborg, Sweden, 2006.

[31] R. I. Laming, M. N. Zervas, and D. N. Payne, "Erbium-doped fiber amplifier with 54 dB gain and 3.1 dB noise figures," *IEEE Photonics Technology Letters,* vol. 4, pp. 1345-1347, 1992.
[32] E. Desurvire, M. Papuchon, J. P. Pocholle, J. Raffy, and D. B. Ostrowsky, "High-gain optical amplification of laser diode signal by Raman scattering in single-mode fibres," *IET Electronics Letters,* vol. 19, pp. 751-753, 1983.
[33] H. Masuda, A. Mori, K. Shikano, K. Oikawa, K. Kato, and M. Shimizu, "Ultra-wide-band Raman amplifier using tellurite and silica fibres," *Electronics Letters,* vol. 38, pp. 867-868, 2002.
[34] P. L. Voss, R. Tang, and P. Kumar, "Measurement of the photon statistics and the noise figure of a fiber-optic parametric amplifier," *Optics Letters,* vol. 28, pp. 549-551, 2003.
[35] K. Krastev and J. Rothman, "Crosstalk in fiber parametric amplifier " in *Proceedings of the 27th European Conference on Optical Communication (ECOC '01)*, pp. 378-379, Amsterdam, 2001.
[36] T. Torounidis, H. Sunnerud, P. O. Hedekvist, and P. A. Andrekson, "Amplification of WDM signals in fiber-based optical parametric amplifiers," *IEEE Photonics Technology Letters,* vol. 15, pp. 1061-1063, 2003.
[37] J. M. C. Boggio, F. A. Callegari, J. D. Marconi, A. Guimara˜es, and H. L. Fragnito, "Influence of zero dispersion wavelength variations on cross-talk in single-pumped fiber optic parametric amplifiers," *Optics Communications,* vol. 242, pp. 471–478, 2004.
[38] J. M. C. Boggio, E. A. M. Fagotto, M. E. Marhic, F. A. Callegari, and H. L. Fragnito, "Amplification of 12 × 10 Gb/s WDM signals with negligible FWM crosstalk in a double-pumped fiber optical parametric amplifier," *Optics Communications,* vol. 280, pp. 468-471, 2007.
[39] K. K. Y. Wong, G.-W. Lu, and L.-K. Chen, "Polarization-interleaved WDM signals in a fiber optical parametric amplifier with orthogonal pumps," *Optics Express,* vol. 15, pp. 56-61, 2007.
[40] M. Jamshidifar, A. Vedadi, and M. E. Marhic, "Reduction of Four-Wave-Mixing Crosstalk in a Short Fiber-Optical Parametric Amplifier," *IEEE Photonics Technology Letters,* vol. 21, pp. 1244-1246, 2009.
[41] B. P.-P. Kuo, P. C. Chui, and K. K.-Y. Wong, "A Comprehensive Study on Crosstalk Suppression Techniques in Fiber Optical Parametric Amplifier by Modulation Format," *IEEE Journal of Selected Topics in Quantum Electronics,* vol. 14, pp. 659-665, 2008.
[42] N. E. Dahdah, D. S. Govan, M. Jamshidifar, N. J. Doran, and M. E. Marhic, "1-Tb/s DWDM Long-Haul Transmission Employing a Fiber Optical Parametric Amplifier," *IEEE Photonics Technology Letters,* vol. 22, pp. 1171-1173, 2010.
[43] K. Inoue, "Arrangement of fiber pieces for a wide wavelength conversion range by fiber four-wave mixing," *Optics Letters,* vol. 19, pp. 1189-1191, 1994.
[44] M. N. Islam and Ö. Boyraz, "Fiber Parametric Amplifiers for Wavelength Band Conversion," *IEEE Journal of Selected Topics in Quantum Electronics,* vol. 8, pp. 527-537, 2002.
[45] A. T. Clausen, L. Oxenlowe, C. Peucheret, H. N. Poulsen, P. Jeppesen, S. N. Knudsen, and L. Gruner-Nielsen, "10-GHz return-to-zero pulse source tunable in wavelength with a single- or multiwavelength output based on four-wave

mixing in a newly developed highly nonlinear fiber," *IEEE Photonics Technology Letters,* vol. 13, pp. 70-72, 2001.

[46] P. O. Hedekvist, M. Karlsson, and P. A. Andrekson, "Fiber four-wave mixing demultiplexing with inherent parametric amplification," *Journal of Lightwave Technology,* vol. 15, pp. 2051-2058, 1997.

[47] J. Hansryd and P. A. Andrekson, "O-TDM Demultiplexer with 40-dB Gain Based on a Fiber Optical Parametric Amplifier," *IEEE Photonics Technology Letters,* vol. 13, pp. 732-734, 2001.

[48] L. Jie, J. Hansryd, P. O. Hedekvist, P. A. Andrekson, and S. N. Knudsen, "300-Gb/s eye-diagram measurement by optical sampling using fiber-based parametric amplification," *IEEE Photonics Technology Letters,* vol. 13, pp. 987-989, 2001.

[49] M. Jinno and T. Matsumoto, "Ultrafast, low power, and highly stable all-optical switching in an all polarization maintaining fiber Sagnac interferometer," *IEEE Photonics Technology Letters,* vol. 2, pp. 349-351, 1990.

[50] S. Radic, C. J. McKinstrie, R. M. Jopson, A. H. Gnauck, J. C. Centanni, and A. R. Chraplyvy, "Multiple-band bit-level switching in two-pump fiber parametric devices," *IEEE Photonics Technology Letters,* vol. 16, pp. 852-854, 2004.

[51] Q. Lin, R. Jiang, C. F. Marki, C. J. McKinstrie, R. Jopson, J. Ford, G. P. Agrawal, and S. Radic, "40-gb/s optical switching and wavelength multicasting in a two-pump parametric device," *IEEE Photonics Technology Letters,* vol. 17, pp. 2376-2378, 2005.

[52] T. Sakamoto, F. Futami, K. Kikuchi, S. Takeda, Y. Sugaya, and S. Watanabe, "All-optical wavelength conversion of 500-fs pulse trains by using a nonlinear-optical loop mirror composed of a highly nonlinear DSF," *IEEE Photonics Technology Letters,* vol. 13, pp. 502-504, 2001.

[53] O. Aso, A. Shin-Ichi, T. Yagi, M. Tadakuma, Y. Suzuki, and S. Namiki, "Broadband four-wave mixing generation in short optical fibres," *IET Electronics Letters,* vol. 36, pp. 709-711, 2000.

[54] T. Tanemura and K. Kikuchi, "Polarization-independent broad-band wavelength conversion using two-pump fiber optical parametric amplification without idler spectral broadening," *IEEE Photonics Technology Letters,* vol. 15, pp. 1573-1575, 2003.

[55] T. Yamamoto, E. Yoshida, and M. Nakazawa, "Ultrafast nonlinear optical loop mirror for demultiplexing 640 Gbit/s TDM signals," *Electronics Letters,* vol. 34, pp. 1013-1014, 1998.

[56] D. M. F. Lai, C. H. Kwok, T. I. Yuk, and K. K. Y. Wong, "Picosecond All-Optical Logic Gates (XOR, OR, NOT, and AND) in a Fiber Optical Parametric Amplifier," in *Proceedings of Optical Fiber Communication Conference (OFC 2008)*, 2008.

[57] B. Adonis, V. Pantelis, and S. Dimitris, "Numerical Investigation of a 160-Gb/s Reconfigurable Photonic Logic Gate Based on Cross-Phase Modulation in Fibers," *IEEE Photonics Technology Letters* vol. 19, pp. 402-404, 2007.

[58] S. H. Lee, K. Chow, and C. Shu, "Spectral filtering from a cross-phase modulated signal for RZ to NRZ format and wavelength conversion," *Optics Express,* vol. 13, pp. 1710-1715, 2005.

[59] C. H. Kwok and L. Chinlon, "Simultaneous 4x10 Gb/s NRZ-to-RZ Modulation Format Conversion in Nonlinear Optical Loop Mirror With a

Photonic Crystal Fiber," *IEEE Photonics Technology Letters*, vol. 19, pp. 1825-1827, 2007.
[60] L. Ju Han, T. Nagashima, T. Hasegawa, O. Seiki, N. Sugimoto, H. Young-Geun, L. Sang Bae, and K. Kikuchi, "Output performance investigation of self-phase-modulation-based 2R regenerator using bismuth oxide nonlinear fiber," *IEEE Photonics Technology Letters*, vol. 18, pp. 1296-1298, 2006.
[61] E. Ciaramella, F. Curti, and S. Trillo, "All-optical signal reshaping by means of four-wave mixing in optical fibers," *IEEE Photonics Technology Letters*, vol. 13, pp. 142-144, 2001.
[62] R. H. Hardin and F. D. Tappert, "Applications of the split-step Fourier method to the numerical solution of nonlinear and variable coefficient wave equations," *SIAM Rev. Chronicle*, vol. 15, p. 423, 1973.
[63] G. P. Agrawal, *Nonlinear Fiber Optics*, Fourth ed.: Academic Press, 2007.
[64] Y. P. Yatsenko, A. D. Pryamikov, V. M. Mashinsky, M. E. Likhachev, A. O. Mavritsky, E. M. Dianov, A. N. Guryanov, V. F. Khopin, and M. Y. Salgansky, "Four-wave mixing with large Stokes shifts in heavily Ge-doped silica fibers," *Optics Letters*, vol. 30, pp. 1932-1934, 2005.
[65] T. Nakanishi, M. Hirano, T. Okuno, and M. Onishi, "Silica-based highly nonlinear fiber with gamma = 30/W/km and its FWM-based conversion efficiency," in *Proceedings of Optical Fiber Communication Conference and the 2006 National Fiber Optic Engineers Conference (OFC 2006)*, 2006.
[66] http://en.wikipedia.org/wiki/Self-phase_modulation.
[67] F. Yaman, Q. Lin, and G. P. Agrawal, "Fiber-optic parametric amplifiers for lightwave systems," in *Guided wave optical components and devices*, ed: Academic press, 2005.
[68] G. Cappellini and S. Trillo, "Third-order three-wave mixing in single-mode fibers: exact solutions and spatial instability effects," *Journal of the Optical Society of America B*, vol. 8, pp. 824-838, 1991.
[69] G. Cerullo and S. De Silvestri, "Ultrafast optical parametric amplifiers," *Review of Scientific Instruments* vol. 74, pp. 1-18, 2003.
[70] R. W. Boyd, *Nonlinear Optics*: Academic Press, 2003.
[71] G. P. Agrawal, *Fiber-Optic Communication Systems*: Wiley InterScience, 2002.
[72] S. Radic, R. M. Jopson, C. J. McKinstrie, J. C. Centanni, and A. R. Chraplyvy, "Stimulated-Brillouin-scattering suppression using a single modulator in two-pump parametric architectures," in *Proceedings of Optical Fiber Communication Conference (OFC/NFOEC 2005)*, 2005.
[73] G. P. Agrawal, *Lightwave Technology: Components and Devices*: John Wiley, 2004.
[74] C. V. Raman, "A new radiation," *Indian Journal of Physics*, vol. 2, pp. 387-398, 1928.
[75] E. J. Woodbury and W. K. Ng, "Ruby Laser Operation in the Near IR," *Proceedings of the Institute of Radio Engineers*, vol. 50, pp. 2367-2367, 1962.
[76] M. E. Marhic, *Fiber Optical Parametric Amplifiers, Oscillators and Related Devices*, First ed.: Cambridge University Press, 2008.
[77] J. M. C. Boggio, J. D. Marconi, and H. L. Fragnito, "Double-pumped fiber optical parametric amplifier with flat gain over 47-nm bandwidth using a conventional dispersion-shifted fiber," *IEEE Photonics Technology Letters*, vol. 17, pp. 1842-1844, 2005.

[78] S. Radic and C. J. McKinstrie, "Two-pump fiber parametric amplifiers," *Optical Fiber Technology,* vol. 9, pp. 7-23, 2003.

[79] P. O. Hedekvist, M. Karlsson, and P. A. Andrekson, "Polarization dependence and efficiency in a fiber four-wave mixing phase conjugator with orthogonal pump waves," *IEEE Photonics Technology Letters,* vol. 8, pp. 776-778, 1996.

[80] J. M. C. Boggio, A. Guimaraes, F. A. Callegari, J. D. Marconi, M. L. Rocha, M. R. X. deBarros, and H. L. Fragnito, "Parametric amplifier for mid-span phase conjugation with simultaneous compensation of fiber loss and chromatic dispersion at 10 Gb/s," *Microwave and Optical Technology Letters,* vol. 42, pp. 503-505, 2004.

[81] J. L. Blows and S. E. French, "Low-noise-figure optical parametric amplifier with a continuous-wave frequency-modulated pump," *Optics Letters,* vol. 27, pp. 491-493, 2002.

[82] S. K. Korotky, P. B. Hansen, L. Eskildsen, and J. J. Veselka, "Efficient phase modulation scheme for suppressing stimulated Brillouin scattering," in *Proceedings of Conference of Integrated Optics and Optical Fiber Communication*, pp. 110-111, Hong Kong, 1995.

[83] M. E. Marhic, N. Kagi, T. K. Chiang, and L. G. Kazovsky, "Broadband fiber optical parametric amplifiers," *Optics Letters,* vol. 21, pp. 573-575, 1996.

[84] J. M. C. Boggio, J. D. Marconi, S. R. Bickham, and H. L. Fragnito, "Spectrally flat and broadband double-pumped fiber optical parametric amplifiers," *Optics Express,* vol. 15, pp. 5288-5309, 2007.

[85] C. Florida, M.L. Sundheimer, L. de S. Menezes and A. S. L. Gomes, "Optimization of spectrally flat and broadband single-pump fiber optic parametric amplifiers," *Optics Communications,* vol. 223, pp. 381-388, 2003.

[86] L. Provino, A. Mussot, E. Lantz, T. Sylvestre, and H. Maillotte, "Broadband and flat parametric amplifiers with a multisection dispersion-tailored nonlinear fiber arrangement," *Journal of the Optical Society of America B (Optical Physics),* vol. 20, pp. 1532-7, 2003.

[87] M. Gao, C. Jiang, W. Hu, and J. Wang, "Optimized design of two-pump fiber optical parametric amplifier with two-section nonlinear fibers using genetic algorithm," *Optics Express,* vol. 12, pp. 5603-13, November 2004 2004.

[88] X. Zhang and C. Jiang, "Gain characteristics and optimization of dual-pump fiber optical parametric amplifier using two-section highly nonlinear fibers," *Optics & Laser Technology,* vol. 39, pp. 638-643, 2007.

[89] W. Zhang, C. Wang, J. Shu, C. Jiang, and W. Hu, "Design of fiber-optical parametric amplifiers by genetic algorithm," *IEEE Photonics Technology Letters,* vol. 16, pp. 1652-1654, 2004.

[90] M. Hirano, T. Nakanishi, T. Okuno, and M. Onishi, "Broadband Wavelength Conversion over 193-nm by HNL-DSF Improving Higher-order Dispersion Performance," in *Proceedings of European Conference on Optical Communications (ECOC 2005)*, pp. 43-44, 2005.

[91] M. Hirano, T. Nakanishi, T. Okuno, and M. Onishi, "Selective FWM-based wavelength conversion realized by highly nonlinear fiber," in *Proceedings of European Conference on Optical Communications (ECOC 2006)*, pp. 21-22, Cannes, France, 2006.

[92] M. Hirano, T. Nakanishi, and T. Sasaki, "Highly nonlinear fiber with reduced dispersion slope and efficient wavelength conversion with sub-ps walk-off," in *Proceedings of Optical Fiber Communication Conference (OFC 2008)*, 2008.

[93] M. Hirano, T. Nakanishi, T. Okuno, and M. Onishi, "Silica-Based Highly Nonlinear Fibers and Their Application," *IEEE Journal of Selected Topics in Quantum Electronics,* vol. 15, pp. 103-113, 2009.
[94] M. Takahashi, R. Sugizaki, J. Hiroishi, M. Tadakuma, Y. Taniguchi, and T. Yagi, "Low-Loss and Low-Dispersion-Slope Highly Nonlinear Fibers," *Journal of Lightwave Technology,* vol. 23, pp. 3615-3624, 2005.
[95] M. Hirano, "Evolution of silica-based highly nonlinear fibers for FWM-based wavelength conversion application," in *IEEE/LEOS Winter Topical Meeting Series*, pp. 84-85, Sorrento, 2008.
[96] J. H. Holland, *Adaptation in Natural and Artificial Systems: An Introductory Analysis with Applications to Biology, Control, and Artificial Intelligence*: The MIT Press, 1992.
[97] J. McCall, "Genetic algorithms for modelling and optimisation," *Journal of Computational and Applied Mathematics,* vol. 184, pp. 205-222, 2005.
[98] M. Gao, C. Jiang, W. Hu, J. Zhang, and J. Wang, "The effect of phase mismatch on two-pump fiber optical parametrical amplifier," *Optics & Laser Technology,* vol. 39, pp. 327-332, 2007.
[99] M. Karlsson, "Four-wave mixing in fibers with randomly varying zero-dispersion wavelength," *Journal of the Optical Society of America B (Optical Physics),* vol. 15, pp. 2269-2275, August 1998.
[100] F. Yaman, Q. Lin, S. Radic, and G. P. Agrawal, "Impact of Dispersion Fluctuations on Dual-Pump Fiber-Optic Parametric Amplifiers," *IEEE Photonics Technology Letters,* vol. 16, pp. 1292-1294, May 2004 2004.
[101] P. Velanas, A. Bogris, and D. Syvridis, "Impact of Dispersion Fluctuations on the Noise Properties of Fiber Optic Parametric Amplifiers," *Journal of Lightwave Technology,* vol. 24, pp. 2171-2178, May 2006 2006.
[102] M. Farahmand and M. d. Sterke, "Parametric amplification in presence of dispersion fluctuations," *Optics Express,* vol. 12, pp. 136-142, 2004.
[103] X. Liu, W. Zhao, K. Lu, T. Zhang, Y. Wang, X. Ouyang, S. Zhu, G. Chen, and X. Hou, "Optimization and Comparison of Single- and Dual-Pump Fiber-Optical Parametric Amplifiers with Dispersion Fluctuations," *Japanese Journal of Applied Physics,* vol. 45, pp. 4074-4082, 2006.
[104] P. Kylemark, P. O. Hedekvist, H. Sunnerud, M. Karlsson, and P. A. Andrekson, "Noise Characteristics of Fiber Optical Parametric Amplifiers," *Journal of Lightwave Technology,* vol. 22, pp. 409-416, 2004.
[105] D. M. Baney, P. Gallion, and R. S. Tucker, "Theory and Measurement Techniques for the Noise Figure of Optical Amplifiers," *Optical Fiber Technology,* vol. 6, pp. 122-154, 2000.
[106] M. E. Marhic, G. M. Williams, L. Goldberg, and J.-M. P. Delavaux, "Tunable Fiber Parametric Wavelength Converter with 900 mW of CW Output Power at 1665 nm," in *Nonlinear Frequency Generation and Conversion: Materials, Devices, and Applications V*, San Jose, CA, USA, 2006.
[107] K. Mori, T. Morioka, and M. Saruwatari, "Optical parametric loop mirror," *Optics Letters,* vol. 20, pp. 1424-1426, 1995.
[108] K. Mori, T. Morioka, and M. Saruwatari, "Wavelength-shift-free spectral inversion with an optical parametric loop mirror," *Optics Letters,* vol. 21, pp. 110-112, 1996.
[109] J. Yu and P. Jeppesen, "Wavelength conversion by use of four-wave mixing in a novel optical loop configuration," *Optics Letters,* vol. 25, pp. 393-395, 2000.

[110] M.-Y. Jeon, H. K. Lee, J. T. Ahn, D. S. Lim, D. I. Chang, and K. H. Kim, "All-optical demultiplexing scheme using an optical parametric loop mirror," *Optics Communications,* vol. 175, pp. 253-256, 2000.
[111] Y. Z. He, H. L. An, X. Z. Lin, and H. D. Liu, "Four-wave mixing in a fiber loop mirror constructed from two polarization-maintaining dispersion-shifted fibers," *Optics Communications,* vol. 184, pp. 277-282, 2000.
[112] G. P. Agrawal, *Applications of Nonlinear Fiber Optics,* second ed.: Academic Press, 2008.
[113] J. Li, B.-E. Olsson, M. Karlsson, and P. A. Andrekson, "OTDM Add–Drop Multiplexer Based on XPM-Induced Wavelength Shifting in Highly Nonlinear Fiber," *Journal of Lightwave Technology,* vol. 23, pp. 2654-2661, 2005.
[114] S. Nakamura, Y. Ueno, and K. Tajima, "Ultrafast all-optical switching using a frequency shift accompanied by cross-phase modulation in a semiconductor optical amplifier," in *The Conference on Lasers and Electro-Optics (CLEO '01)*, pp. 348-349, 2001.
[115] S. L. Jansen, M. Heid, S. Spalter, E. Meissner, C.-J. Weiske, A. Schopflin, D. Khoe, and H. d. Waardt, "Demultiplexing 160 Gbit/s OTDM signal to 40Gbit/s by FWM in SOA," *IET Electronics Letters,* vol. 38, pp. 978-980, 2002.
[116] H.-F. Chou, J. E. Bowers, and D. J. Blumenthal, "Compact 16O-Gb/s Add-Drop Multiplexing with a 4O-Gb/s Base-Rate," in *Proceedings of Optical Fiber Communication Conference (OFC 2004)*, 2004.
[117] E. J. M. Verdurmen, A. M. J. Koonen, and H. d. Waardt, "Time domain add-drop multiplexing for RZ-DPSK OTDM signals," *Optics Express,* vol. 14, pp. 5114-5120, 2006.
[118] G.-W. Lu, K. S. Abedin, T. Miyazaki, and M. E. Marhic, "RZ-DPSK OTDM demultiplexing using fibre optical parametric amplifier with clock-modulated pump," *Electronics Letters,* vol. 45, pp. 221-222, 2009.
[119] M. P. Fok and C. Shu, "Delay-asymmetric nonlinear loop mirror for DPSK demodulation," *Optics Letters,* vol. 33, pp. 2845-2847, 2008.
[120] K. Chan, C.-K. Chan, L.-K. Chen, and F. Tong, "Demonstration of 20-Gb/s All-Optical XOR Gate by Four-Wave Mixing in Semiconductor Optical Amplifier With RZ-DPSK Modulated Inputs," *IEEE Photonics Technology Letters,* vol. 16, pp. 897-899, 2004.
[121] M. P. Fok and C. Shu, "Exclusive-OR Gate for RZ-DPSK Signals Using Four-Wave Mixing in a Highly Nonlinear Bismuth-Oxide Fiber," in *European Conference on Lasers and Electro-Optics, 2007 and the International Quantum Electronics Conference. CLEOE-IQEC 2007*, 2007.
[122] M. Galili, B. Huettl, C. Schmidt-Langhorst, R. Ludwig, F. Futami, S. Watanabe, and C. Schubert, "All-Optical Combination of DPSK and OOK to 160 Gbit/s DQPSK Data Signals," in *Proceedings of Optical Fiber Communication and the National Fiber Optic Engineers Conference (OFC/NFOEC 2007)*, pp. 1-3, Anaheim, CA, 2007.
[123] Y. Miyamoto, A. Hirano, K. Yonenaga, A. Sano, H. Toba, K. Murata, and O. Mitomi, "320 Gbit/s (8 x 40 Gbit/s) WDM transmission over 367 km with 120 km repeater spacing using carrier-suppressed return-to-zero format," *Electronics Letters,* vol. 35, pp. 2041-2042, 1999.
[124] W. Li, M. Chen, Y. Dong, and S. Xie, "All-Optical Format Conversion From NRZ to CSRZ and Between RZ and CSRZ Using SOA-Based Fiber Loop Mirror," *IEEE Photonics Technology Letters,* vol. 16, pp. 203-205, 2004.

[125] J. Wang, J. Sun, X. Zhang, and D. Huang, "Proposal for PPLN-Based All-Optical NRZ-to-CSRZ, RZ-to-CSRZ, NRZ-DPSK-to-CSRZ-DPSK, and RZ-DPSK- to-CSRZ-DPSK Format Conversions," *IEEE Photonics Technology Letters,* vol. 20, pp. 1039-1041, 2008.
[126] B. Wu, S. Fu, J. Wu, P. Shum, N. Q. Ngo, K. Xu, X. Hong, and J. Lin, "40 Gb/s Multifunction Optical Format Conversion Module With Wavelength Multicast Capability Using Nondegenerate Four-Wave Mixing in a Semiconductor Optical Amplifier," *Journal of Lightwave Technology,* vol. 27, pp. 4446-4454, 2009.
[127] P. J. Winzer and R.-J. Essiambre, "Advanced Optical Modulation Formats," *Proceedings of the IEEE,* vol. 94, pp. 952-985, 2006.
[128] K. E. Stubkjaer, "Semiconductor Optical Amplifier-Based All-Optical Gates for High-Speed Optical Processing," *IEEE Journal of Selected Topics in Quantum Electronics,* vol. 6, pp. 1428-1435, 2000.
[129] T. Fjelde, A. Kloch, D. Wolfson, B. Dagens, A. Coquelin, I. Guillemot, F. Gaborit, F. Poingt, and M. Renaud, "Novel scheme for simple label-swapping employing XOR logic in an integrated interferometric wavelength converter," *IEEE Photonics Technology Letters,* vol. 13, pp. 750-752, 2001.
[130] A. J. Poustie, K. J. Blow, R. J. Manning, and A. E. Kelly, "All-optical pseudorandom number generator," *Optics Communications,* vol. 159, pp. 208-214, 1999.
[131] A. J. Poustie, K. J. Blow, A. E. Kelly, and R. J. Manning, "All-optical parity checker," in *Proceedings of Optical Fiber Communication Conference and the International Conference on Integrated Optics and Optical Fiber Communication (OFC/IOOC '99)*, pp. 137-139 vol.1, 1999.
[132] M. Zhang, L. Wang, and P. Ye, "All-optical XOR logic gates: Technologies and experiment demonstrations," *IEEE Communications Magazine,* vol. 43, pp. S19-S24, 2005.
[133] K. Jae Hun, J. Young Min, B. Young Tae, L. Seok, W. Deok Ha, and K. Sun Ho, "All-optical XOR gate using semiconductor optical amplifiers without additional input beam," *IEEE Photonics Technology Letters,* vol. 14, pp. 1436-1438, 2002.
[134] S. Kumar and A. E. Willner, "Simultaneous four-wave mixing and cross-gain modulation for implementing an all-optical XNOR logic gate using a single SOA," *Optics Express,* vol. 14, pp. 5092-5097, 2006.
[135] J. H. Lee, T. Nagashima, T. Hasegawa, S. Ohara, N. Sugimoto, and K. Kikuchi, "40 Gbit/s XOR and AND gates using polarisation switching within 1 m-long bismuth oxide-based nonlinear fibre," *Electronics Letters,* vol. 41, pp. 1074-1075, 2005.
[136] J. Wang, Q. Sun, and J. Sun, "All-optical 40 Gbit/s CSRZ-DPSK logic XOR gate and format conversion using four-wave mixing," *Optics Express,* vol. 17, pp. 12555-12563, 2009.
[137] Z. Liu, S. Xiao, L. Cai, and Z. Liang, "Multi-format receiver for non-return-to-zero binary-phase-shift-keyed and non-return-to-zero amplitude-shift-keyed signals," *Optics Express,* vol. 17, pp. 2918-2925, 2009.
[138] I. Kaminow, T. Li, and A. E. Willner, *Optical Fiber Telecommunications V B: systems and networks*, 5 ed., 2008.
[139] G. Charlet, "Progress in optical modulation formats for high-bit rate WDM transmissions," *IEEE Journal of Selected Topics in Quantum Electronics,* vol. 12, pp. 469-483, 2006.

[140] Y. Yadin, M. Orenstein, and M. Shtaif, "Optical DPASK and DQPSK: A Comparative Analysis for Linear and Nonlinear Transmission," *IEEE Journal of Selected Topics in Quantum Electronics,* vol. 12, pp. 581-588, 2006.
[141] N. Kikuchi, K. Mandai, K. Sekine, and S. Sasaki, "Incoherent 32-Level Optical Multilevel Signaling Technologies," *Journal of Lightwave Technology,* vol. 26, pp. 150-157, 2008.
[142] K. Sekine, N. Kikuchi, S. Sasaki, S. Hayase, C. Hasegawa, and T. Sugawara, "40 Gbit/s, 16-ary (4 bit/symbol) optical modulation/demodulation scheme," *Electronics Letters,* vol. 41, pp. 430-432, 2005.
[143] A. Maruta and S. Kitagawa, "All-optical modulation format conversion from NRZ-OOK to RZ-multilevel APSK based on fiber nonlinearity," presented at the The IEEE/LEOS Winter Topical Meeting Series, Innsbruck, Austria, 2009.
[144] G.-W. Lu and T. Miyazaki, "Experimental demonstration of RZ-8-APSK generation through optical amplitude and phase multiplexing," *IEEE Photonics Technology Letters,* vol. 20, pp. 1995-1997, 2008.